Immunological basis of abscopal antitumor responses induced by combination of distinct radiotherapy fractionation schedules with autologous tumor vaccines and checkpoint inhibition

Immunologische Grundlage der abskopalen Antitumorreaktionen, induziert durch die Kombination unterschiedlicher Strahlentherapie-Fraktionierungen mit autologen Tumorimpfstoffen und Checkpoint-Inhibition

Der Naturwissenschaftlichen Fakultät

der Friedrich-Alexander-Universität Erlangen-Nürnberg

zur

Erlangung des Doktorgrades Dr. rer. nat.

vorgelegt von

Michael Karl Rückert

Als Dissertation genehmigt von der Naturwissenschaftlichen Fakultät
der Friedrich-Alexander-Universität Erlangen-Nürnberg.

Tag der mündlichen Prüfung: 16.10.2020

Vorsitzender des Promotionsorgans: Prof. Dr. Wolfgang Achtziger

Gutachter: Prof. Dr. rer. nat. Thomas Winkler

Prof. Dr. med. Rainer Fietkau

This work was performed at the Department of Radiation Oncology

In the group of Radiation Immunobiology, Universitätsklinikum Erlangen.

Table of contents

I. List of Figures

II. List of Tables

III. List of Abbreviations

AF	Autofluorescence
APC	Antigen-presenting cell
ATCC	American Type Culture Collection
ATP	Adenosine triphosphate
AxV	AnnexinA5
BSA	Bovine serum albumin
BSA	Bovine serum albumin
BV	Brilliant Violet
CAF	Cancer-associated fibroblast
CAR	Chimeric antigen receptor
CD	Cluster of differentiation
cDC	Conventional DC
cGAS	Cyclic GMP-AMP synthase
CTL	Cytotoxic T lymphocyte
CTLA	Cytotoxic T-lymphocyte-associated protein
ctrl	Control
CXCL	C–X–C motif ligand
Cy	Cyanin
DAMP	Damage-associated molecular pattern
DC	Dendritic cell
DMSO	Dimethyl sulfoxide
DNA	Deoxyribonucleic acid
EDTA	Ethylenediaminetetraacetic acid
ELISA	Enzyme-linked immunosorbent assay
FACS	Fluorescence-activated cell sorting
FBS	Fetal bovine serum
FDA	Food and Drug Administration
FITC	Fluorescein isothiocyanate
FLT3-L	FMS-like tyrosine kinase 3 ligand
FoxP3	Forkhead box P3
FSC	Forward scatter
GM-CSF	Granulocyte-macrophage colony-stimulating factor
Gy	Gray
HHP	High hydrostatic pressure
HMGB	High-mobility group box
HRP	Horseradish peroxidase
HSP	Heat shock protein
HVEM	Herpesvirus entry mediator
ICD	Immunogenic cell death
ICI	Immune checkpoint inhibitor
ICOS-L	Inducible T cell costimulator ligand
IFN	Interferon
IGF	Insulin-like growth factor
IGFBP	IGF binding protein
IL	Interleukin
iNOS	Inducible nitric oxide synthase
IPP	Immune phenotyping panel
IT	Immunotherapy
iTAM	Immature TAM
LAG	Lymphocyte-activation gene
MACS	Magnetic-activated cell sorting
MDSC	Myeloid-derived suppressor cell
MEM	Minimum essential medium
MFI	Median fluorescence intensity
MHC	Major histocompatibility complex
MN	Monocytes
MoDC	Monocyte-derived DC
MPa	Megapascal
mRNA	Messenger ribonucleic acid
mTAM	Mature TAM
MTT	3-(4,5-dimethylthiazol-2-yl)-2,5-diphenyltetrazolium bromide

NIR	Near-infrared
NK	Natural killer
NKT	Natural killer T cell
NRT	Non-reverse transcription
NSCLC	Non-small cell lung cancer
OD	Absorbance
(D)PBS	(Dulbecco's) Phosphate-Buffered Saline
PCR	Polymerase chain reaction
PD	Programmed death
PDCA	Plasmacytoid dendritic cell antigen
PD-L	Programmed death-ligand
PE	Phycoerythrin
PerCP	Peridinin-Chlorophyll-Protein
PI	Propidium iodide
PMSF	Phenylmethylsulfonyl fluoride
PS	Phosphatidylserine
qPCR	Quantitative PCR
RIT	Radioimmunotherapy
RPMI	Roswell Park Memorial Institute
RT	Radiotherapy
SI	International System of Units
siRNA	Small interfering ribonucleic acid
SSC	Side scatter
STING	Stimulator of interferon genes
TADC	Tumor-associated DC
TAM	Tumor-associated macrophages
TAN	Tumor-associated neutrophil
TCR	T cell receptor
TGF	Transforming growth factor β
TIGIT	T cell immunoreceptor with Ig and ITIM domains
TIM	T cell immunoglobulin mucin
TLR	Toll-like receptor
TMB	Tumor mutational burden
TME	Tumor microenvironment
UV	Ultraviolet
VEGF	Vascular endothelial growth factor
VISTA	V-domain Ig suppressor of T cell activation

IV. Summary

Ionizing radiation is commonly used in radiotherapy (RT) for the local treatment of solid tumors to kill cancer cells and to stop tumor progression. Meanwhile, RT is also known to have immune-stimulatory properties by causing immunogenic tumor cell death turning tumors into *in situ* cancer vaccines eventually leading to anti-tumor immune responses. However, due to the immunosuppressive tumor microenvironment, after RT alone the immune system often fails to completely eradicate residual tumor masses of locally irradiated lesions or distant metastases. Although therapies are continuously improving, these systemic immune responses after RT that also target distant metastases outside of the radiation field, the so called abscopal effects, are still rarely seen in the clinic. Thus, immunotherapies are needed to break immunosuppression or to amplify RT-induced anti-tumor immune responses. The latter can be addressed by autologous whole tumor cell-based vaccines which comprise tumor-associated or -specific antigens of a particular patient. Since their approval for the treatment of several tumor entities, immune checkpoint inhibitors, counteracting tolerance induction and repressed tumor cell killing by immune cells, have achieved great success. The combined treatment with RT is currently under investigation in many clinical trials but is by far not standard yet. Here we aimed to generate inactivated whole tumor cell vaccines with high hydrostatic pressure (HHP) which are safe but still immunogenic to boost RT-induced immune responses. We hypothesized that RT and such HHP-vaccines synergize to generate a tumor microenvironment fostering tumor growth retardation in locally irradiated tumors and that systemic anti-tumor immune reactions can also be triggered when anti-PD-1 immune checkpoint inhibitors are applied in addition.

In pre-clinical model systems we subcutaneously (s.c.) injected mice with syngeneic B16 melanoma or CT26 colon carcinoma cells, respectively. To evaluate the efficiency of RT in combination with HHP vaccines, established tumors were locally irradiated with a hypofractionated schedule and mice were injected next to the tumor with HHP-vaccines generated with 200 MPa. In an abscopal tumor model with local irradiation of only one of two B16 tumors (one on each flank) using two differently hypofractionated schedules with 2x8 Gy or 3x8 Gy, HHP-vaccines were injected s.c. in the neck. Additionally, mice concurrently received anti-PD-1 antibodies. Tumor growth and survival of the mice was monitored and the immunological tumor microenvironment was analyzed via multi-color flow cytometry, qPCR and ELISA.

Tumor cells treated with a pressure of 200 MPa were completely inactivated and lost the potential to form colonies *in vitro* or tumors *in vivo*. Combined treatment of local irradiation and therapeutic HHP-vaccination resulted in retarded tumor growth and prolonged survival of the mice in both tumor models. The number of cells per gram of tumor across several immune cell subtypes was only significantly increased in B16 tumors that were treated with both, RT and HHP-vaccines.

Irradiated tumors showed higher expression of suppressive immune checkpoint ligands and most of the tumor-infiltrating T cells were positive for PD-1 expression, providing a rationale for the combination with anti-PD-1 checkpoint inhibition. Although injected distantly in the abscopal setting, HHP-vaccines also further retarded the growth of locally irradiated tumors even though in all radioimmunotherapy combinations the total number of immune cells was decreased in primary tumors and the peripheral blood. However, HHP-vaccination combined with RT failed to significantly induce abscopal anti-tumor immune responses and even partly abrogated those which were induced with RT plus anti-PD-1. In this group, the abscopal effects were accompanied by an elevated infiltration of CD8+ T cells. Adding another fraction of 8 Gy completely abrogated abscopal effects and *in vitro* data revealed that multiple immunosuppressive and oncogenic pathways including cell death, cytokine release, and checkpoint expression were differently modulated with 3x8 Gy when compared to 2x8 Gy. We further found that high intratumoral concentrations of IGFBP-6 correlated with abscopal responses. Surprisingly, knockdown of IGFBP-6 inhibited tumor growth *in vitro* and *in vivo*.

We conclude that autologous whole tumor cell-based vaccines generated with HHP are safe and suitable to be combined with RT and work irrespective of the injection site of the vaccine if the tumor was previously irradiated. However, HHP-vaccines without any additional adjuvant do not increase abscopal anti-tumor immune responses induced with RT plus anti-PD-1 and thus need further optimization in the future.

V. Zusammenfassung

Ionisierende Strahlung wird üblicherweise in der Strahlentherapie (RT) zur lokalen Behandlung von soliden Tumoren verwendet, um Krebszellen abzutöten und das Fortschreiten des Tumors zu stoppen. Mittlerweile ist auch bekannt, dass RT immunstimulierende Eigenschaften hat, indem es immunogenen Tumorzelltod verursacht und Tumore in *in-situ*-Krebsimpfstoffe verwandelt, die schließlich zu anti-Tumor-Immunantworten führen. Aufgrund der immunsuppressiven Tumormikroumgebung kann das Immunsystem jedoch die verbleibenden Tumormassen lokal bestrahlter Läsionen oder Fernmetastasen außerhalb des Bestrahlungsfeldes nach RT allein oft nicht vollständig eliminieren. Obwohl sich die Therapien kontinuierlich verbessern, werden diese systemischen Immunantworten nach RT, welche auch unter dem Begriff abskopaler Effekt bekannt sind, in der Klinik immer noch selten beobachtet. Daher sind Immuntherapien erforderlich, um die Immunsuppression zu unterbrechen oder RT-induzierte anti-Tumor-Immunantworten zu verstärken. Letzteres kann durch autologe Impfstoffe auf der Basis ganzer Tumorzellen realisiert werden, die tumorassoziierte oder -spezifische Antigene eines bestimmten Patienten beinhalten. Seit ihrer Zulassung für die Behandlung mehrerer Tumorentitäten haben Immun-Checkpoint-Inhibitoren, die der Toleranzinduktion und der unterdrückten Abtötung von Tumorzellen durch Immunzellen entgegenwirken, große Erfolge erzielt. Die Behandlung in Kombination mit RT wird derzeit in vielen klinischen Studien untersucht, ist jedoch bei weitem noch nicht Standard. In dieser Arbeit war es unser Ziel inaktivierte Ganzzell-Tumorimpfstoffe mit hohem hydrostatischem Druck (HHP) zu erzeugen, die sicher und immunogen sind, um RT-induzierte Immunantworten zu verstärken. Wir stellten die Hypothese auf, dass RT und solche HHP-Impfstoffe zusammenwirken, um eine Tumormikroumgebung zu erzeugen, die die Verzögerung des Tumorwachstums bei lokal bestrahlten Tumoren fördert, und dass darüber hinaus systemische anti-Tumor-Immunreaktionen ausgelöst werden können, wenn zusätzlich anti-PD-1-Immun-Checkpoint-Inhibitoren angewendet werden.

In präklinischen Modellsystemen injizierten wir Mäusen subkutan (s.c.) syngene B16-Melanom- oder CT26-Kolonkarzinomzellen. Um die Effizienz von RT in Kombination mit HHP-Impfstoffen zu untersuchen, wurden etablierte Tumoren lokal mit einem hypofraktionierten Schema bestrahlt und Mäusen wurden neben dem Tumor HHP-Impfstoffe injiziert, die mit 200 MPa erzeugt wurden. In einem abskopalen Tumormodell mit lokaler Bestrahlung von nur einem von zwei B16-Tumoren (einer an jeder Flanke) unter Verwendung von zwei unterschiedlich hypofraktionierten Zeitplänen mit 2×8 Gy oder 3×8 Gy wurden HHP-Impfstoffe s.c. im Nacken injiziert. Zusätzlich erhielten Mäuse gleichzeitig anti-PD-1-Antikörper. Das Tumorwachstum und das Überleben der Mäuse wurden überwacht und die immunologische Tumormikroumgebung wurde mittels Mehrfarben-Durchflusszytometrie, qPCR und ELISA analysiert.

Mit einem Druck von 200 MPa behandelte Tumorzellen wurden vollständig inaktiviert und verloren das Potenzial zur Bildung von Kolonien *in vitro* oder von Tumoren *in vivo*. Die kombinierte Behandlung mit lokaler Bestrahlung und therapeutischer HHP-Impfung führte in beiden Tumormodellen zu einem verzögerten Tumorwachstum und einem verlängerten Überleben der Mäuse. Die Menge an Zellen pro Gramm Tumor über mehrere Immunzell-Subtypen hinweg war nur bei B16-Tumoren, die sowohl mit RT als auch mit HHP-Impfstoffen behandelt wurden, signifikant erhöht. Bestrahlte Tumoren zeigten eine höhere Expression von supprimierenden Immun-Checkpoint-Liganden und die meisten Tumor-infiltrierenden T-Zellen waren PD-1 positiv, was eine Begründung für die Kombination mit anti-PD-1-Checkpoint-Inhibition liefert. Obwohl HHP-Impfstoffe entfernt von den Tumoren verabreicht wurden, verzögerten sie trotzdem das Wachstum lokal bestrahlter Tumoren weiter, obwohl in allen Radioimmuntherapiekombinationen die Gesamtzahl der Immunzellen in Primärtumoren und im peripheren Blut verringert war. Eine mit RT kombinierte HHP-Impfung induzierte jedoch keine signifikanten abskopalen anti-Tumor-Immunantworten und hob sogar diejenigen, die mit RT plus Anti-PD-1 induziert wurden, teilweise auf. In dieser Gruppe gingen die abskopalen Effekte mit einer erhöhten Infiltration von CD8+ T-Zellen einher. Eine zusätzliche Fraktion von 8 Gy hob die abskopalen Effekte vollständig auf und *in-vitro*-Daten zeigten, dass mit 3×8 Gy im Vergleich zu 2x8 Gy eher immunsuppressive und onkogene Signalwege, einschließlich Zelltod, Zytokinfreisetzung und Checkpoint-Expression, moduliert wurden. Außerdem fanden wir heraus, dass hohe intratumorale Konzentrationen von IGFBP-6 mit abskopalen Reaktionen korrelierten. Überraschenderweise hemmte ein IGFBP-6 knockdown allerdings das Tumorwachstum *in vitro* und *in vivo*.

Wir schließen daraus, dass mit HHP erzeugte autologe Impfstoffe auf der Basis ganzer Tumorzellen sicher und geeignet sind, mit RT kombiniert zu werden und unabhängig von der Injektionsstelle des Impfstoffs wirken, wenn der Tumor zuvor bestrahlt wurde. HHP-Impfstoffe ohne zusätzliches Adjuvans erhöhen jedoch nicht die mit RT plus Anti-PD-1 induzierten abskopalen Antitumor-Immunantworten und müssen daher in Zukunft weiter optimiert werden.

1. Introduction

1.1 Cancer and the immune system

It is widely known that mutations in oncogenes or tumor suppressor genes transform normal tissue cells in cancer cells. For cancer development multiple of these driver mutations need to accumulate (Martincorena et al., 2017) eventually providing the tumor with characteristic malignant properties, such as evasion of apoptosis, insensitivity to anti-growth signals, self-sufficiency in growth signals, sustained angiogenesis, tissue invasion and metastasis, and limitless replicative potential as proposed by Hanahan and Weinberg in their well-known "hallmarks of cancer" (Hanahan & Weinberg, 2000). The role of the immune system in cancer prevention and development, however, was neglected for a long time (Schreiber, Old, & Smyth, 2011). Higher incidence rates of cancer in immunocompromised patients under immunosuppressive medication after transplantation (Mortaz et al., 2016) and in immunodeficient mice and men (Schreiber et al., 2011; Mayor et al., 2018) clearly indicate that immunosurveillance is important for tumor cell eradication. Therefore, the avoidance of immune destruction was later included in an updated version of the "hallmarks of cancer" (Hanahan & Weinberg, 2011).

1.1.1 Anti-tumor immune responses

In general, cytotoxic T lymphocyte (CTL) responses against tumors have a similar course of events as they do against pathogens (Murphy, Weaver, Mowat, & Janeway, 2017). Chen and Mellman described this process as the cancer-immunity cycle (Figure 1, 1.2 Cancer immunotherapies (IT)). First, if tumor antigens are released by dying tumor cells in a pro-inflammatory context and taken up by dendritic cells (DCs) they get activated and migrate to the next lymph node. There, they cross-present the processed antigen on MHC-I to CD8+ T cells. After this priming, the activated effector T cells exit the lymph node and traffic to the tumor via the peripheral blood. In the tumor, they recognize their cognate antigen with the T cell receptor presented on MHC-I by the tumor cells. Killing their target tumor cell releases further neoantigens and the cycle revolves once again (D. S. Chen & Mellman, 2013). After CD8+ T cells are primed by activated DCs, CD4+ T cells help to initiate CTL clonal expansion and differentiation into effector and memory T cells (Janssen et al., 2003). Thus, the functional quality of the anti-tumor immune response is improved and might protect from recurrent disease (Borst, Ahrends, Babala, Melief, & Kastenmuller, 2018).

NK cells contribute to tumor surveillance by recognizing tumor cells in different ways. Activation of NK cells and subsequent killing of target cells with perforin, granzyme or death-inducing ligands, such as FasL, depends on the balance between stimulatory and inhibitory signals they sense

via several receptors on their surface (Morvan & Lanier, 2016). Missing MHC-I on tumors cells can be a strong activating signal but even if MHC-I is expressed engagement of other receptors, e.g. NKG2D, is enough to induce killing of the tumor cell (Cerwenka, Baron, & Lanier, 2001). Antibody-dependent cell-mediated cytotoxicity might not be involved in immunosurveillance but could be partially responsible for the success of therapies with antibodies directed against tumor cells (Valipour et al., 2019).

1.1.2 Immunoediting

In fact, the immune system is not only responsible for cancer immunosurveillance as a host-protective function to clear transformed cells in early stages but has a more complex and dual role in cancer development. The finding that tumor cells isolated from immunocompetent mice are less immunogenic than the ones from immunodeficient tumors suggests that the immune system actively selects less immunogenic tumor cells by killing the immunogenic clones (Shankaran et al., 2001). This led to the development of the cancer immunoediting hypothesis with its "three Es": *elimination*, *equilibrium* and *escape* (G. P. Dunn, Old, & Schreiber, 2004). In the elimination phase cancer cells are recognized by cells of the innate and adaptive immune system and are cleared before they form tumors. If some tumor cells survive they enter the equilibrium phase in which immune cells keep the tumor cells in a dormant state. Tumor outgrowth is prevented and this phase might last for a long period throughout the life of the host. Pathologically visible tumors are already in the escape phase and have fully circumvented immune recognition to promote tumor outgrowth. Escape mechanisms can occur in the form of loss of tumor antigens or resistance to immune cell-mediated killing. In detail, loss of antigen can be achieved by tumor cells through a defective antigen processing and presentation machinery via MHC-I or if tumor cell clones lacking tumor-associated antigens emerge from the strong selection pressure by immunosurveillance and immunoediting. To prevent an attack by effector cells of the adaptive immune system or NK cells, the tumor creates a surrounding immunosuppressive microenvironment with conditions in which those immune cells are not able to exert their anti-tumor activity (Schreiber et al., 2011).

1.1.3 The immunosuppressive tumor microenvironment

The tumor microenvironment (TME) consists of tumor cells as well as all surrounding non-cancerous cells, non-cellular components and particular physiological conditions. Latter comprise low pH, hypoxia, nutrient deprivation and immunosuppressive metabolites, such as lactate and arginase-1 which are responsible for the low pH, suppress CTL and NK cell functions, and support regulatory T cells (Tregs) and pro-tumorigenic M2 polarization of tumor-associated macrophages

(TAMs) (Yu & Ho, 2019). Tumor and stroma cells secrete vascular endothelial growth factor (VEGF), a key driver of angiogenesis which is crucial for tumor progression and metastatic spread. In tumors, angiogenesis is defective and leads to structurally and functionally impaired vasculature. Together with the high metabolic rate of tumor cells, this contributes to a limited nutrient supply for immune cells, the infiltration of immune cells is restricted and hypoxic areas inside the tumor are generated (Griffioen, Damen, Blijham, & Groenewegen, 1996; Fukumura et al., 1998). The cells of the tumor stroma largely consist of cancer-associated fibroblasts (CAFs), endothelial cells and immune cells. CAFs contribute to tumor progression via secretion of extracellular matrix components, metabolites, growth factors and also directly shape the immune system within the TME by releasing a wide variety of cytokines and chemokines (LeBleu & Kalluri, 2018). Especially cytokines released by Th2 cells, such as IL-4, IL-6 or IL-13 have immunosuppressive and pro-tumorigenic roles such as polarizing macrophages towards an M2 phenotype (D. Chen et al., 2018). TGF-β exerts multiple functions in tumor progression and immunosuppression by dampening effector immune cells and supporting tumor-promoting cells (Knudson et al., 2018; P. Zhao et al., 2018). CXCL12 is overexpressed in many cancer entities, induces VEGF expression and recruits M2 TAMs and Tregs into the TME (Guo et al., 2016). Myeloid-derived suppressor cells (MDSCs) are a heterogeneous population of immature myeloid cells that suppress CTL, NK cell and B cell responses and are able to differentiate into TAMs, tumor-associated neutrophils (TANs) and tumor-associated DCs (TADCs) (Veglia, Perego, & Gabrilovich, 2018). Tumor-infiltrating macrophages originate from inflammatory monocytes from the periphery and per se can have pro- as well as anti-tumoral activity depending on their polarization mediated by the surrounding micromilieu (Porrello et al., 2018). In the TME, however, as mentioned before, TAMs are more likely to acquire an anti-inflammatory M2 phenotype and in turn, themselves function as important regulators of immunosuppression by secreting TGF-β or IL-10 (Liu, Kuang, Zhou, & Zhang, 2018). Just like M1/M2macrophages, TANs have equivalent subtypes, albeit they are prone to acquire an anti-inflammatory N2 phenotype in the TME and thereafter convey the same signals that led to their polarization to sustain these TME conditions (Albini, Bruno, Noonan, & Mortara, 2018). TADCs are maintained in an immature state by the TME and have impaired antigen cross-presentation and co-stimulation functionality. On top of that, TADCs exhibit tolerogenic and proangiogenic properties (Albini et al., 2018). The role of B cells in tumor immunity is controversial. Wouters and Nelson reported a positive prognostic effect of tumor-infiltrating B cells in half of the studies they analyzed and a negative effect in less than 10 % of the publications (Wouters & Nelson, 2018). However, emerging evidence in mice and humans suggests that B cells can also contribute to the immunosuppressive TME by acquiring a regulatory phenotype and secreting anti-inflammatory cytokines (Sarvaria, Madrigal, & Saudemont, 2017). In tumors Tregs show a highly activated phenotype and, compared to conventional T cells, express high-affinity T cell receptors (TCRs) against

self-antigens (Sainz-Perez, Lim, Lemercier, & Leclerc, 2012). Tregs mediate their immunosuppressive properties by multiple mechanisms. Via high-affinity IL-2 receptor expression they deprive cytotoxic T cells and NK cells from IL-2 and thereby mitigate their proliferation, differentiation, and activation. Effector T cells and antigen-presenting cells (APCs) can also be directly killed by perforin and granzyme released by Tregs. Additionally, regulatory T cells are another source of suppressive cytokines (TGF-β, IL-10, IL-35) and the surface expression of CTLA-4 inhibits APC maturation (Shitara & Nishikawa, 2018). CTLA-4 and PD-1 are the best-known representatives of the immune checkpoint molecules which are expressed on T cells. The ligands of immune checkpoint receptors, such as PD-L1, PD-L2 or HVEM are usually expressed on APCs to shut down T cells responses after successful elimination of pathogens and thus prevent autoimmunity. Tumor cells, however, adopt this mechanism for the inhibition of T cell priming and to circumvent the elimination by CTLs (Dyck & Mills, 2017). Immune checkpoint functions and the importance of tumor immunotherapies will be described in more detail in 1.2.2 Immune checkpoint inhibitors.

Taken together, the TME is a very complex interplay of tumor cells with numerous physiological, cellular and humoral factors having highly redundant and self-sustaining mechanisms to generate and maintain tumor progression and immunosuppression. Thus, treatments can either directly target tumor cells or modulate the surrounding TME to induce anti-tumor immune responses.

1.2 Cancer immunotherapies (IT)

Cancer immunotherapies are basically all immune system modulating treatments that help the body's own immune system to fight the tumor in two fundamental ways. Immunotherapy (IT) can either stimulate and initiate new immune responses, or support pre-existing immune responses by strengthening effector functions or counteracting the immunosuppressive TME. Referring to the cancer immunity cycle (D. S. Chen & Mellman, 2013) there are numerous targets in the course of an anti-tumor immune response which can be addressed by ITs (Figure 1). Therefore, a multitude of approaches in clinical and pre-clinical trials already exists and are further being developed.

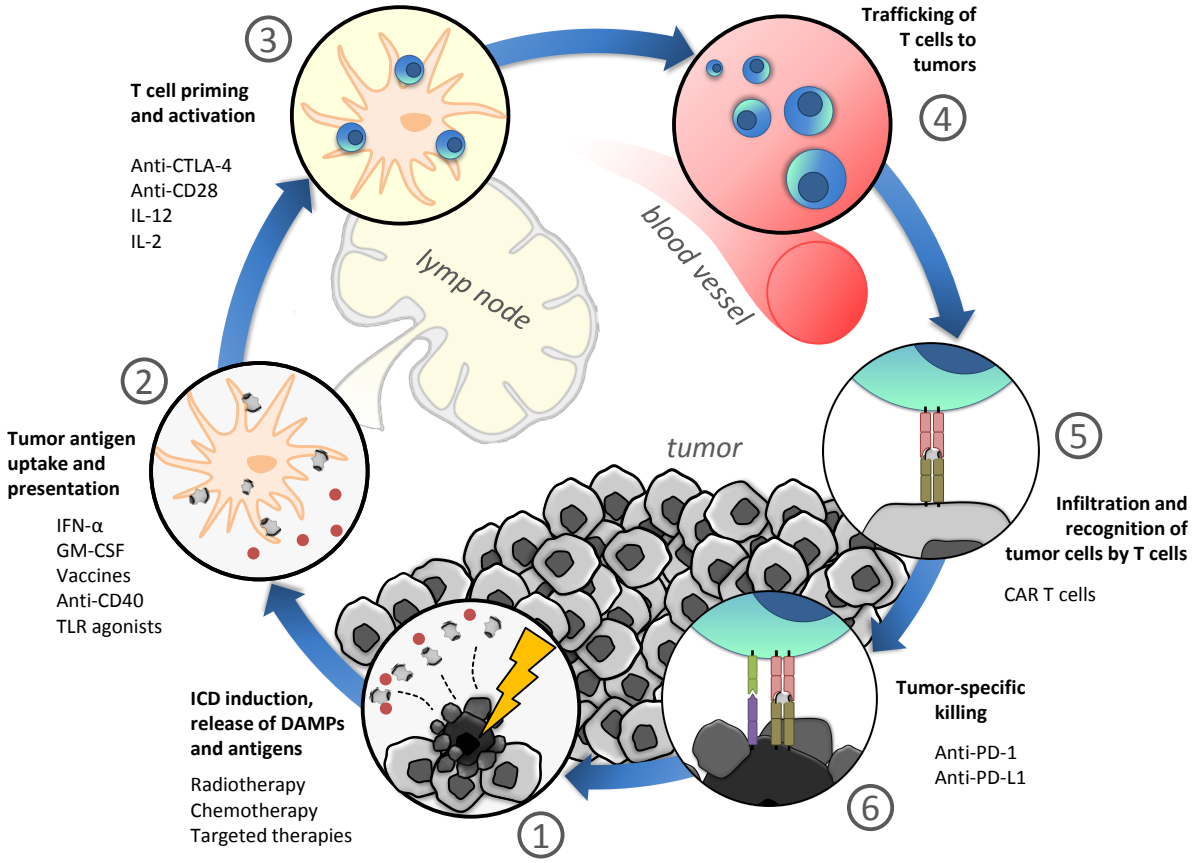

Figure 1: Cancer immunotherapy targets in the cancer immunity cycle. *ICD* immunogenic cell death, *DAMPs*, damage-associated molecular patterns, *CAR* chimeric antigen receptor. Adapted from (D. S. Chen & Mellman, 2013).

Immune checkpoint inhibitors targeting the immunosuppression of CTLs in the priming (anti-CTLA-4) and effector phase (anti-PD-1, anti-PD-L1/2) have become the most promising and effective ITs in the last decade and will be explained in detail in 1.2.2 Immune checkpoint inhibitors. Receptor agonists triggering co-stimulatory pathways on T cells (anti-CD28) or APCs (anti-CD40) and cytokines, such as interleukins (e.g IL-2, IL-12), interferons (IFN-α) and GM-CSF can be applied either alone to rather unspecifically differentiate, activate, and mature different immune cells or can be combined as an adjuvant with cancer vaccines (Peggs, Quezada, & Allison, 2009; S. Lee & Margolin, 2011). In contrast, adoptive T cell therapies represent a more tumor-specific approach in which patient-derived T cells are genetically engineered *ex vivo* to express recombinant T cell receptors or chimeric antigen receptors (CARs) recognizing tumor antigens and are then reinjected into the same patient. Unlike MHC-dependent recombinant TCRs, CARs are basically antigen recognition domains of different receptor or antibody origins fused to intracellular T cell signaling domains enabling the MHC-independent binding of non-peptide antigens as well. However, adoptive T cell therapies, so far, have only proven to be effective in hematological malignancies rather than in solid cancers (Riley, June, Langer, & Mitchell, 2019).

Therapeutic cancer vaccination aims to provide the immune system with tumor antigens and this strategy alone has originated manifold different approaches. Although historically seen classical cancer therapies, such as radiotherapy and chemotherapy, and most targeted therapies were not intended to be immunostimulatory treatments per se. However, by killing cancer cells, tumor-associated or -specific antigens are made available for antigen-presenting cells and therefore these treatments act as a kind of *in situ* cancer vaccine and are able to initiate anti-tumor immune responses (L. Galluzzi, Buque, Kepp, Zitvogel, & Kroemer, 2015; Rückert, Deloch, Fietkau, Frey, & Gaipl, 2017). Tumor-associated antigens are endogenous antigens on tumor cells which are not expressed in normal tissues but are involved in tissue differentiation or which are overexpressed by tumor cells. Tumor-specific antigens comprise oncogenic viral antigens and neoantigens as products of somatic mutations. These antigens are foreign to the body, lack control of central tolerance, and are therefore highly immunogenic (Velcheti & Schalper, 2016). All approaches rely on the uptake and presentation by APCs. Therefore, some approaches also focus on directly targeting DCs via the coupling of tumor antigens to monoclonal antibodies directed against endocytosis receptors on DCs. In most cases however, antigens in *ex vivo* generated cancer vaccines are solely delivered in various sizes and forms ranging from nucleic acids (mRNA, DNA), peptides, proteins, up to whole tumor cells. These antigens are usually formulated with adjuvants, such as different TLR agonists, anti-CD40, saponins or GM-CSF as a general immune stimulant to increase their immunogenicity (Hu, Ott, & Wu, 2018).

Contrary to tumor-associated antigens which are often overexpressed in the same type of cancer, tumor-specific antigens are not only tumor-specific but also patient-specific and therefore need to be identified for each individual patient for the targeting in adoptive T cell therapies and therapeutic cancer vaccines. This makes these approaches costly and technically challenging but much more promising. Personalized whole tumor cell vaccines would overcome the issue of prospective antigen identification and would provide the whole spectrum of tumor-associated as well as tumor-specific neoantigens. Additionally, unlike targeting a single tumor antigen, this would address tumor heterogeneity and minimize the risk of immune escape by immunoediting and clonal evolution (Rosenberg, Yang, & Restifo, 2004). Here we focus on two therapy modalities, autologous whole tumor cell vaccines generated with high hydrostatic pressure to boost anti-tumor immune responses and immune checkpoint inhibitors used to counteract immunosuppression of CTLs.

1.2.1 Whole tumor cell vaccines generated with high hydrostatic pressure

One potential treatment to further boost anti-tumor immune responses induced by ionizing radiation are whole tumor cell vaccines generated with high hydrostatic pressure (HHP).

Physiological pressure on earth reaches from 0.1 MPa (1 bar) atmospheric pressure at sea level to ~110 MPa at almost 11 km below sea level in the Challenger Deep located in the Mariana Trench (Lauro & Bartlett, 2008). One technical use of high hydrostatic pressure in industry is the preservation of food and has the advantage that, compared to thermal treatment, aromas, flavors, and vitamins are not affected (Adkins et al., 2018). Additionally, bone or cartilage transplants can be sterilized by HHP prior to orthopedic surgery (Diehl et al., 2004; Diehl, Schauwecker, Mittelmeier, & Schmitt, 2008). Higher pressure levels in the physiological range do not only change the morphology of eukaryotic cells but can also induce cellular stress which resembles a heat shock response. However, these effects are reversible when the pressure is back at a physiological level and the cell viability is not affected (Haskin, Athanasiou, Klebe, & Cameron, 1993; Wilson, Trogadis, Zimmerman, & Zimmerman, 2001). In contrast, non-physiological high hydrostatic pressure above 100 MPa has irreversible effects and eventually leads to cell death (Frey et al., 2008). Without changing the primary structure, HHP denatures proteins only by affecting their tertiary and quaternary structure and thereby inactivates enzymes (Boonyaratanakornkit, Park, & Clark, 2002). While DNA is mostly resistant to HHP, cytoplasm and plasma membranes acquire gel-like properties (Macgregor, 1998; Mentre, Hamraoui, Hui Bon Hoa, & Debey, 1999). Therefore, cells are smaller after HHP treatment but their round shape is retained over weeks and they do not degrade (Frey et al., 2008). Although human cells tend to be more resistant to HHP than murine cells, pressure of at least 200 MPa effectively and reproducibly kills tumor cells of both species (Weiss, Meister, et al., 2010). HHP treated cells predominantly die a necrotic and thus immunogenic cell death characterized by DNA degradation at later time points, phosphatidylserine exposure, loss of membrane integrity and the release of HMGB1, HSP70, HSP90 and ATP (Frey et al., 2004; Weiss, Meister, et al., 2010; Fucikova et al., 2014). Therefore, HHP was included in the list of immunogenic cell death inducers (L. Galluzzi, Buque, Kepp, Zitvogel, & Kroemer, 2017). In addition to the adjuvanticity these DAMPs give the HHP treated tumor cells, Urbanova et al. have reported that HHP preserves tumor antigens if the pressure is not too high, HHP treated tumor cells are phagocytosed by DCs and subsequently stimulate CD8+ T cells (Urbanova et al., 2017). They treated human lung, prostate and ovarian cancer cell lines with pressures of 150 MPa to 300 MPa and found that tumor antigens are degraded predominantly at pressures of 250 MPa and higher, however, the degradation varied with the tissue origin of the cells and within the tumor antigens. Although DC phagocytosis increased with the pressure the tumor cells were treated with and the DC activation peaked at 200 MPa, the best stimulation of tumor-specific CD8+ T cells *in vitro* was detected when DCs were pulsed with tumor cells treated with

150 MPa. However, 150 MPa did not fully inactivate the tumor cells and is therefore not suitable for vaccine preparation. Urbanova et al. conclude that 200 MPa is the optimal pressure as a compromise of antigen degradation and immunogenicity (Urbanova et al., 2017).

Compared to other tumor cell vaccine preparation methods such as freeze-thaw, irradiation or heat inactivation, the aforementioned properties make HHP a suitable method to generate whole tumor cell vaccines as it fulfills three major requirements for the application of such cancer vaccines. The reproducible complete inactivation of tumor cells would guarantee the safety of the vaccine by preventing residual viable tumor cells to form new tumors after injection into patients and it has no intrinsic toxicity. Additionally, this enables HHP vaccine generation to be in accordance with legal requirements and good manufacturing practices. Thirdly, in agreement with the current consensus guidelines on the definition of immunogenic cell death (Lorenzo Galluzzi et al., 2020) HHP vaccines possess a certain immunogenicity as they combine antigenicity and adjuvanticity by containing preserved tumor antigens along with the release of DAMPs (Weiss, Frey, et al., 2010; Seitz et al., 2019). Currently, HHP treated tumor cells are tested as therapeutic cancer vaccines in two phase I/II clinical trials for ovarian and lung cancer (NCT03657966, NCT02470468) and one phase III trial for prostate cancer (NCT02111577). In these trials monocyte-derived DCs from patients are loaded with HHP treated allogeneic tumor cell lines (DCVAC) followed by the injection of these pulsed DCs back into the patient.

1.2.2 Immune checkpoint inhibitors

Uncontrolled, long-lasting immune responses and self-reactive T cells bear the risk of inducing autoimmunity. Thus, the immune system installed several checkpoints to prevent damage of lymphocytes directed against the own body. Central tolerance is the process of deleting T cells with strong reactivity to self-antigens during their development in the thymus. Additionally, T cells which do not bind to MHC at all are sorted out as well. Only T cells weakly interacting with MHC and a low affinity to self-peptides are released into secondary lymphatic organs or the blood and are subsequently regulated by mechanisms of peripheral tolerance, such as anergy, regulatory T cells (Tregs), activation-induced cell death or immune checkpoint molecules (Murphy et al., 2017). Of the inhibitory receptors, CTLA-4 and PD-1 are the most studied representatives of the latter. For their discovery and envisioning how to exploit them for cancer immunotherapy James P. Allison and Tasuku Honjo were awarded with the Nobel Prize in physiology or medicine in 2018 (Leach, Krummel, & Allison, 1996; Freeman et al., 2000; NobelPrize.org, 2020). In order to mount a proper CTL response, T cells need three signals for their activation. First, the antigen-specific T cell receptor (TCR) recognizes a peptide presented on MHC by APCs. Second, APCs deliver co-stimulatory signals

via CD80/CD86 to CD28 on the T cell. Third, cytokines, such as IL-12 or type 1 IFNs are required to promote activation and proliferation (Williams & Bevan, 2007). Upon activation induced by TCR binding T cells immediately start to express CTLA-4 which outcompetes CD28 signaling by binding CD80 and CD86 with a higher affinity and avidity than CD28. Thereby, CTLA-4 dampens the co-stimulatory signal two provided by APCs and thus, is a regulator of early-stage T cell responses in the priming phase in secondary lymphoid organs against weak antigens including self- as well as tumor antigens (Fife & Bluestone, 2008). In addition, binding of CTLA-4 can also remove CD80/86 from APCs via trans-endocytosis reducing its availability to other T cells (Qureshi et al., 2011). T cell activation by TCR engagement or cytokine (e.g. TGF-β, IL-2, IL-21) exposure also induces PD-1 expression (Seidel, Otsuka, & Kabashima, 2018). On APCs, IFN-γ is the main stimulus for the expression of both PD-1 ligands, PD-L1 and PD-L2 (Brown et al., 2003). Although both eventually interfere with CD28 signaling, in contrast to CTLA-4, PD-1 thus regulates CTL suppression rather during the effector phase of the immune response. PD-L1 and PD-L2 can be expressed by different cells of TME and also tumor cells exploit this mechanism to circumvent CTL-mediated killing (Seidel et al., 2018). Albeit an anti-tumor immune response was initiated and activated tumor-specific CTLs infiltrate into the tumor, in the presence of immune checkpoint molecules they hence fail to exert their effector function.

Immune checkpoint inhibitors (ICIs) are monoclonal antibodies designed to block the interaction of the immune checkpoint receptor with its ligands in the immunological synapse. Thus, they can be directed against CTLA-4 or either PD-1 or one of its ligands PD-L1 and PD-L2. In 2011 anti-CTLA-4 antibody ipilimumab for the treatment of advanced melanoma was the first ICI being approved by the FDA and only four months later in Europe. Striking results have been achieved ever since with ICIs against CTLA-4 and PD-1 with increased overall survival of patients with melanoma, lung cancer and carcinomas (Seidel et al., 2018). Historically seen, novel cancer therapies, such as chemotherapies, were considered successful and thus, approved for the clinic even if they added only few weeks or months to the median survival of cancer patients. In contrast, immune checkpoint therapy for the treatment of patients with advanced diseases results in a plateau in the overall survival curve with long-term survivors. For example, in a retrospective analysis about 20 % of patients with unresectable or metastatic melanoma treated with ipilimumab who reached the plateau after three years had a good chance of still being alive after ten years (Schadendorf et al., 2015). This indicates that patients initially responding to checkpoint inhibition are likely to be among the long-term survivors, although a large proportion of patients remains refractory to the treatment, which calls for further improvements, such as combined therapies. Based on the success of ICIs targeting the CTLA-4 and PD-1 axis, increasing interest emerged to develop ICIs against other immune checkpoints, such as TIM-3, VISTA, TIGIT or LAG-3, and to discover new immunosuppressive

immune checkpoint pathways. Although some of them showed promising results in pre-clinical and firs clinical trials none of them made its way into the clinic, so far (Qin et al., 2019).

1.3 Radiotherapy (RT)

About 60 % of the patients with solid tumors receive radiotherapy (RT) in the course of their disease either as monotherapy or in combination with surgery, chemotherapy, and others (Prasanna, Ahmed, Mohiuddin, & Coleman, 2014). The primary goal of radiotherapy for the treatment of cancer always was to control the disease either by stopping the proliferation of tumor cells or the induction of their cell death. At the same time, localized irradiation spares as much surrounding normal tissue as possible, thus, the damage to organs in the irradiation field is minimized. However, it has become more and more evident that ionizing radiation does not only have direct targeted effects on tumor cells but also induces bystander or distant effects on neighboring cells and systemic effects by modulating the immune system.

1.3.1 Ionizing radiation

Radiation travels through space and matter at high speeds in the form of particles or electromagnetic waves and, if carrying sufficient energy, radiation ionizes atoms by detaching an electron. Ionizing radiation occurs as a consequence of radioactivity in radioactive decay (alpha- beta- gamma- or neutron radiation) or can be produced artificially (e.g. X-rays, radiotherapy). Depending on the medium they are passing through, particle radiation, such as alpha- and beta radiation are readily absorbed by matter (e.g. air or water) and thus have only a short range of a few millimeters or centimeters to few meters, respectively, and can be shielded quite easily with a piece of paper or thin aluminum plates. Alpha particles, which are helium nuclei consisting of two protons and two neutrons, can only penetrate the outer layers of the human skin but as they deposit their energy in this short distance alpha-ray emitters such as radon can cause severe damage to the tissue upon ingestion. Beta radiation is emitted as electrons or positrons from radioactive decays and causes damage to tissues as well but has lower biological effectiveness than alpha radiation because it deposits less energy per distance. Electromagnetic radiation is characterized by its frequency or wavelength with higher energies at higher frequencies or shorter wavelengths. Radiation in the form of massless photons without electric charge in the electromagnetic spectrum above UV-light is ionizing and can be divided, depending on its origin, inside or outside of the atomic nucleus in X-radiation and gamma radiation. The latter is emitted from the atomic nucleus at alpha- or beta decays and easily penetrates matter which makes heavy shielding with lead and concrete necessary. X-radiation is also a product of radioactive decay but is mostly know for technical or medical

applications, such as X-ray diagnostics and radiotherapy, where it is produced artificially. There, electrons are accelerated at high-speeds and when they hit the anode, are slowed down and X-rays are emitted with an energy proportional to the applied voltage. Electromagnetic radiation has lower biological effectiveness than particle radiation but penetrates tissue deeper which makes it suitable for the irradiation of tumors inside the body (BfS, 2019).

The radiation dose is defined by the unit Gray (Gy) as the amount of energy absorbed by matter in the SI units Joule per kilogram (1 J/kg). As Gy is independent of the target material, biological effects are not considered. However, each organ and tissue in the human body is different in its radiosensitivity and each type of radiation (e.g. particle and electromagnetic radiation) is more or less harmful. Therefore, the unit Sievert (Sv) was introduced and is also defined as J/kg but takes into account the biological effectiveness with weighing factors for the type of radiation in the equivalent dose and additionally tissue-specific susceptibilities in the effective dose. Unlike Gy which is used in cancer therapy for high dose irradiation where biological effects can be directly compared to the absorbed dose, Sv is found for low doses in radiation protection for example for the exposition of humans to natural radiation and technical radiation at workplaces (Frey, Rückert, Deloch, et al., 2017).

1.3.2 Biological effects of RT

Ionizing radiation has directly targeted effects on cells when it deposits its energy in molecules inside the cell as well as non-targeted effects which are mostly mediated by the immune system. These targeted effects are mostly caused by DNA damage. The DNA can be ionized either directly by ionizing radiation or indirectly via highly reactive radicals including reactive oxygen and nitrogen species which are generated inside the cell when other molecules are ionized. These reactions cause base damage, single or clustered DNA single-strand breaks or double-strand breaks. If the damage is detected by the cell and exceeds its repair mechanism capabilities the cell undergoes cell death to protect the whole organism from tumorigenesis caused by these mutations or chromosomal aberrations. Radiation-induced forms of cell death can be mitotic catastrophe, apoptosis, necrosis, and autophagy but also senescence can occur (Frey, Rückert, Deloch, et al., 2017). In the latter, cells remain viable and metabolically active, but undergo permanent cell cycle arrest. The mitotic catastrophe is a well-known response to RT which appears upon premature, faulty entrance of cells into mitosis as a result of irreparable DNA damage and eventually leads to cell death. Apoptosis is a physiological process during cell differentiation, growth and development to maintain tissue homeostasis and is the best characterized form of cell death. Typical morphological characteristics of this programmed form of cell death are chromatin condensation, nuclear

fragmentation, cellular shrinkage, membrane blebbing and exposure of phosphatidylserine on the outer cell membrane. Unlike apoptosis, necrosis was thought to be a non-physiological uncontrolled form of cell death induced by extracellular traumata but it was found that there are also cell-intrinsic pathways leading to the so-called necroptosis. Irrespective of that it results in swelling of cells and organelles, a ruptured plasma membrane and therefore loss of intracellular contents (Deloch et al., 2016; Rückert et al., 2018).

1.3.3 Immunological effects of RT

Additional to the targeted effects RT has also immunological effects which are mostly related to cancer cell death. Here, the most important forms of cell death induced by RT are apoptosis and necrosis. As mentioned before, apoptosis is a physiological process in the body. Therefore, if apoptotic cells are taken up by phagocytes they subsequently release anti-inflammatory cytokines and thus promote tumor tolerance. Among those cytokines, TGF-β is found in large amounts in an inactive form in the TME and can be converted by RT into its active form. Furthermore, other suppressive factors such as adenosine, chemokines and VEGF-A can be found in the TME after RT eventually promoting recruitment, differentiation and polarization of immunosuppressive immune cell subtypes (Wennerberg et al., 2017). Additionally, it was found that RT or radiochemotherapy results in upregulated expression of immune checkpoint ligands on melanoma and glioblastoma cells (Derer et al., 2016).

Unlike apoptosis, necrosis is considered to be a form of immunogenic cell death. By the loss of membrane integrity, damage-associated molecular patterns (DAMPs) are released by necrotic cells. In general, molecules which are usually only present inside of cells under physiological conditions act as alarm signals for immune cells when they detect them on the cell surface or in the extracellular space indicating damaged cells and tissue. Among those DAMPs are chaperones belonging to the family of heat shock proteins (HSPs) and calreticulin, the chromatin stabilization protein high-mobility group box 1 (HMGB1) or the energy providing ATP. Both, HMGB1 and ATP have adjuvant-like effects and extracellular ATP also mediates chemotaxis of APCs. Calreticulin, HSP70 and HSP90 act as “eat-me” signals for APCs and foster the maturation, antigen uptake and presentation and thus the priming of CTLs (L. Galluzzi et al., 2017; Rückert et al., 2018). Further, membrane-bound HSP70 on tumor cells directly activates NK cells and triggers their cytolytic activity (Gaipl et al., 2014). In addition to the release of DAMPs, RT increases the immunogenicity of tumor cells by inducing the release of pro-inflammatory cytokines and chemokines, and the surface expression on tumor cells of adhesion molecules, death receptors, stress ligands, CD80 and MHC-I (Reits et al., 2006; Frey et al., 2014).

1.3.4 The abscopal effect

In an ideal situation for a patient with metastasized disease, local RT of the primary tumor or a metastasis triggers a systemic immune response directed against all lesions in the body including distant, non-irradiated tumors. This shrinkage of tumor masses outside the irradiation field is the so-called abscopal effect ("ab" – away from, "scopus" – target) and was first described and termed by Mole et al. in 1953 (Mole, 1953). However, the abscopal effect is very seldom seen in the clinic, as there was only about one reported case per year in the literature between 1969 and 2014 (Abuodeh, Venkat, & Kim, 2016).

In consequence of the ambivalent effects of RT with simultaneous immune stimulation and modulation of the TME but also suppression of emerging and pre-existing anti-tumor immune responses, RT alone is often not enough to fully eradicate tumors and to induce abscopal effects. Therefore, ITs have great potential to complement RT by further boosting RT-induced immune responses and counteracting tumor-intrinsic as well as RT-mediated immunosuppression (Ainhoa Arina, Gutiontov, & Weichselbaum, 2020). This beneficial liaison of radioimmunotherapies is reflected by the continuously increasing case reports of abscopal effects since the approval of ipilimumab in 2011 (S. Demaria & Formenti, 2020).

1.4 Radio-Immunotherapy (RIT) combinations

Upon approval for the clinic, immune checkpoint inhibitors were mostly used as monotherapies. Since the past few years however, increasing amounts of clinical trials are conducted evaluating the safety and efficacy of combining ICIs with RT. So far, in most reported cases RT had no effect on the immunotherapy-related side-effects (Xing, Siva, & Hanna, 2019). In a more recent review on case reports of abscopal effects the authors compared patients receiving RT alone or RIT combinations. Between 1960 and 2018 they found 94 cases of which 47 were patients treated with RT alone. Consequently, the other half of the documented abscopal effects originated from combined treatments. Strikingly, these reports were all found in the short period from 2012 until 2018, indicating a strong increase in the frequency in the past few years since combined therapies have become more frequent (Dagoglu, Karaman, Caglar, & Oral, 2019).

Pre-clinical evidence from several studies for the synergy of radiotherapy with immunotherapies and the induction of abscopal effects exists since many years. All of them have in common that abscopal effects were most pronounced or only visible if RT was combined with different kinds of IT, including growth factors, cytokines and ICIs (Ainhoa Arina et al., 2020). In an early study using a metastatic lung cancer model, Chakravarty et al. found that FLT3-L injections expand DCs *in vivo* and, together with irradiation of the primary tumor (1x60 Gy), significantly

prolonged the survival by reducing the number of metastases (Chakravarty et al., 1999). In a poorly immunogenic breast cancer model these results were further confirmed and it was demonstrated that the immune response was tumor-specific and T cell dependent (S. Demaria et al., 2004). Intratumoral administration of IL-12 with an adenoviral vector together with RT improved local tumor control and prevented microscopic tumor growth at distant sites (Seetharam et al., 1999). Demaria et al. were the first to test the combination of RT and checkpoint inhibition. Anti-CTLA-4 antibody 9H10 had no impact on the poorly immunogenic metastatic mammary carcinoma 4T1 tumor. However, combined treatment with RT resulted in delayed tumor growth and inhibited formation of lung metastases (Sandra Demaria et al., 2005). Whole tumor cell vaccines generated with HHP in combination with RT have not been tested so far.

Increasing evidence suggests that RT has potential for optimization in terms of dose and fractionation to elicit the most favorable immune response. Additionally, IT needs to be well-matched with RT concerning both, the type of IT and the chronological order in which they are administered.

1.4.1 Impact of RT dose and fractionation on the immune response

For therapy of most tumor entities, classically fractionated treatment schedules are applied with approximately 2 Gy per fraction, five times a week; this scheme is therefore called normfractionation. This fractionation exploits the impaired DNA damage repair and cell cycle processes in tumor cells to increase tumor cell death and, at the same time, minimize side effects on the surrounding normal tissue (Asur, Butterworth, Penagaricano, Prise, & Griffin, 2015). In preclinical experiments single doses of 1 Gy or 2 Gy were found to be favorable for the tumor infiltration of iNOS expressing M1 macrophages which release nitric oxide. Subsequently, this resulted in vasculature normalization and accumulation of T cells (Klug et al., 2013).

Technical advances of treatment planning, linear accelerators and irradiation techniques facilitate an increasing precision of dose deposition in the target tumor volume with minimized dose in the healthy tissue (Deloch et al., 2016; Herskind et al., 2017). This enables the application of hypofractionated treatment schedules with less fractions and higher doses per fraction. In stereotactic ablative RT even the irradiation of small lesions with few very high doses, often called radiosurgery, is possible. In pre-clinical models with oral and colon carcinoma Morisada et al. compared norm- (10x2 Gy) and hypofractionation (2x8 Gy). Both fractionations achieved similar local tumor control, however, in the hypofractionation protocol CTL accumulation and activation was preserved in tumors and the periphery. Further, RT plus anti-PD1 was much more efficient to induce local and abscopal responses with 2x8 Gy than 10x2 Gy (Morisada et al., 2018). Similar results were

found by Dewan et al. when they compared hypofractionation with a single high dose. In combination with anti-CTLA-4, local and abscopal tumor growth inhibition with 1x20 Gy was inferior to both hypofractionation schemes of which 3x8 Gy was more effective than 5x6 Gy (Dewan et al., 2009). Schaue et al. conducted a dose escalation experiment with single doses from 5 Gy to 15 Gy and found that the tumor control and number of tumor-reactive T cells increased with the dose. Fractionation of the 15 Gy with different doses per fraction was most effective with a medium dose of 2x7.5 Gy (Schaue, Ratikan, Iwamoto, & McBride, 2012). The idea of a certain threshold for an immunogenic dose with possible disadvantageous outcomes if applied doses exceed a certain upper limit was also suggested by the work of Vanpouille-Box and colleagues. They have demonstrated that the immunogenicity of higher doses of ionizing irradiation is dependent on the sensing of DNA released into the cytosol after irradiation by the cGAS/STING pathway and subsequent type I IFN responses. If the applied single dose is above 12-18 Gy, however, the exonuclease Trex1 is also expressed which in turn degrades the cytosolic DNA (Vanpouille-Box et al., 2017). Type I IFNs released after hypofractionated RT subsequently induce expression of IFN-responsive genes such as MHC-I but also PD-L1 on tumor cells *in vivo* (Morisada et al., 2018). Increased PD-L1 expression after (hypo-)fractionated RT and radiochemotherapy but not high single doses has also been shown *in vitro* for melanoma and glioblastoma cells (Derer et al., 2016) and also in biopsies of patients after radiochemotherapy (Lim et al., 2017). These results might explain why ICIs predominantly synergize with hypofractionated RT.

In conclusion, normfractionation rather favors recruitment of immune cells into the tumor whereas hypofractionation induces ICD to elicit robust local and systemic immune responses. Future treatment plans might exploit the advantages of both by combining them in consecutive schedules.

1.4.2 Sequencing of RIT combinations

As mentioned before, most of the cancer patients do not respond to checkpoint inhibition. Neglecting this fact could end up being a personal burden for patients in case alternative treatments would have been more effective at the same time and a financial burden for the healthcare system as ICIs are too expensive to be given to every patient. Therefore, biomarkers need to be found for the identification of responders and non-responders in advance, and determining the most effective radioimmunotherapy for each tumor entity or individual patient is desired. One critical aspect for the combination of RT and IT is the chronological order of the treatment schedule. Dovedi et al. treated CT26 tumor bearing mice with fractionated RT of 5x2 Gy and compared the onset of anti-PD-L1 therapy at three different time points. The mice received the antibodies either beginning with the first dose of RT, together with, or five days after the last dose, respectively. The latter schedule did

not prolong the survival of the mice. Only concomitant treatment significantly improved the survival with a slight advantage of simultaneous treatment start of both therapies (Dovedi et al., 2014). Another group followed a similar approach to compare administration sequencing of anti-CTLA-4 and an agonistic antibody against OX40, a co-stimulatory receptor expressed by activated T cells. CT26 colon carcinomas were treated with a single dose of 20 Gy and IT was given seven days before, one day following, or five days following RT. In the case of anti-CTLA-4 the best outcome was observed for the administration before RT, whereas anti-OX40 was most effective right after RT and had no effect five days after RT (Young et al., 2016). Additionally, in almost all cases of abscopal effects reviewed by Dagoglu et al. patients received RT immediately after, or concurrent with IT (Dagoglu et al., 2019). Given the distinct mechanisms of the CTLA-4 and PD-1 axis the different results for both ICIs are explainable. Together, these results indicate that there might not be a generally accepted schedule for all ITs and that the impact of the RT fractionation scheme should be considered as well.

The immunogenicity of a tumor is determined by factors such as its antigenicity and the efficacy of the antigen processing and presentation machinery (Wang, He, Wang, Li, & Liu, 2019). High tumor mutational burden (TMB) was found to be a predictive biomarker for the immunogenicity of the tumor and its response to ICI (Thomas et al., 2018; Klempner et al., 2020). Consequently, TMB and the resulting immune recognition could provide a rationale why some patients do not respond to ICI and why they profit from a combined treatment when it is applied in the right order. As depicted in Figure 2, it is thought that immunogenic tumors of patients are recognized by the immune system and, thus, the tumor cells have to express immune checkpoint ligands to counteract the immune attack. If ICIs are given to those patients as a monotherapy the immune response is re-initiated and the tumors respond to the treatment. In contrast, non-immunogenic tumors lack a pre-existing immune response and consequently expression of immune checkpoint ligands. Hence, ICI is not effective and those patients represent the non-responder group. Using therapies, such as RT, therapeutic vaccination or other ITs to increase the immunogenicity of the tumor could convert the non-immunogenic tumors to “hot” tumors that are recognized by effector cells. In turn, tumor cells would try to rebalance immunosuppression by immune checkpoint expression. ICIs applied in a combined treatment would then be effective again, resulting in higher response rates (Frey, Rückert, & Gaipl, 2019).

Previous work of our group provides another hint that the timing of ITs might be critical. There, we irradiated CT26 tumors with 2x5 Gy and monitored tumor-infiltrating immune cells. Right after RT we observed enhanced infiltration of macrophages and APCs for about four days, followed by a sharp peak of CD8 T cell infiltration lasting only one day and appearance of Tregs thereafter (Frey, Rückert, Weber, et al., 2017). Similar results were reported after irradiation of melanomas with 2x12 Gy. In those tumors, leukocytes in general and CD8 T cells were present in higher percentages

five days after RT before they declined (Hettich, Lahoti, Prasad, & Niedermann, 2016). This clearly shows that immune cell infiltration into tumors following irradiation is a dynamic process and that RT fractionation protocols might have to be optimized to prevent re-irradiation in a phase of high immune cell infiltration. Therefore, Zhang and Niedermann conducted a pre-clinical trial where they investigated the effect of hypofractionated irradiation extended in the phase of T cell infiltration. Importantly, anti-PD-1 and irradiation with 5x6.43 Gy spread over ten days had similar effects as treatment with 3x9.18 Gy distributed over three or five days on the local and abscopal tumor growth as well as immune cell infiltration and tumor-specific CD8 T cell responses (X. Zhang & Niedermann, 2018). Still, the addition of immunotherapies needs to be well-matched to the treatment schedule based on the type of immunotherapy to achieve optimal outcomes.

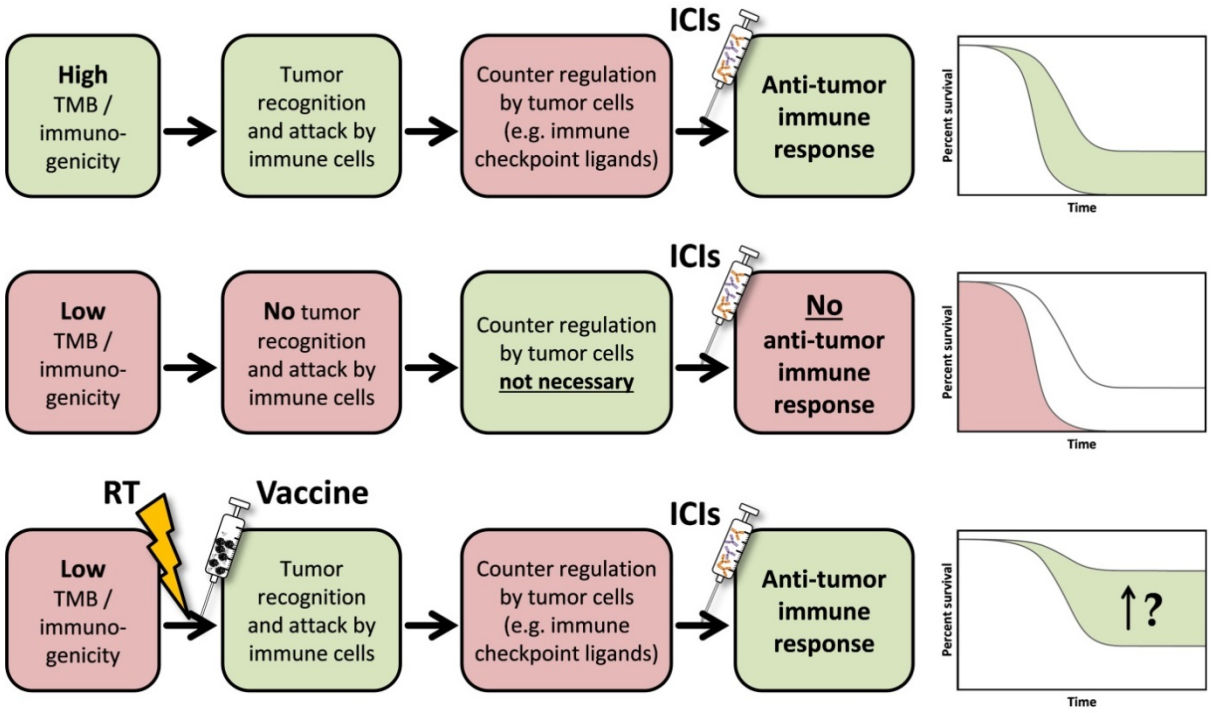

Figure 2: Immunological rationale for the combination of radio(immuno)therapy with immune checkpoint inhibition. *TMB* tumor mutational burden, *RT* radiotherapy, *ICIs* immune checkpoint inhibitors. Adapted from (Frey et al., 2019).

1.5 Aim of the project

RT alone often fails to induce strong anti-tumor immune responses. In clinical and pre-clinical trials ITs appear to be promising complementary treatment options. HHP has been shown to induce immunogenic cell death in tumor cells and to reproducibly inactivate them completely, which makes HHP-treated cells suitable for the use in therapeutic cancer vaccines. In this project, we first aimed to evaluate the safety of whole tumor cell vaccines generated with HHP and their efficacy in combination with RT in a murine ectopic B16-F10 melanoma and CT26 colon carcinoma model. Analyzing the tumor-infiltrating immune cell subtypes should give insight into the immunological tumor microenvironment generated by the treatment modalities.

As a second aim we wanted to augment the therapy with immune checkpoint inhibition to assess the induction of abscopal effects in a setting with a tumor on each flank of the mouse of which only one was irradiated. As depicted in Figure 3, we hypothesized that by induction of immunogenic cell death in tumor cells local RT provides antigens and DAMPs to activate immune cells (1). HHP vaccines would further boost the anti-tumor immune response and increase the accumulation of activated immune cells into the tumor (2). Infiltrating effector T cells would however face immunosuppression mediated by immune checkpoint molecules. By the systemic application of anti-PD-1 antibodies as a third therapy option we aimed to counteract this shutdown of the immune response to enable the eradication of the primary irradiated tumor (3) as well as the non-irradiated abscopal tumor (4). Further, we hypothesized that by performing immune phenotyping of tumor-infiltrating and circulating immune cells by multi-color flow cytometry and analysis of the cytokine milieu inside the tumors we would get further insight into the underlying mechanism of abscopal effects and that there will be differences between primary and abscopal tumors as well as between the treatment groups. So far, pre-clinical trials often only focus on the T cell response. With our approach we aimed to gain a broader overview on immune cell infiltration to identify additional subtypes which might contribute to the orchestration of anti-tumor immune responses.

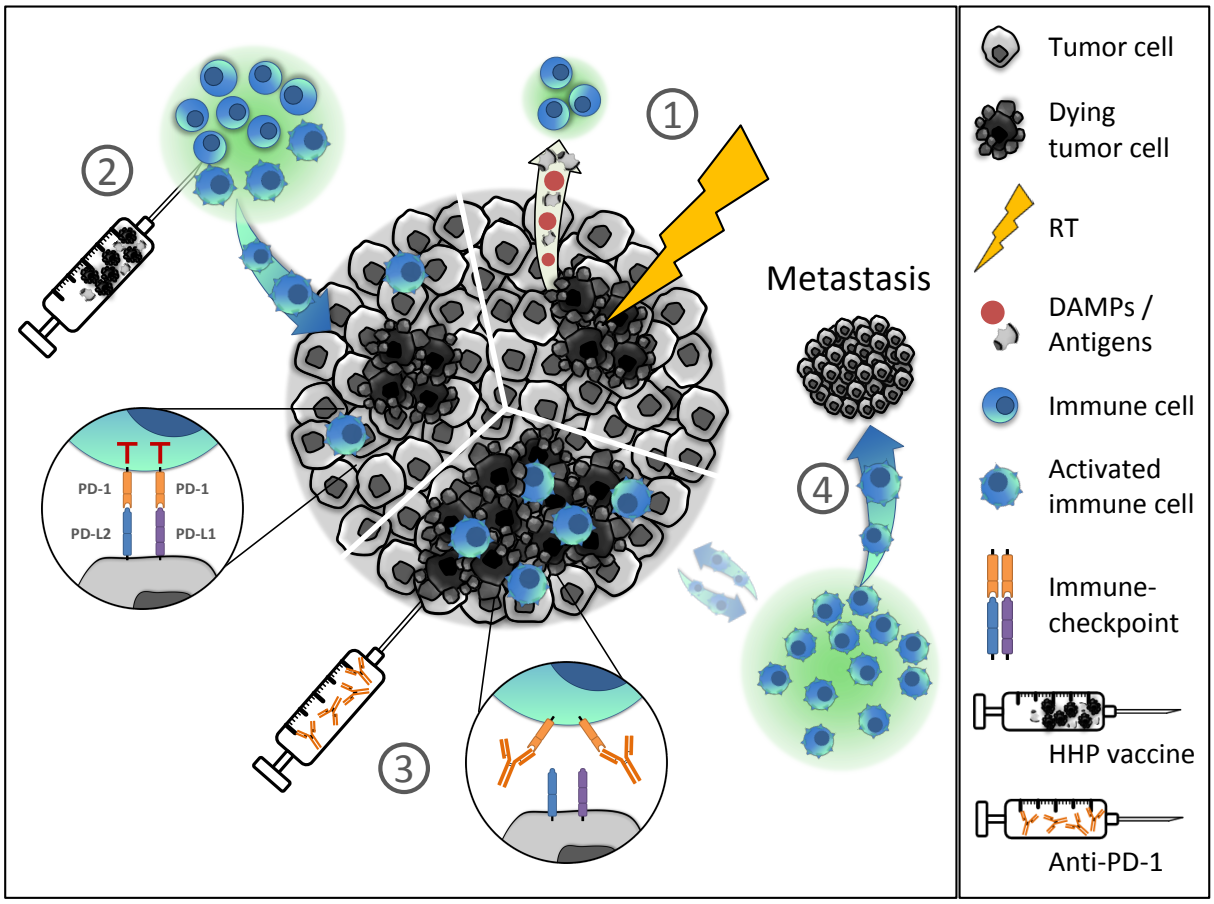

Figure 3: Induction of local and abscopal anti-tumor immune responses by the combination of RT, HHP vaccination and anti-PD-1. (1) Local RT provides antigens and DAMPs to activate immune cells by inducting immunogenic cell death in tumor cells.(2) HHP vaccines further boost the anti-tumor immune response and increase the accumulation of activated immune cells into the tumor. However, infiltrating effector T cells face immunosuppression mediated by immune checkpoint molecules. (3) The systemic application of anti-PD-1 antibodies counteracts this shutdown of the immune response to enable the eradication of the primary irradiated tumor (4) as well as the non-irradiated abscopal tumor. Adapted from (Rückert et al., 2018).

2. Material & Methods

2.1 Material

2.1.1 Chemicals and reagents

Table 1: List of chemicals and reagents

Chemical	Product number	Supplier	
2-Propanol	1.00995.6010	Merck	Darmstadt, Germany
2X Lysis Buffer	AA-LYS-16ML	RayBiotech	Peachtree Corners, GA, USA
AnnexinV-FITC (1 mg/ml)	-	GeneArt	Regensburg, Germany
Antifoam Y-30 Emulsion	A5758-100ML	Sigma-Aldrich	Munich, Germany
Aqua ad iniectabilia	2351744	B.Braun Melsungen AG	Melsungen, Germany
Bovine serum albumin (BSA)	A7030-S04	Sigma-Aldrich	Munich, Germany
Chloroform	1.02445.0250	Merck	Darmstadt, Germany
Dimethyl sulfoxide (DMSO)	D8418	Sigma-Aldrich	Munich, Germany
DNase I, RNase-free (1 U/µL)	EN0521	Thermo Fisher Scientific	Waltham, MA, USA
Ethanol	9065.1	Carl Roth	Karlsruhe, Germany
Ethylenediaminetetraacetic acid (EDTA)	8040.1	Carl Roth	Karlsruhe, Germany
Halt Phosphatase Inhibitor Single-Use Cocktail	78428	Thermo Fisher Scientific	Waltham, MA, USA
Invivofectamine 3.0 Reagent	IVF3001	Thermo Fisher Scientific	Waltham, MA, USA
InVivoPlus anti-mouse PD-1	BP0146	Bio X Cell	West Lebanon, NH, USA
Isofluran CP	1214	CP-Pharma	Burgdorf, Germany
Methylene blue	03978-250ml	Sigma-Aldrich	Munich, Germany
Monopotassium phosphate	4873	Merck	Darmstadt, Germany
peqGold Glycogen RNase free	37-1810	VWR International	Darmstadt, Germany
peqGold TriFast	30-2010	VWR International	Darmstadt, Germany
PMSF Protease Inhibitor	36978	Thermo Fisher Scientific	Waltham, MA, USA
Potassium chloride	4936.1000	Merck	Darmstadt, Germany
Propidium Iodide (1 mg/ml)	P4170	Sigma-Aldrich	Munich, Germany
RNase A	10109169001	Merck	Darmstadt, Germany
Sodium chloride	39571	Carl Roth	Karlsruhe, Germany
Sodium fluoride	S6776-100G	Sigma-Aldrich	Munich, Germany
Sodium orthovanadate	450243-10G	Sigma-Aldrich	Munich, Germany
Sodium phosphate dibasic	S5136	Sigma-Aldrich	Munich, Germany
Sulfuric acid (2 N)	X873.1	Carl Roth	Karlsruhe, Germany
Triton X-100	T8787	Sigma-Aldrich	Munich, Germany
Tween 20	9127.1	Carl Roth	Karlsruhe, Germany
UltraPure DNase/RNase-Free Distilled Water	10977035	Thermo Fisher Scientific	Waltham, MA, USA
Yellow Sample Buffer (40X)	R1381	Thermo Fisher Scientific	Waltham, MA, USA
β-Glycerophosphate	G9422	Sigma-Aldrich	Munich, Germany

2.1.2 Media and additives

Table 2: List of media and supplements

Media/Additive	Product number	Supplier	
0.5 % Trypsin-EDTA (10X)	15400-054	Gibco Life Technologies	Carlsbad, CA, USA
Accutase solution	A6964-100ML	Merck	Darmstadt, Germany
CASYton	5651808	OLS OMNI Life Science	Bremen, Germany
CytoFLEX Sheath Fluid	B51503	Beckman Coulter	Brea, CA, USA
Dulbecco's Phosphate-Buffered Saline (DPBS)	D8537-500ML	Sigma-Aldrich	Munich, Germany
Fetal bovine serum (FBS) Superior	S0615	Biochrom	Berlin, Germany
Lipofectamine RNAiMAX Transfection Reagent	13778075	Thermo Fisher Scientific	Waltham, MA, USA
MACS BSA Stock Solution	130-091-376	Miltenyi Biotec	Bergisch Gladbach, Germany
Opti-MEM I Reduced Serum Medium	31985070	Thermo Fisher Scientific	Waltham, MA, USA
Recombinant Mouse IGFBP-6 (carrier-free)	752404	BioLegend	San Diego, CA, USA
Ringer's solution	2610813	Fresenius Kabi	Bad Homburg, Germany
RPMI-1640 medium	R8758-500ML	Merck	Darmstadt, Germany
Silencer Select Igfbp6 siRNA	AM16830, ID: 62477	Thermo Fisher Scientific	Waltham, MA, USA
Silencer Select Negative Control No. 1 siRNA	4404020	Thermo Fisher Scientific	Waltham, MA, USA

2.1.3 Consumables

Table 3: List of consumables

Material	Product number	Supplier	
BD Microtainer SST Tubes	365951	BD	Franklin Lakes, NJ, USA
CASYcups	5651808	OLS OMNI Life Science	Bremen, Germany
Cellstar 96-, 6-well culture plate sterile, F-bottom	655180, 657160	Greiner bio-one	Frickenhausen, Germany
Cellstar 96-well culture plate sterile, V bottom	651180	Greiner bio-one	Frickenhausen, Germany
Cellstar cell culture flask (T75, T175 cm^2)	658175, 660175	Greiner bio-one	Frickenhausen, Germany
Cellstar serological pipettes (2, 5, 10, 25, 50 ml)	710180, 606180, 607180, 760180, 768180	Greiner bio-one	Frickenhausen, Germany
Centrifuge tubes (15, 50 ml)	227261, 188271	Greiner bio-one	Frickenhausen, Germany
Combitips advanced (1, 5, 10 ml)	0030089790, 0030089456, 0030089464	Eppendorf	Hamburg, Germany
CRYO.S 2 ml round bottom tube	121263	Greiner bio-one	Frickenhausen, Germany
Disposable pipette tips (10, 200, 1250 µl)	771258, 737240, 750250	Greiner bio-one	Frickenhausen, Germany
EASYstrainer™, 70 µm, sterile	542070	Greiner bio-one	Frickenhausen, Germany
Filter tips (10, 20, 300, 1250 µl)	771261, 773261, 737261, 738261, 750261	Greiner bio-one	Frickenhausen, Germany

gentleMACS C Tubes	130-093-237	Miltenyi Biotec	Bergisch Gladbach, Germany
gentleMACS M Tubes	130-093-236	Miltenyi Biotec	Bergisch Gladbach, Germany
GripTips pipette tips (125, 300 µl)	4425, 4435	Integra bioscience	Zizers, Switzerland
Hematocrit capillary	9100275	Hirschmann	Eberstadt, Germany
Herd-shell skirted 96-Well PCR plate	HSP9601	BioRad	Hercules, CA, USA
Injekt-F syringe	9166017V	B.Braun Melsungen	Melsungen, Germany
LS Columns	130-042-401	Miltenyi Biotec	Bergisch Gladbach, Germany
MicroFine+ Insulin Syringe	324827	BD	Franklin Lakes, NJ, USA
Microlance 3 needles (0.4x19mm)	30220	BD	Franklin Lakes, NJ, USA
Microvette 500 LH	20.1345	Sarstedt	Nümbrecht, Germany
Nunc Maxisorb plates (96-well format)	442404	Thermo Fisher Scientific	Waltham, MA, USA
Nunclon surface petri dishes	150288	Nunc A/S	Roskilde, Denmark
Parafilm	PM-996	Bemis	Oshkosh, WI, USA
Pre-Separation Filters (30 µm)	130-041-407	Miltenyi Biotec	Bergisch Gladbach, Germany
Reaction tubes (0.5, 1.5, 2.5, 5.0 ml)	72.706.400, 72.704.400, 72.695.500	Sarstedt	Nümbrecht, Germany
Round bottom tube	55.1578	Sarstedt	Nümbrecht, Germany
Scalpel, sterile	200130011	pfm medical	Cologne, Germany
Syringes Discardit II (10 ml)	309110	BD	Franklin Lakes, NJ, USA

2.1.4 Laboratory equipment

Table 4: List of laboratory equipment

Material	Supplier	
Beaker (100, 200, 500, 1000 ml)	Duran Group	Wertheim, Germany
Measuring cylinder	Duran Group	Wertheim, Germany
Multichannel pipette m300	Sartorius	Goettingen, Germany
Multipette M4	Eppendorf	Hamburg, Germany
Neubauer counting chamber	Paul Marienfeld	Lauda-Königshofen, Germany
Pipetboy comfort	Integra bioscience	Zizers, Switzerland
VIAFLO II multichannel pipette (125, 300 µl)	Integra bioscience	Zizers, Switzerland

2.1.5 Instruments

Table 5: List of instruments

Instrument	Supplier	
Analytical balance Mettler AC100	Mettler Toledo	Columbus, OH, USA
Aqua dest. TKA-Lab Tower	TKA Wasseraufbereitungssysteme	Niederelbert, Germany
Autoclave Varioclav	HP Medizintechnik	Oberschleißheim, Germany
AxioCam ERc5s	Carl Zeiss Microscopy	Jena, Germany
CASY Cell Counter	OLS OMNI Life Science	Bremen, Germany
Centrifuge Hettich Rotina 420R	Hettich	Tuttlingen, Germany
Centrifuge Megafuge 1.0RS	Heraeus Instruments	Hanau, Germany

Centrifuge Mikro 200R	Hettich	Tuttlingen, Germany
CytoFLEX S	Beckman Coulter	Brea, CA, USA
DNA/RNA UV-cleaner box UVC/T-M-AR	Biosan	Riga, Latvia
Epoch Microplate Spectrophotometer	BioTek	Bad Friedrichshall, Germany
Freezer (-20 °C)	Liebherr,	Biberach an der Riß, Germany
Freezer (-80 °C)	Heraeus Instruments	Hanau, Germany
Fridge	Liebherr	Biberach an der Riß, Germany
gentleMACS Dissociator	Miltenyi Biotec	Bergisch Gladbach, Germany
High Hydrostatic Pressure (HHP) treatment system	Lehrstuhl für Prozessmaschinen und Anlagentechnik" (iPAT)	Erlangen, Germany
Hotplate	Kunz Instruments	Nynashamn, Sveden
iBright™ FL1000 Imaging System	Thermo Fisher Scientific	Waltham, MA, USA
Ice machine	Ziegra	Isernhagen, Germany
Incubator BBD 6220	Heraeus Instruments	Hanau, Germany
Laminar flow cabinet Hera Safe	Heraeus Instruments	Hanau, Germany
Laminar flow cabinet LaminAir LFM 2448S	Heraeus Instruments	Hanau, Germany
Lead shielding chamber	Seifert	Ahrensberg, Germany
MACS MultiStand	Miltenyi Biotec	Bergisch Gladbach, Germany
MESO QuickPlex SQ 120	Meso Scale Diagnostics	Rockville, MD, USA
Microscope Primo Vert	Carl Zeiss Microscopy	Jena, Germany
Nanophotometer P330	Implen	München, Germany
PCR machine C1000 Touch Thermal Cycler, CFX96 Real Time System	BioRad,	Hercules, CA, USA
PRIMART linear accelerator	Siemens	Munich, Germany
QuadroMACS Separator	Miltenyi Biotec	Bergisch Gladbach, Germany
Sprout Mini-Centrifuge	Heathrow Scientific	Vernon Hills, IL, USA
TQ-Prep Workstation	Beckman Coulter	Krefeld, Germany
Vortexer MS1 Minishaker	IKA-Labortechnik	Staufen, Germany
Water bath	GFL Gesellschaft für Labortechnik	Burgwedel, Germany
X-ray generator Isovolt Titan	GE Inspection Technologies	Frankfurt a.M., Germany

2.1.6 Kits and ELISAs

Table 6: List of kits and ELISAs

Material	Product number	Supplier	
CD45 (TIL) MicroBeads, mouse	130-110-618	Miltenyi Biotec	Bergisch Gladbach, Germany
DyNAmo ColorFlash SYBR Green qPCR Kit	F416XL	Thermo Fisher Scientific	Waltham, MA, USA
FoxP3 Staining Buffer Set	130-093-142	Miltenyi Biotec	Bergisch Gladbach, Germany
High-Capacity cDNA Reverse Transcription Kit	4368814	Thermo Fisher Scientific	Waltham, MA, USA
HMGB1 ELISA	ST51011	IBL International	Hamburg, Germany
Human/Mouse/Rat Total HSP70/HSPA1A ELISA	DYC1663	R&D Systems	Minneapolis, MN, USA
Mouse CXCL1/KC ELISA	DY453	R&D Systems	Minneapolis, MN, USA
Mouse Cytokine Array C3	AAM-CYT-3-8	RayBiotech	Peachtree Corners, GA, USA
Mouse IFN-β ELISA	DY8234	R&D Systems	Minneapolis, MN, USA
Mouse IGFBP-6 ELISA	DY776	R&D Systems	Minneapolis, MN, USA

MTT Cell Proliferation/Viability Assay	4890-025-K	R&D Systems	Minneapolis, MN, USA
Pierce BCA Protein Assay Kit	23225	Thermo Fisher Scientific	Waltham, MA, USA
Tumor Dissociation Kit, mouse	130-096-730	Miltenyi Biotec	Bergisch Gladbach, Germany
V-PLEX Proinflammatory Panel 1 Mouse Kit	K15048D-1	Meso Scale Diagnostics	Rockville, MD, USA

2.1.7 Animals

Table 7: List of mouse strains

Strain	Supplier	
BALB/cJRj	Janvier Labs	Le Genest-Saint-Isle, France
C57Bl/6NRj	Janvier Labs	Le Genest-Saint-Isle, France

2.1.8 Software

Table 8: List of analysis softwares

Software	Supplier	
CFX Manager Software 3.1	Bio-Rad Laboratories	Hercules, CA, USA
CytExpert Acquisition and Analysis Software 2.3	Beckman Coulter	Brea, CA, USA
EndNote X9	Clarivate Analytics	Philadelphia, PA, USA
Gen5 3.0	BioTek	Bad Friedrichshall, Germany
GraphPad Prism 8	GraphPad Software	La Jolla, CA, USA
iBright Analysis Software	Thermo Fisher Scientific	Waltham, MA, USA
Kaluza 2.1	Beckman Coulter	Brea, CA, USA
Microsoft Office Professional Plus 2010	Microsoft Corporation	Redmond, WA, USA
RAYBIO Analysis Tool	RayBiotech	Peachtree Corners, GA, USA

2.1.9 Flow cytometry antibodies and dyes

Table 9: List of flow cytometry antibodies and dyes

Target antigen	Fluorochrome	Product number	Supplier	
4-1BBL	VioBright-FITC	130-105-857	Miltenyi Biotec	Bergisch Gladbach, Germany
CD11b	APC	17-0112	eBioscience	San Diego, CA, USA
CD11c	BV 510	562949	BD	Franklin Lakes, NJ, USA
CD16/32	purified	14-0161-86	eBioscience	San Diego, CA, USA
CD19	APC-Cy7	561737	BD	Franklin Lakes, NJ, USA
CD25	PE-Cy7	552880	BD	Franklin Lakes, NJ, USA
CD3e	V450	560801	BD	Franklin Lakes, NJ, USA
CD4	FITC	553729	BD	Franklin Lakes, NJ, USA
CD45.2	PerCP-Cy5.5	45-0454	eBioscience	San Diego, CA, USA
CD49b	APC	108910	BioLegend	San Diego, CA, USA
CD62L	PE-Cy7	560516	BD	Franklin Lakes, NJ, USA
CD70	PE	12-0701	eBioscience	San Diego, CA, USA
CD8a	BV 605	100744	BioLegend	San Diego, CA, USA
FcεR1α	PE	134308	BioLegend	San Diego, CA, USA
FoxP3	APC	130-093-013	Miltenyi Biotec	Bergisch Gladbach, Germany
Galectin-9	BV421	566028	BD	Franklin Lakes, NJ, USA

HVEM	APC	136305	BioLegend	San Diego, CA, USA
ICOS-L	PE	107405	BioLegend	San Diego, CA, USA
Live/dead	Zombie NIR	423106	BioLegend	San Diego, CA, USA
Live/dead	Zombie Aqua	423102	BioLegend	San Diego, CA, USA
Ly-6C	FITC	553104	BD	Franklin Lakes, NJ, USA
Ly-6G	PE-Cy7	560601	BD	Franklin Lakes, NJ, USA
MHC-II (I-A/I-E)	eFluor 450	48-5321	eBioscience	San Diego, CA, USA
OX40L	PerCP-eFluor710	46-5905-80	eBioscience	San Diego, CA, USA
PD-1	PE-Dazzle 594	109116	BioLegend	San Diego, CA, USA
PDCA-1	BV 650	127019	BioLegend	San Diego, CA, USA
PD-L1	PE-Cy7	25-5982	eBioscience	San Diego, CA, USA
PD-L2	APC	107210	BioLegend	San Diego, CA, USA
Siglec-F	PE	552126	BD	Franklin Lakes, NJ, USA
γδTCR	PE	12-5711-82	eBioscience	San Diego, CA, USA

2.1.10 qPCR primers

Table 10: List of Bio-Rad Prime PCR Primers

Gene symbol	Gene name	Assay ID
Cd274	CD274 antigen (PD-L1)	qMmuCID0011907
Cxcl1	chemokine (C-X-C motif) ligand 1	qMmuCED0047655
E330016A19Rik	RIKEN cDNA E330016A19 gene (cGAS)	qMmuCID0025813
Hprt	hypoxanthine guanine phosphoribosyl transferase	qMmuCED0045738
Ifnb1	interferon beta 1	qMmuCED0050444
Igf1r	Insulin-like growth factor I receptor	qMmuCID0005315
Igf2	insulin-like growth factor 2	qMmuCED0025029
Igf2r	Insulin-like growth factor II receptor	qMmuCED0046384
Igfbp6	Insulin-like growth factor binding protein 6	qMmuCID0006112
Pdcd1lg2	programmed cell death 1 ligand 2 (PD-L2)	qMmuCID0011922
Rps18	ribosomal protein S18	qMmuCED0045430
Tbp	TATA box binding protein	qMmuCID0040542
Tmem173	transmembrane protein 173 (STING)	qMmuCED0046127
Trex1	three prime repair exonuclease 1	qMmuCED0061616

2.1.11 Buffer, media and staining solutions:

Cell culture medium R10-:

- RPMI 1640
- 10 % fetal bovine serum

Permeabilization buffer (cell cycle):

- 192 ml 0.2 M Na_2HPO_4 (in H_2O)
- 8 ml 0.1 X (v/v) Triton X-100 (in H_2O)
- pH 7.8

DNA staining buffer:

- 5 µl PI (1 mg/ml in H_2O))
- 20 µl RNase (200 µg/ml in PBS)
- Ad 1 ml PBS

Cell death staining solution

- 1 ml Ringer's solution
- 1 µl Propidium Iodide (1 mg/ml)
- 0.75 µl AnnexinV-FITC (1 mg/ml)

MACS buffer:

- PBS
- BSA stock solution 1:20

Tumor lysis buffer:

- 2X Lysis Buffer
- 1:1 H_2O
- 1:30 Antifoam Y-30 Emulsion
- 1:100 HALT phosphatase inhibitor
- 1:100 PMSF protease inhibitor (0.1 M in 99 % EtOH)
- 1:1000 Sodium fluoride (1 M in H_2O)
- 1:1000 ß-Glycerophosphate (1 M in H_2O)
- 1:1000 Sodium orthovanadate (0.2 M in H_2O)

PBS (10X):

- H_2O
- Sodium chloride (1.37 M)
- Potassium chloride (27 mM)
- Sodium phosphate dibasic (100 mM)
- Monopotassium phosphate (18 mM)
- pH 7.4

PBS-T:

- H_2O
- PBS (10X) 1:10
- 0.05 % Tween 20

Reagent diluent (ELISA):

- PBS
- 1 % BSA
- pH 7.2-7.4

FACS buffer:

- PBS
- 2 % fetal bovine serum
- 2 mM EDTA

Fc-block solution:

- FACS buffer
- Anti-CD16/32 antibody 1:100

Immune checkpoint panel 1:

Table 11: Antibodies and dyes of immune checkpoint panel 1

Target antigen	Fluorochrome	Dilution
PD-L1	PE-Cy7	1:1600
PD-L2	APC	1:100
OX40L	PerCP-eFluor710	1:800
ICOS-L	PE	1:200
Live/dead	Zombie Aqua	1:500
		in FACS buffer

Immune checkpoint panel 2:

Table 12: Antibodies and dyes of immune checkpoint panel 2

Target antigen	Fluorochrome	Dilution
4-1BBL	VioBright-FITC	1:10
Galectin-9	BV421	1:100
HVEM	APC	1:800
CD70	PE	1:200
Live/dead	Zombie Yellow	1:250
		in FACS buffer

Immune phenotyping panel 1 (IPP1):

Table 13: Antibodies and dyes of immune phenotyping panel 1

Target antigen	Fluorochrome	Dilution
Live/dead	Zombie NIR	1:1000
MHC-II (I-A/I-E)	eFluor 450	1:1000
Ly-6G	PE-Cy7	1:1000
Ly-6C	FITC	1:800
CD11b	APC	1:500
Siglec-F	PE	1:500
CD45.2	PerCP-Cy5.5	1:400
PDCA-1	BV 650	1:250
CD11c	BV 510	1:250
		in FACS buffer

Immune phenotyping panel 2 (IPP2):

Table 14: Antibodies and dyes of immune phenotyping panel 2

Target antigen	Fluorochrome	Dilution
CD62L	PE-Cy7	1:1000
CD8a	BV 605	1:1000
FcεR1α	PE	1:1000
Live/dead	Zombie Aqua	1:500
CD4	FITC	1:500
CD19	APC-Cy7	1:500
CD3e	V450	1:500
CD45.2	PerCP-Cy5.5	1:400
CD49b	APC	1:400
PD-1	PE-Dazzle 594	1:250
		in FACS buffer

Immune phenotyping panel 3 (IPP3):

Table 15: Antibodies and dyes of immune phenotyping panel 3

Target antigen	Fluorochrome	Dilution
Live/dead	Zombie NIR	1:1000
CD8a	BV 605	1:1000
CD4	FITC	1:500
CD3e	V450	1:500
γδTCR	PE	1:400
CD45.2	PerCP-Cy5.5	1:400
CD25	PE-Cy7	1:200
FoxP3	APC	1:40
		in FACS buffer

2.2 Methods

2.2.1 Cell lines and cell culture

Commercially available murine B16-F10 melanoma cell derived from C57Bl/6 mice and CT26 colon carcinoma cells derived from BALB/c mice (both cell lines from ATCC) were cultured in RPMI 1640 supplemented with 10 % fetal bovine serum without addition of any antibiotics (R10-medium) in T75 or T175 flasks under standard conditions in an incubator with 37 °C, 95 % humidity, 5 % CO_2.The cell lines were tested negatively for mycoplasma contamination and were stored in a cell bank format. A new vial of cells was thawed for each *in vivo* experiment or set of *in vitro* experiments and the cells were regularly passaged with Trypsin twice a week for a maximum of ten passages.

2.2.2 High hydrostatic pressure (HHP) treatment

For the preparation of the whole tumor cell vaccine adherent tumor cells were detached with Accutase to obtain single cell suspensions. To get rid of any medium and serum the cells were washed with PBS and resuspended in Ringer solution at a concentration of $25x10^6$ cells/ml. Cryogenic vials were completely filled with cell suspension to avoid any air bubbles, tightly closed and additionally sealed with Parafilm. The vials were put in the autoclave (Figure 4C) of the computer-controlled HHP treatment system (Figure 4A, B) which was provided by the "*Lehrstuhl für Prozessmaschinen und Anlagentechnik*" (iPAT, Friedrich-Alexander-Universität Erlangen-Nürnberg). The high hydrostatic pressure treatment of the vials with tumor cells was conducted with a pressure build-up velocity of 50 MPa/s and a final pressure of 100 to 500 MPa for 300 s. Autoclaved water was used as pressure transmitting medium. Before using the pressurized tumor cells for *in vitro* experiments or as a vaccine *in vivo* they were incubated for 24 h in the incubator without changing the medium to avoid the loss of any released DAMPs.

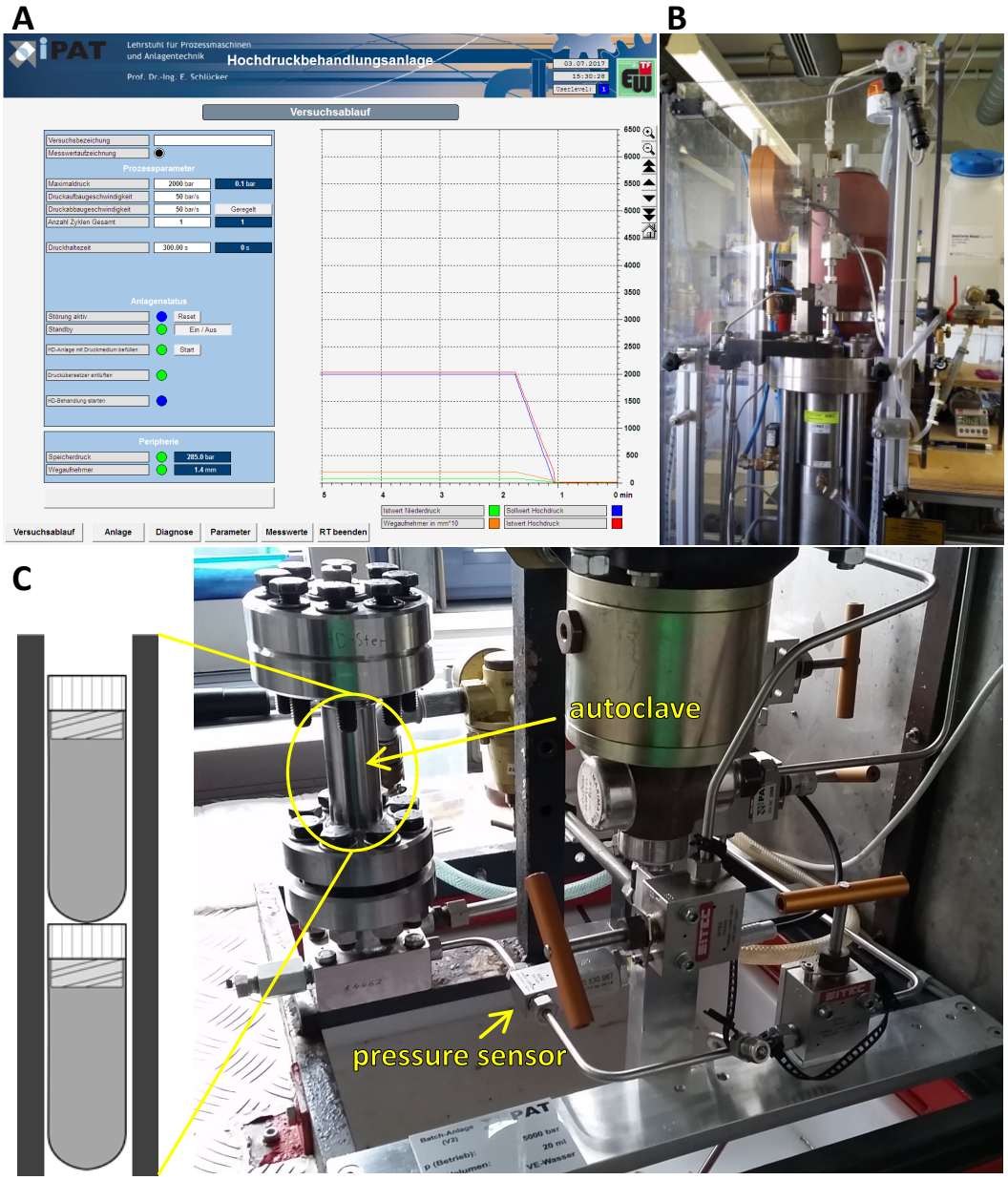

Figure 4: High hydrostatic pressure treatment. The device was kindly provided by the "*Lehrstuhl für Prozessmaschinen und Anlagentechnik*" (iPAT, Friedrich-Alexander-Universität Erlangen-Nürnberg). A: fully computer monitored treatment process; B: hydraulic system; C: cryogenic vial containing autoclave and pressure sensor.

2.2.3 Animal experiments

For all animal experiments male wildtype C57Bl/6 or BALB/c mice were ordered from Janvier and were kept at the Präklinisches Experimentelles Tierzentrum animal facility of the Friedrich-Alexander-Universität Erlangen-Nürnberg. At the age of six to eight weeks the mice were used for the experiments. All experiments were approved by the government of Unterfranken and conducted according to the guidelines of the "Federation of European Laboratroy Animal Science Associations" (FELASA) and the "Gesellschaft für Versuchstierkunde" (GV-SOLAS).

2.2.3.1 Tumorigenicity of HHP treated cells

To test for the ability of HHP treated (0-500 MPa) tumor cells to form tumors *in vivo* $2x10^6$ B16 tumor cells in Ringer solution were injected subcutaneously in C57Bl/6 mice. The mice were observed for 39 days to detect any subsequent tumor growth.

2.2.3.2 Radioimmunotherapy combinations

For the investigation of radio-immunotherapy combinations ectopic B16-F10 melanoma and CT26 colon carcinoma models were established in syngeneic mice. In all *in vivo* vaccination approaches with the HHP generated whole tumor cell vaccine the tumor cells were prepared with a pressure of 200 MPa as described above (2.2.2 High hydrostatic pressure (HHP) treatment).

Single tumor model:

In the experiments with a single tumor $1x10^6$ viable B16-F10 or $1.2x10^6$ CT26 tumor cells in Ringer solution were subcutaneously injected into the previously shaved right flank of C57Bl/6 or BALB/c mice, respectively. The treatment of the tumors started when palpable, vascularized tumors had formed after eight (B16) or 14 days (CT26). The local irradiation of the tumors with X-rays at the PRIMART linear accelerator (Figure 5A) was performed as previously published (Werthmöller et al., 2016). The mice were positioned in the irradiation field in a plexiglas box with isoflurane anesthesia (Figure 5B) and irradiated tangentially in a 20° angle to completely irradiate the tumor and at the same time sparing as much surrounding tissue as possible. The tumors were irradiated with a dose of 5 Gy per fraction on days 0 and 2 of the treatment period or were left untreated. Half of the irradiated or untreated mice were additionally vaccinated subcutaneously with $5x10^6$ HHP treated tumor cells (200 µl) next to the tumor on day 3. Tumor and blood samples were collected from some animals on day 7 for immune phenotyping.

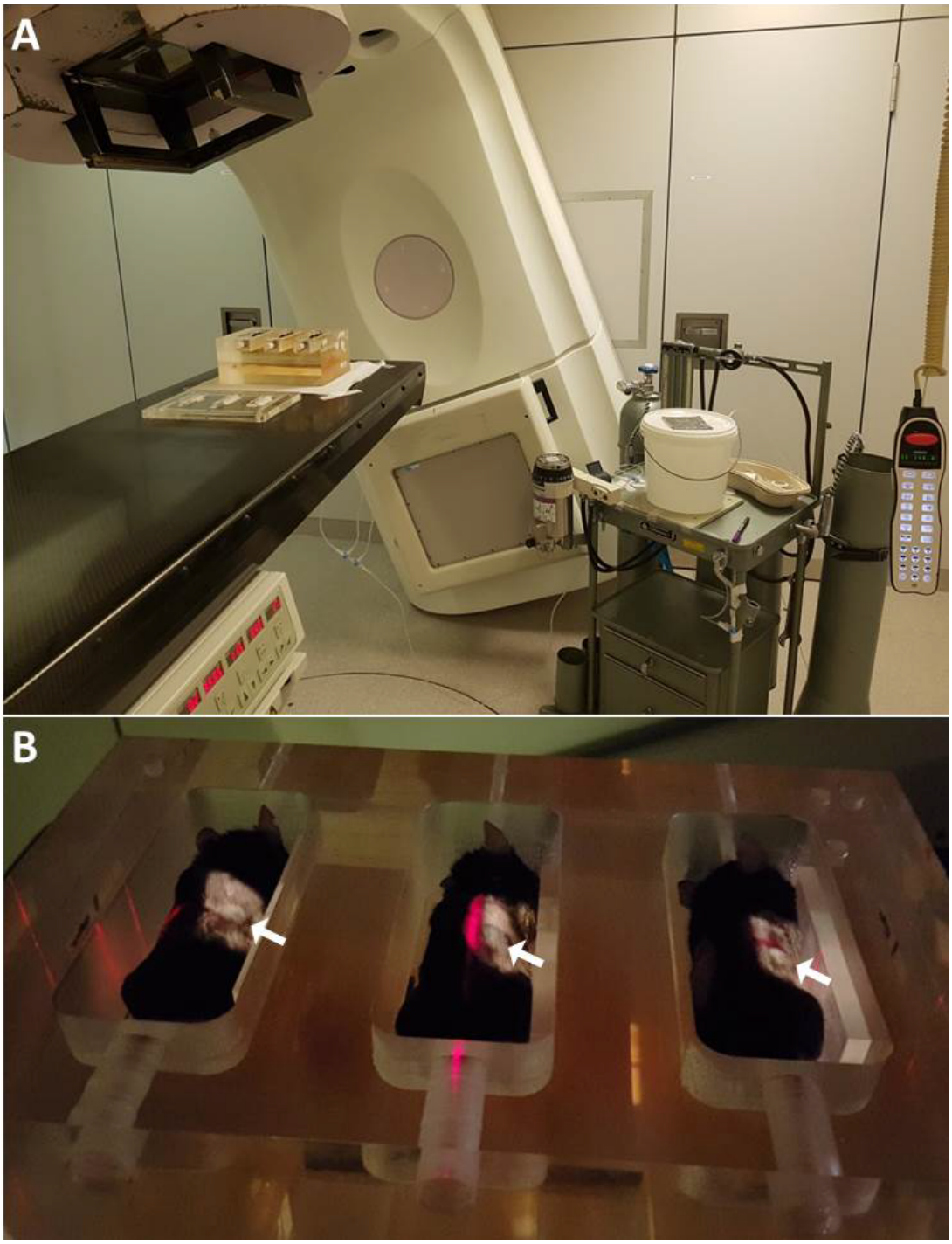

Figure 5: Animal irradiation set-up. A: PRIMART linear accelerator with anesthesia device and mouse irradiation box; B: mice in the irradiation box with their tumor positioned in the irradiation field (indicated by white arrows) for the local irradiation.

Abscopal tumor model:

For the investigation of systemic immune responses of radioimmunotherapies an abscopal tumor models was established. $0.2x10^6$ B16-F10 tumor cells in 200 µl Ringer's solution were injected subcutaneously into the previously shaved right flank of C57Bl/6 mice. Four days afterwards a second tumor was injected the same way on the left flank which later served as the non-irradiated abscopal

tumor. The following describes the maximum triple treatment whereas some groups were only received some of the treatment modalities. Only the first injected primary right flank tumor was irradiated after seven days (d0) as described in the single tumor model with 8 Gy. On day 3 (2x8 Gy experiments) or on days 1 and 3 (3x8 Gy experiments) the mice received another dose of 8 Gy. Beginning with the first irradiation on d0 the mice were intraperitoneally injected with 200 µg anti-PD-1 antibody (αPD-1) dissolved in 200 µl PBS every three to four days for a total of four injections. Additionally, HHP vaccine ($5x10^6$ cells, 200 µl) was injected twice subcutaneously into the shaved neck on days 2 and 8. Tumor and blood samples were collected from some animals on day 8 for cytokine analyses and on day 10 for immune phenotyping.

2.2.3.3 IGFBP-6 siRNA knockdown in vivo

The *in vivo* siRNA knockdown of IGFBP-6 in abscopal tumors was conducted in mice treated with αPD-1 and 2x8 Gy as described in the abscopal tumor model (2.2.3.2 Radioimmunotherapy combinations). Additionally, Igfbp-6 siRNA (2.5 nmol) was formulated with Invivofectamine 3.0 Reagent in a total volume of 40 µl according to the manufacturer's protocol and injected intratumorally only into the abscopal tumor on days 0, 4 and 8. Negative control siRNA and PBS without Invivofectamine 3.0 Reagent served as control groups. To check for successful knockdown of IGFBP-6 three mice of each group were sacrificed on day 4 to collect serum and abscopal tumors for an IGFBP-6 ELISA.

During and after the treatment in all *in vivo* experiments the tumor growth of the mice was examined. The tumor volume was calculated with the formula (length x $width^2$)/2. Once one of the tumors exceeded a volume of 1500 mm^3 the mice were sacrificed due to ethical reasons.

2.2.4 In vitro experiments

2.2.4.1 Clonogenicity of HHP treated cells

To test the ability of HHP treated cells (0-500 MPa) to form colonies *in vitro* they were seeded at various concentrations in triplicates in petri dishes and cultivated for 10 days. The cells were stained with methylene blue and colonies consisting of more than 50 cells were counted.

2.2.4.2 In vitro irradiation experiments

For the investigation of the influence of different fractionations on tumor cells the amount of cells indicated in Table 16 was seeded in two T75 flasks per treatment in 20 ml R10- medium 16 h before the experiment.

Table 16: Amount of cells seeded for *in vitro* irradiation experiments

Treatment	Amount of seeded cells
Untreated	$1.8x10^4$
1x8 Gy	$4.5x10^4$
2x8 Gy	$4x10^5$
3x8 Gy	$7x10^5$
1x20 Gy	$5x10^4$

For *in vitro* experiments the cells were irradiated with X-rays using an X-ray tube in a lead shielding chamber. The 2x8 Gy treatment group was irradiated on d0 and d3, the 3x8 Gy group on d0, d1 and d3. The single dose treatment groups (1x8 Gy, 1x20 Gy) were irradiated on d3 only and one group was left untreated. On d4 24 h after the last irradiation the cells of one flaks including the dead cells were detached with Accutase and used for subsequent flow cytometric analysis. Cell-free supernatant was collected from the other flask before detaching the cells with Accutase as well. Those cells were resuspended in TriFast for qPCR analysis.

2.2.4.3 Incubation of tumor cells with IGFBP-6

The influence of IGFBP-6 on B16 tumor cell proliferation and viability was analyzed using a MTT assay. For this, 1,700 (48 h) or 6,800 (24 h) B16 cells were seeded in 50 µl R10- in a 96 well plate and 50 µl R10- containing IGFBP-6 recombinant mouse protein in a final concentration of 0.1, 0.5 or 1 µg/ml were added. After 24 h or 48 h the MTT assay was performed according to the manufacturer's protocol. The OD at 570 nm and 700 nm as reference wavelength was recorded with an Epoch Microplate Spectrophotometer.

2.2.4.4 IGFBP-6 siRNA knockdown in vitro

To investigate the effects of IGFBP-6 knockdown on tumor cell proliferation, viability and cell cycle a siRNA mediated knockdown approach via lipofection was used. $5x10^4$ B16 cells per well were seeded in 2.25 ml R10- in 6 well plates. A final concentration of 10 nM Igfbp-6 or negative control siRNA was formulated with Lipofectamine RNAiMAX Transfection Reagent in Opti-MEM medium according to the protocol provided by the manufacturer. Lipofectamine without any siRNA and pure medium served as controls. 250 µl per well of these solutions were added to the tumor cells. After 48 h in the incubator the cells were harvested for flow cytometric cell death and cell cycle analyses. Additionally, cells were lysed with 1 ml TriFast for subsequent confirmation of the siRNA knockdown via qPCR analysis.

2.2.5 Flow cytometric analyses

2.2.5.1 Cell death analysis

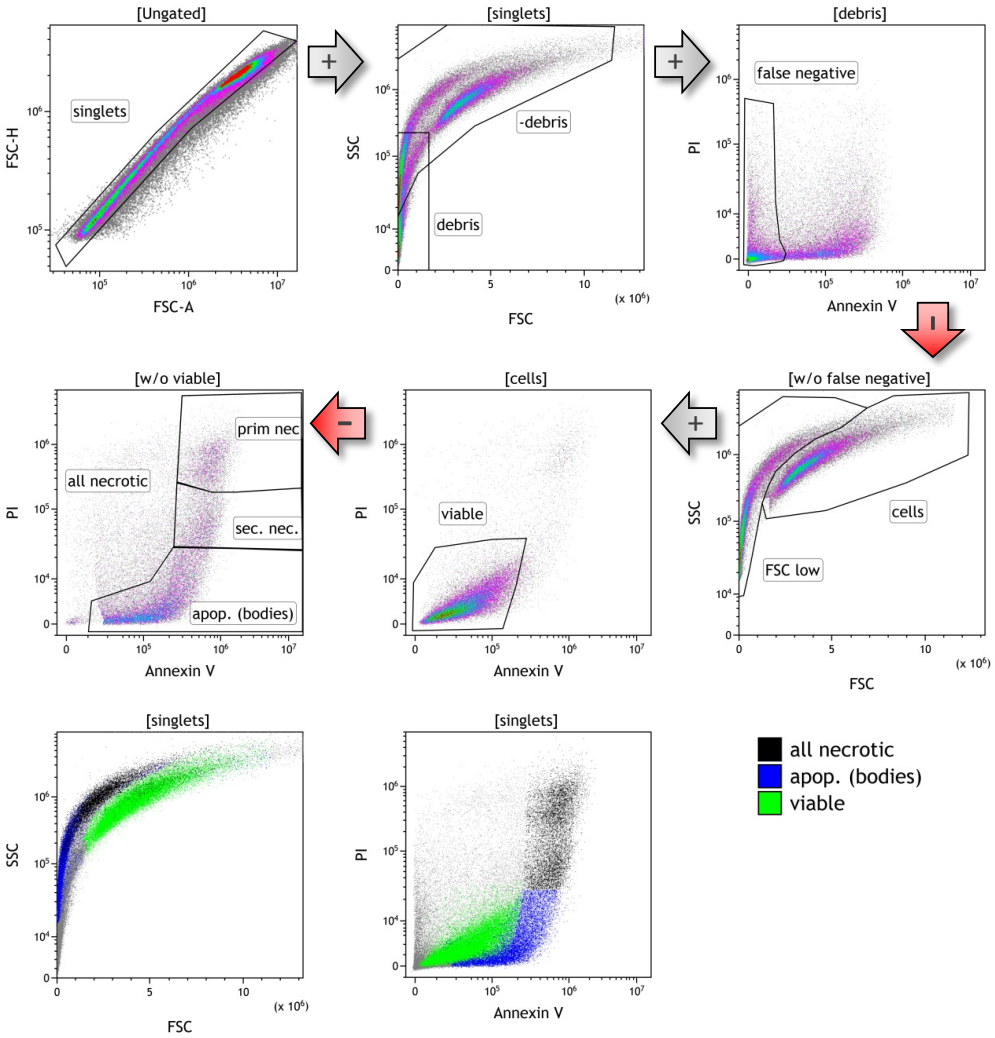

Figure 6: Gating strategy for the AxV, PI cell death analysis. Doublets were excluded by plotting FSC-A against FSC-H. In the FSC/SSC plot debris was selected and then excluded with a Boolean gate as false negative AxV^-, PI^- events for further analysis. Viable cells were determined based on their morphological properties and in the AxV/PI plot as double negative events. In another AxV/PI plot cleared from viable cells by Boolean gating apoptotic (AxV^+, PI^-) and necrotic cells (primary necrotic AxV^+, PI^{hi}; secondary necrotic AxV^+, PI^{med}) were selected. Backgating of viable, apoptotic and necrotic cells is displayed in the FSC/SSC and AxV/PI plot. Grey arrows with a "+" indicate subgating of the previous population. The exclusion of the previously gated population from further analysis by Boolean gating is indicated by red arrows with a "-".

Apoptotic and necrotic cell death of tumor cells was determined via flow cytometry. The staining was performed with FITC-labeled AnnexinA5 (AxV) and propidium iodide (PI). $0.2x10^6$ tumor cells were resuspended in 100 µl of cell death staining solution (1 µl PI and 0.75 µl AxV-FITC per 1 ml Ringer solution). After incubation for 30 min at 4 °C the cells were analyzed with a CytoFLEX S flow cytometer. AxV binds to phosphatidylserine (PS) which is actively translocated to the inner side of the plasma membrane in viable cells. If cells undergo apoptosis or necrosis this asymmetry in the plasma membrane cannot be maintained any longer and PS is accessible for AxV on the outside of the cell. In apoptotic cells the membrane integrity is preserved and therefore apoptotic and necrotic

cells can be distinguished with the DNA intercalating membrane impermeable PI. Thus, AxV^-, PI^- cells are defined as viable, AxV^+, PI^- as apoptotic and AxV^+, PI^+ as necrotic. The gating in the Kaluza analysis software (Figure 6) was done as follows: single cells were determined by FSC-A/FSC-H doublet exclusion. After gating on debris in the FSC/SSC plot false negative AxV-, PI^- events were excluded with a Boolean gate. Viable cells were gathered by first selecting them on their morphological properties in the FSC/SSC plot and then gating on AxV^-, PI^- events. Apoptotic cells, apoptotic bodies and necrotic cells were determined in the viable cell-excluded AxV/PI plot. In the final analysis primary and secondary necrotic cells were combined and depicted as necrotic cells in total.

2.2.5.2 Cell cycle analysis

For cell cycle analysis 900 µl ethanol (70 %, -20 °C) was added to $0.4x10^6$ tumor cells resuspended in 100 µl PBS. After incubation of at least 20 min at -20 °C the cells were centrifuged at 300 x g at room temperature. The pellet was resuspended in 500 µl PBS and the cells were permeabilized by adding 500 µl permeabilization buffer for 5 min. After centrifugation the cell pellet was resuspended in 500 µl DNA staining solution containing PI and RNase and was then incubated for 30 min at room temperature in the dark. At least $0.2x10^6$ cells were analyzed with a CytoFLEX S flow cytometer. The gating in the Kaluza analysis software (Figure 7) was done as follows: doublets were excluded by plotting PI-A against PI-H and debris was excluded based on FSC/SSC properties. G1- S- and G2/M-phases were gated based on the DNA content (PI staining intensity). Degraded DNA of dying tumor cells below G1 phase was labeled sub-G1.

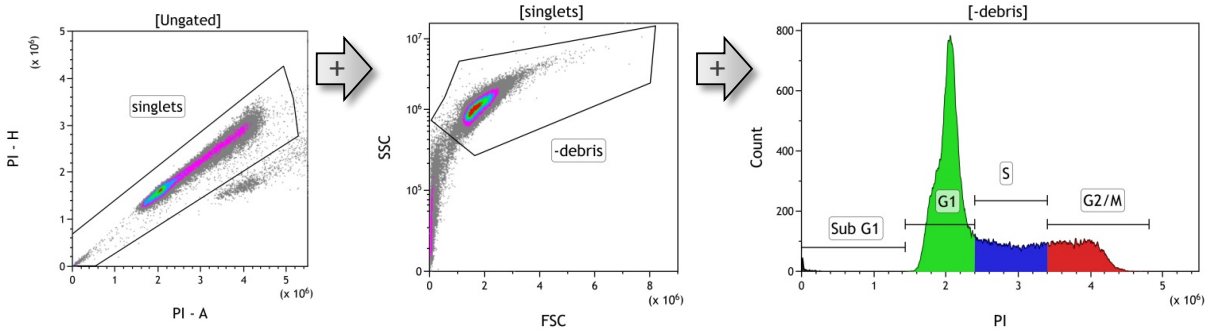

Figure 7: Gating strategy of the cell cycle analysis. Doublets were excluded by plotting PI-A against PI-H and debris in the FSC/SSC plot. G1-, S- and G2/M-phases were gated based on the DNA content (PI staining intensity). Everything below G1-phase was regarded as sub-G1. Grey arrows with a "+" indicate subgating of the previous population.

2.2.5.3 Immune checkpoint ligands

The surface expression of immune checkpoint ligands on tumor cells was analyzed by flow cytometry. For this, 4x 0.2x10^6 cells were resuspended in 50 µl Fc-block solution in a 96-well V-bottom plate and incubated for 10 min at room temperature to block unspecific binding of staining antibodies. After centrifugation at 400 x g for 4 min the supernatant was discarded, the cells were resuspended in 50 µl antibody mix of "checkpoint panel 1", "checkpoint panel 2", or the respective autofluorescence control (AF ctrl) mix only containing the viable/dead stain and incubated for 30 min at 4 °C. The cells were then washed two times with FACS buffer and analyzed with a CytoFLEX S flow cytometer. The gating in the Kaluza analysis software (Figure 8) was done as follows: in the pre-gating doublets (FSC-A/FSC-H) and dead cells (FSC/SSC) were excluded. Additionally, it was gated on viable cells based on a viable/dead stain. As irradiated tumor cells tend to have a higher autofluorescence (AF) than untreated cells the median fluorescence intensity (MFI) of each immune checkpoint ligand in the stained sample was corrected for this background with the AF ctrl. Thus, the ΔMFI was calculated by subtracting the MFI of the AF ctrl from the MFI of the stained sample.

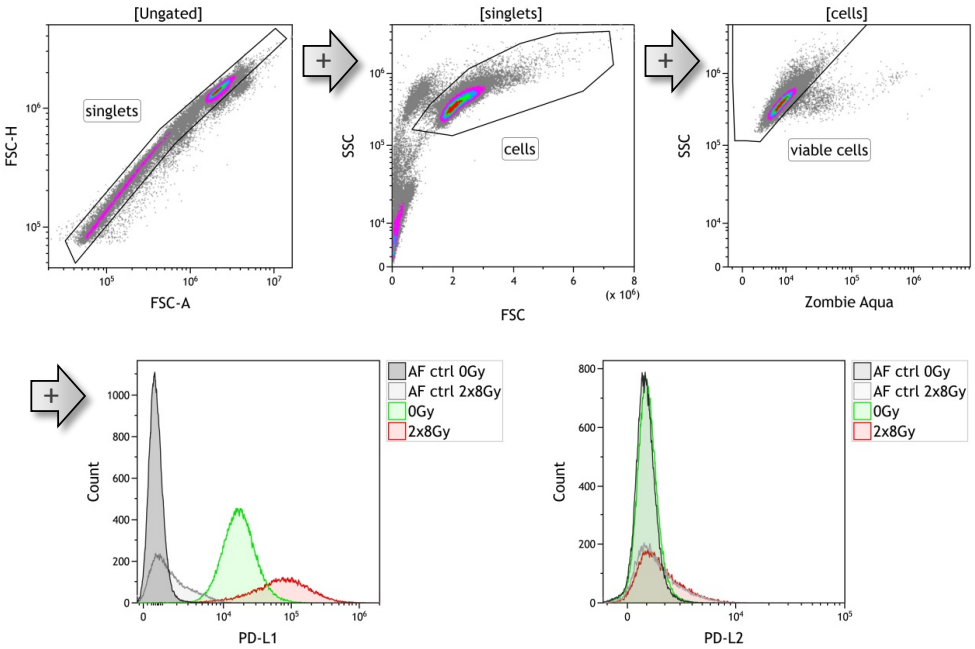

Figure 8: Gating strategy of the immune checkpoint analysis. After pre-gating on singlets (FSC-A/FSC-H) and viable cells based on morphological properties (FSC/SSC) and live/dead stain (Zombie Aqua$^-$), the median fluorescence intensity (MFI) of each checkpoint ligand was analyzed. To correct for a higher autofluorescence of irradiated tumor cells the MFI of each stained sample was subtracted by the MFI of the same sample which was not stained for the checkpoint ligands (AF ctrl). PD-L1 and PD-L2 analysis is shown exemplarily for all immune checkpoints. Grey arrows with a "+" indicate subgating of the previous population.

2.2.5.4 Immune phenotyping of blood and tumor infiltrating immune cells

Leukocyte subtypes infiltrating into tumors after radioimmunotherapy combinations and in the peripheral blood were analyzed on day 10 of the treatment period. First, blood was drawn from the retro-orbital sinus of isoflurane anesthetized mice with a hematocrit capillary. Part of it was collected in Microtainer serum tubes to obtain serum by centrifugation at 10,000 x g for 2 min. The mice were then sacrificed by cervical dislocation and the tumors were excised. The tumors were weighed before dissociation with the tumor dissociation kit (Miltenyi) according to the manufacturer's instructions in gentleMACS C tubes on a gentleMACS dissociator. The tumor mass was filtered through a 70 µm cell strainer, washed with RPMI and resuspended in MACS buffer. The volume corresponding to up to 0.3 g of tumor was centrifuged (300 x g, 5 min) and resuspended in 270 µl MACS buffer. To isolate immune cells from the multitude of tumor cells by MACS separation 45 µl of CD45 (TIL) MicroBeads were added to the cell suspension. Following steps were performed according to the manufacturer's instructions. The flow through, predominantly containing tumor cells, was collected and the cells were stored in TriFast for further analyses. The eluted immune cell fraction was equally distributed to three wells of a 96 well plate for the immune phenotyping. For the immune phenotyping of the blood erythrocytes of 100 µl whole blood were lysed using a TQ-Prep Workstation. After one washing step with PBS the cells were equally distributed to three wells of a 96 well plate, as well. Both, tumor and blood samples were resuspended in 50 µl Fc-block solution and incubated for 10 min at room temperature to block unspecific binding of staining antibodies. After centrifugation at 400 x g for 4 min the supernatant was discarded, the cells were resuspended in 50 µl antibody mix of "immune phenotyping panel 1" (IPP1), IPP2, or IPP3 (without the FoxP3 antibody) and incubated for 30 min at 4 °C. The cells stained with IPP1&2were then washed two times with FACS buffer and analyzed with a CytoFLEX S flow cytometer. For the intracellular staining of IPP3 for FoxP3 the cells were fixed and permeabilized using the FoxP3 staining buffer set according to the manufacturer's instructions. After the staining for 30 min at 4 °C and one washing step with FACS buffer these samples were also analyzed with the CytoFLEX S flow cytometer.

The gating of IPP1 in the Kaluza analysis software (Figure 9) was done as follows: after pre-gating on singlets (FSC-A/FSC-H) and viable cells (FSC/SSC, Zombie$^-$) all immune cells were gated as CD45$^+$. Neutrophils (CD11b$^+$, Ly6G$^+$) and plasmacytoid dendritic cells (pDCs; PDCA-1$^+$, Ly6C$^+$) were identified and excluded from further analysis by Boolean gating. Eosinophils (CD11b$^+$, Siglec-F$^+$) were pre-gated on CD45$^+$, SSC^{hi} and also excluded from further analysis. DCs (MHC-II$^+$, CD11c$^+$) were excluded from monocytes/macrophages (CD11b$^+$, Ly6C$^+$) gating and vice versa. DCs were further subdivided in conventional typ 1 DCs (cDC1; CD11b$^-$, SSC^{lo}) and cDC2 (CD11b$^+$, SSC^{hi}). In the monocyte/macrophage compartment monocytes (MHC-II$^-$, Ly6C$^+$) were distinguished from mature

tumor associated macrophages (mTAMs; MHC-II$^+$, Ly6C$^+$) and immature TAMs (Ly6C$^-$) (Etzerodt et al., 2019).

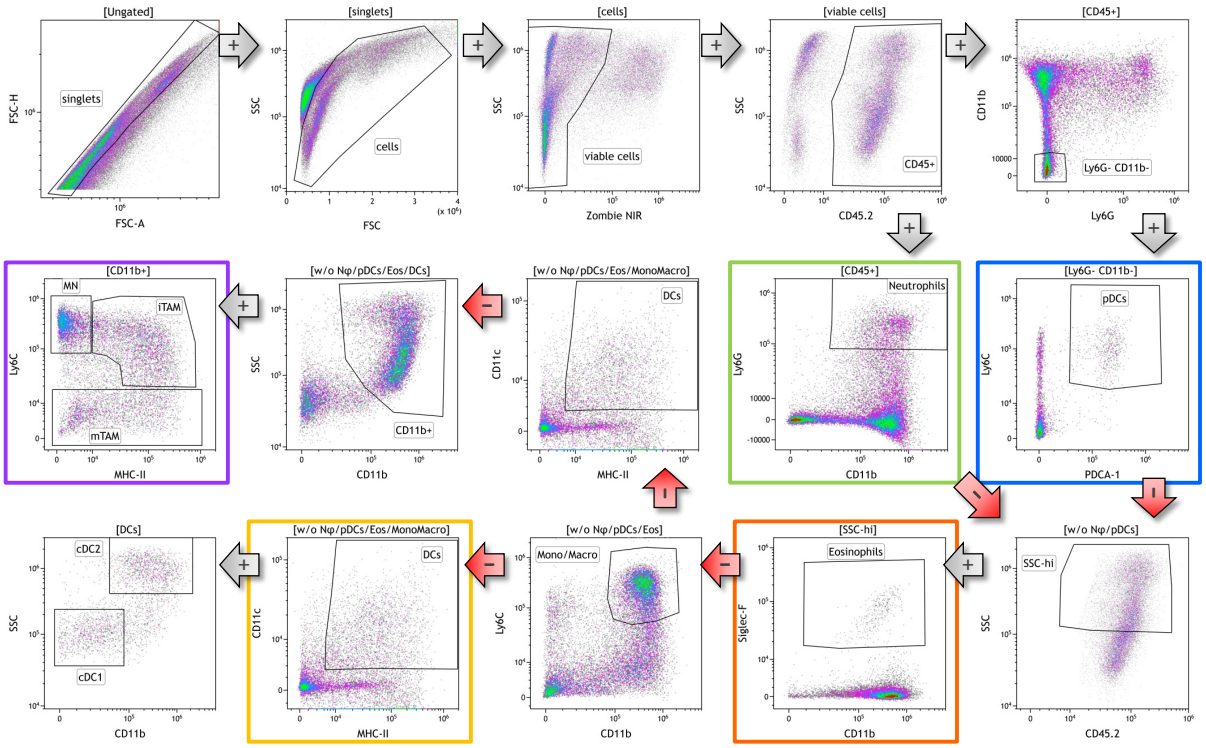

Figure 9: Gating strategy of the immune phenotyping panel 1. After pre-gating on single (FSC-A/FSC-H) viable cells (FSC/SSC, Zombie$^-$) all immune cells were gated as CD45$^+$. Ly6G$^-$, CD11b$^-$ plasmacytoid dendritic cells (pDCs) were identified as Ly6C$^+$, PDCA-1$^+$. Neutrophils were gated as CD11b$^+$, Ly6G$^+$, Eosinophils as SSC^{hi}, CD11b$^+$, Siglec-F$^+$, DCs as MHC-II$^+$, CD11c$^+$ and subdivided in conventional type 1 DCs (cDC1s; CD11b$^-$, SSC^{lo}) and cDC2s (CD11b$^+$, SSC^{hi}). After pre-gating on CD11b$^+$ cells Monocytes (MN) were identified as MHC-II$^-$, Ly6C$^+$, immature tumor associated macrophages (iTAM) as MHC-II$^+$, Ly6C$^+$ and mature TAMs (mTAM) as Ly6C$^-$. Major subtypes are highlighted with colored frames. Grey arrows with a "+" indicate subgating of the previous population. The exclusion of the previously gated population from further analysis by Boolean gating is indicated by red arrows with a "-".

The gating of IPP2 in the Kaluza analysis software (Figure 10) was done as follows: the same pre-gating on single viable immune cells as for IPP1 was applied. First basophils (FcεR1α$^+$ CD49b$^+$) and then B cells (CD19$^+$) were identified and excluded from subsequent analysis. T cells (CD49b$^-$ CD3$^+$) were further subdivided in CD4$^+$ and CD8$^+$ T cells and analyzed for PD-1 and CD62L expression. NK cells were gated as CD49b$^+$ SSC^{lo} CD3$^-$ and NKT cells as CD49b$^+$ SSC^{lo} CD3$^+$.

The gating of IPP3 in the Kaluza analysis software (Figure 11) was done as follows: the same pre-gating on single viable immune cells as for IPP1 was applied. γδ T cells were identified as CD3$^+$ TCRγδ$^+$ and Tregs as CD3$^+$ CD4$^+$ CD25$^+$ FoxP3$^+$.

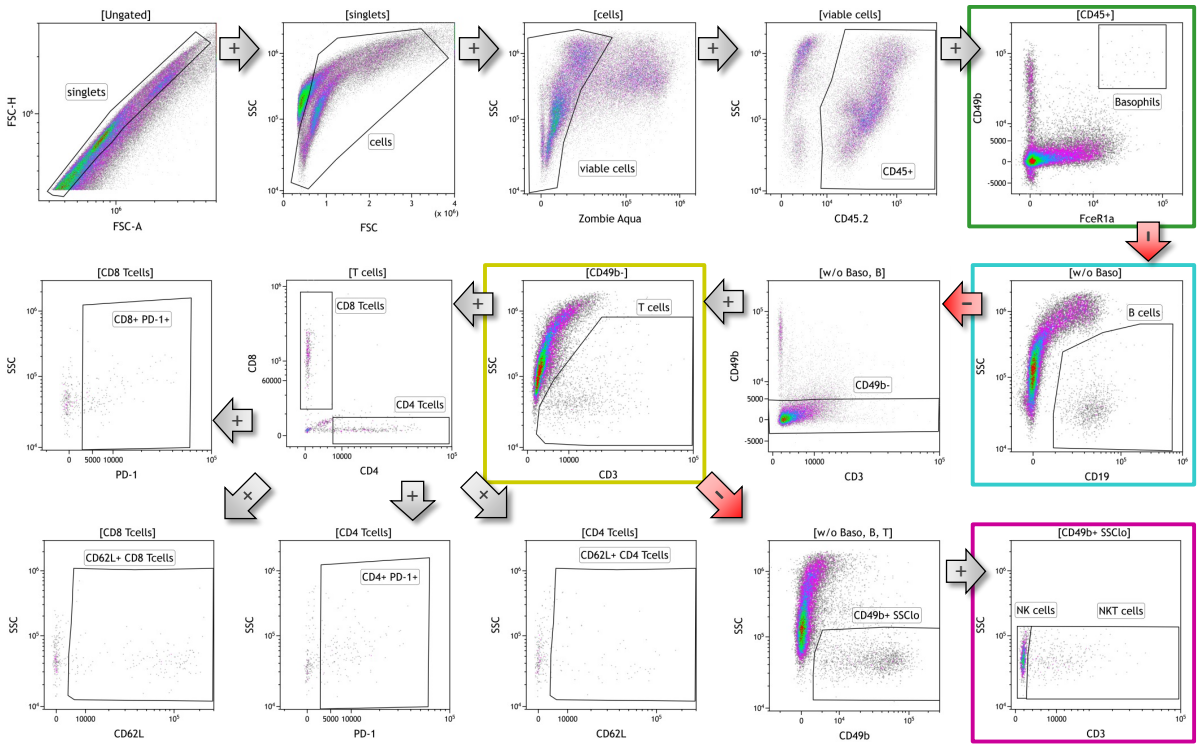

Figure 10: Gating strategy of the immune phenotyping panel 2. After pre-gating on single (FSC-A/FSC-H) viable cells (FSC/SSC, Zombie$^-$) all immune cells were gated as CD45$^+$. Basophils were identified as FcεR1α$^+$ CD49b$^+$, B cells as CD19$^+$, T cells as CD49b$^-$ CD3$^+$, NK cells as CD49b$^+$ SSC^{lo} CD3$^-$ and NKT cells as CD49b$^+$ SSC^{lo} CD3$^+$. T cells were further subdivided in CD4$^+$ and CD8$^+$ T cells and analyzed for PD-1 and CD62L expression. Major subtypes are highlighted with colored frames. Grey arrows with a "+" indicate subgating of the previous population. The exclusion of the previously gated population from further analysis by Boolean gating is indicated by red arrows with a "-".

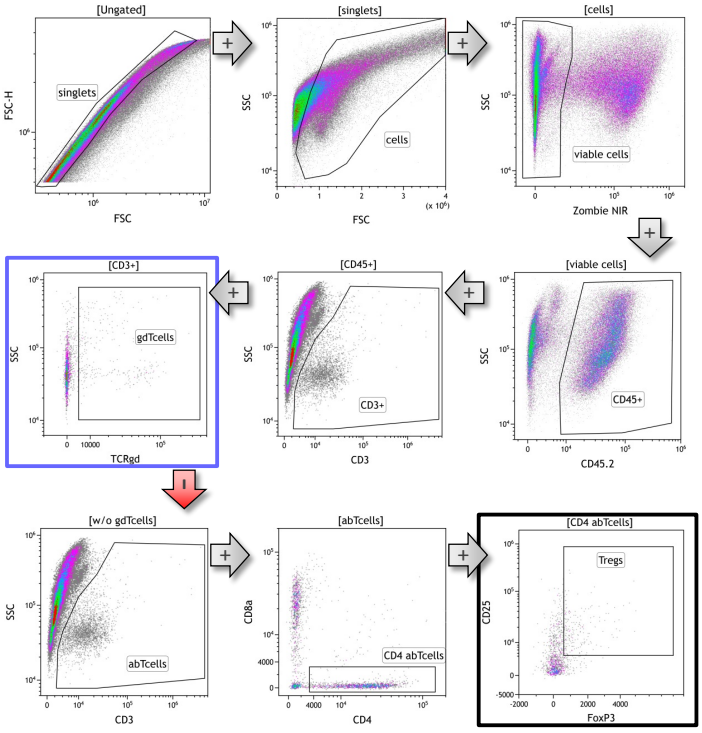

Figure 11: Gating strategy of the immune phenotyping panel 3. After pre-gating on single (FSC-A/FSC-H) viable cells (FSC/SSC, Zombie$^-$) all immune cells were gated as CD45$^+$. γδ T cells were identified as CD3$^+$ TCRγδ$^+$ and Tregs as CD3$^+$ CD4$^+$ CD25$^+$ FoxP3$^+$. Major subtypes are highlighted with colored frames. Grey arrows with a "+" indicate subgating of the previous population. The exclusion of the previously gated population from further analysis by Boolean gating is indicated by red arrows with a "-".

As one sample was evenly distributed to the three immune phenotyping panels the cell numbers were multiplied by 3 and divided by the tumor mass used for MACS cell separation to get concentrations of tumor infiltrating immune cells per gram of tumor.

2.2.6 Protein analyses

2.2.6.1 Preparation of tumor lysates

To prepare tumor lysates for protein analyses the tumors were excised and weighed. A volume of 2.5 ml tumor lysis buffer per 0.1 g of tumor was added in a gentleMACS M tube and the tumors were dissociated with a gentleMACS dissociator. After centrifugation (4,000 x g, 5 min) the supernatant was transferred into a new tube. To completely remove cell debris the lysate was centrifuged two more times at 12,000 x g for 5 min at 4 °C. The protein concentration was determined with the Pierce BCA Protein Assay Kit of a 1:10 dilution of the lysate according to the manufacturer's instructions.

2.2.6.2 Enzyme Linked Immunosorbent Assay (ELISA)

To examine cytokines in cell culture supernatants and tumor lysates the following ELISAs were performed according to the manufacturer's recommendations unless stated otherwise: HSP70 (supernatants, undiluted), HMGB1 (supernatants, undiluted), CXCL1 (supernatants, undiluted), IFN-β (supernatants, undiluted; tumor lysate, 100 µg total protein). The IGFBP-6 ELISA was performed for undiluted supernatant and serum. 100 µg total protein of the tumor lysates and the standard was diluted in 1 % BSA. For the blocking and the dilution of the detection antibody and streptavidin-HRP 5 % Tween was used. The reaction was stopped with sulfuric acid (2 N) and the OD at 450 nm and 540 nm as reference wavelength was recorded with an Epoch Microplate Spectrophotometer.

2.2.6.3 Multiplex ELISA

For the analysis of several cytokines in tumor lysates and in serum with the V-PLEX Proinflammatory Panel 1 Mouse Kit tumor lysate samples were adjusted to a 1 mg/ml concentration with H_2O and 25 µl of this tumor lysate or 25 µl of serum were used. The assay was conducted according to the manufacturer's instructions and the plates were read on a MESO QuickPlex SQ 120.

Another spectrum of cytokines and proteins in the tumor lysates was analyzed with the membrane-based Mouse Cytokine Array C3. Therefore, 300 µg total protein of three tumor lysates was pooled for one membrane (100 µg each). Primary tumors irradiated with 2x8 Gy (RT) and

abscopal tumors of the same mice, or primary and abscopal tumors of the RT plus HHP vaccination group were analyzed (Figure 12). To identify differences in the cytokine milieu in abscopal tumors of the RT + αPD-1 group that do respond to the treatment vs. the ones that don't, the three smallest ("responder") and largest abscopal tumors ("non-responders") were pooled. The respective primary tumors were analyzed as well. The assay was performed according to the kit's instructions with an overnight incubation of the samples on the membranes at 4 °C. The membranes were imaged on an iBright FL1000 Imaging System and were analyzed with the iBright Analysis Software and the RAYBIO Analysis Tool.

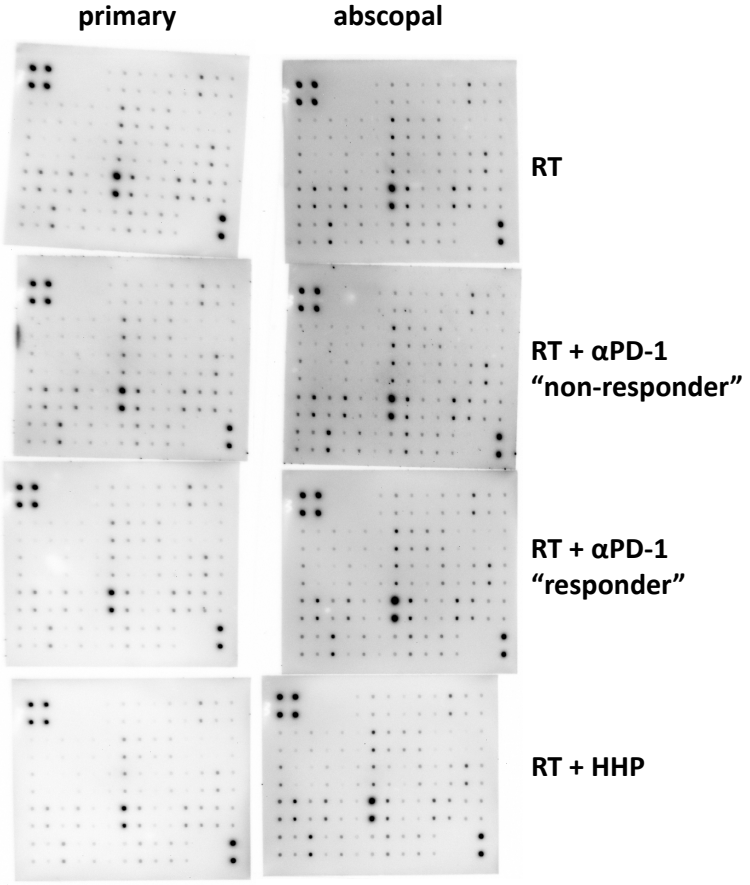

Figure 12: Mouse Cytokine Array C3. Tumor lysates of three 2x8 Gy (RT) irradiated primary tumors and abscopal tumors of the same mice, or primary and abscopal tumors of the RT plus HHP vaccination group were pooled together on one membrane. For the RT + αPD-1 group the three smallest ("responder") and largest abscopal tumors ("non-responder") were pooled.

2.2.7 Quantitative real-time PCR (qPCR)

2.2.7.1 RNA isolation

The phenol/chloroform isolation of RNA from samples resuspended in TriFast was performed according to the manufacturer's protocol. Glycogen was added RNA precipitation step with 70 % isopropanol. RNA pellets were resuspended in RNase free water and the concentration and purity was determined with a P330 nanophotometer.

2.2.7.2 cDNA synthesis

Genomic DNA was digested with DNase I before reverse transcription of the RNA into cDNA following the supplied protocol. 1 µg RNA from *in vitro* tumor cell experiments and 0.7 µg from *in vivo* experiments were then transcribed with the High-Capacity cDNA Reverse Transcription Kit as described in the protocol. Additionally, non-reverse transcription (NRT) controls were prepared. The transcribed cDNA was diluted 1:4 with Yellow Sample Buffer (40X) and RNase free water for qPCR.

2.2.7.3 qPCR

Pre-designed Prime PCR Primers from Bio-Rad were used for all qPCR reactions. The qPCR analysis was carried out with the DyNAmo ColorFlash SYBR Green qPCR Kit with the following components (Table 17) and program (Table 18) on a CFX96 Real-Time System:

Table 17: qPCR components

Component	
2X SYBR Green Mix	1X
20X PrimePCR Primer Mix	1X
cDNA	25 ng
Nuclease free water	ad 20 µl

Table 18: qPCR cycling conditions

Temperature [°C]	Time	
95	7 min	
95	10 s	40X
60	15 s	
60 to 95 in 0.5 °C increments	5 s	

The qPCR results were analyzed with the Bio-Rad CFX Manager software and the gene expression was calculated as normalized gene expression or relative expression normalized to housekeeping genes only (ΔCq) or housekeeping genes plus control samples (ΔΔCq).

2.2.8 Statistical analyses

Statistical analysis was performed with the GraphPad Prism software. Unless indicated otherwise, in most of the cases a Kruskal-Wallis test was calculated to compare all treatment groups against the untreated control with Dunn's correction for multiple testing and a Mann-Whitney U test to compare two treatment groups. For the analysis of the tumor growth a two-way ANOVA with Geisser-Greenhouse correction and for the survival a log-rank test with Holm-Sidak correction for multiple testing was applied. Significances were indicated as follows: *$p < 0.05$, **$p < 0.01$, ***$p < 0.001$

3. Results

Part of this work, as indicated in the figure legends, has been previously published in the following article:

Seitz C., **Rückert M.**, Deloch L., Weiss E.-M., Utz S., Izydor M., … Frey, B. (2019). Tumor Cell-Based Vaccine Generated With High Hydrostatic Pressure Synergizes With Radiotherapy by Generating a Favorable Anti-tumor Immune Microenvironment. *Frontiers in Oncology*, *9*(August), 1–12. https://doi.org/10.3389/fonc.2019.00805

Additionally, data have been presented at the following conferences as a poster:

Frey B., Seitz C., **Rückert M.**, Weiss E.-M., Wunderlich R., Schlücker E., Schaft N., Fietkau R., Gaipl U. S. (2016). Combination of ionizing radiation with an autologous whole tumour cell-based vaccine induces immunogenic melanoma and colorectal cancer cells and significantly retards tumour growth in syngenic mouse models. *Strahlentherapie Und Onkologie*, *192*(S1), 1–161. https://doi.org/10.1007/s00066-016-0974-z
22. Jahrestagung der Deutschen Gesellschaft für Radioonkologie (DEGRO)

Rückert M., Frey B., Fietkau R., Gaipl U. S. (2017). Immunological basis of abscopal antitumor responses induced with radio-immunotherapy. *Strahlentherapie Und Onkologie*, *193*(S1), 1–194. https://doi.org/10.1007/s00066-017-1137-6
23. Jahrestagung der Deutschen Gesellschaft für Radioonkologie (DEGRO)

Frey B., Seitz C., Weiss E. M., **Rückert M.**, Schlücker E., Schaft N., Fietkau R., Gaipl U. S.. (2017). Autologous whole tumor cell-based vaccines generated with high hydrostatic pressure bear immunogenic potential and act synergistically with radiotherapy to retard tumor growth. *European Journal of Immunology*, *47*, 1-333. doi:10.1002/eji.201770300
47. Jahrestagung der Deutschen Gesellschaft für Immunologie (DGfI)

Rückert M., Frey B., Fietkau R., Gaipl U. S. (2018). Anti-tumor immune responses in primary and abscopal tumors differently depend on radiotherapy fractionation and immunotherapy modalities. *Strahlentherapie Und Onkologie*, *194*(S1), 1–222. https://doi.org/10.1007/s00066-018-1301-7
24. Jahrestagung der Deutschen Gesellschaft für Radioonkologie (DEGRO)

Rückert M., Seitz C., Deloch L., Weiss E.-M., Utz S., Izydor M., Ebel N., Schlücker E., Fietkau R., Gaipl U.S., Frey B. (2019). Mit hydrostatischem Hochdruck generierte Ganzzell-Tumorvakzine erzeugen in Kombination mit Strahlentherapie ein immunogenes Tumor-Mikromilieu. *Strahlentherapie Und Onkologie*, *195*(S1), 1–218. https://doi.org/10.1007/s00066-019-01465-2
25. Jahrestagung der Deutschen Gesellschaft für Radioonkologie (DEGRO)

3.1 High hydrostatic pressure treatment of tumor cells generates a whole tumor cell vaccine that synergizes with RT to retard melanoma and colon carcinoma growth

3.1.1 High hydrostatic pressure of at least 200 MPa fully inactivates tumor cells

Applying whole tumor cells as therapeutic tumor vaccines in patients always bears the risk of newly formed tumors if some of the injected tumor cells remain viable. Therefore, high hydrostatic pressure (HHP) used to generate whole tumor cell vaccines first needs to be proven to be a suitable method to fully inactivate tumor cells in a reproducible manner. To address this issue, we treated B16-F10 melanoma cells with various pressures from 100 to 500 MPa (1,000 to 5,000 bar) and analyzed the viability and their ability to form colonies *in vitro* or tumors *in vivo*.

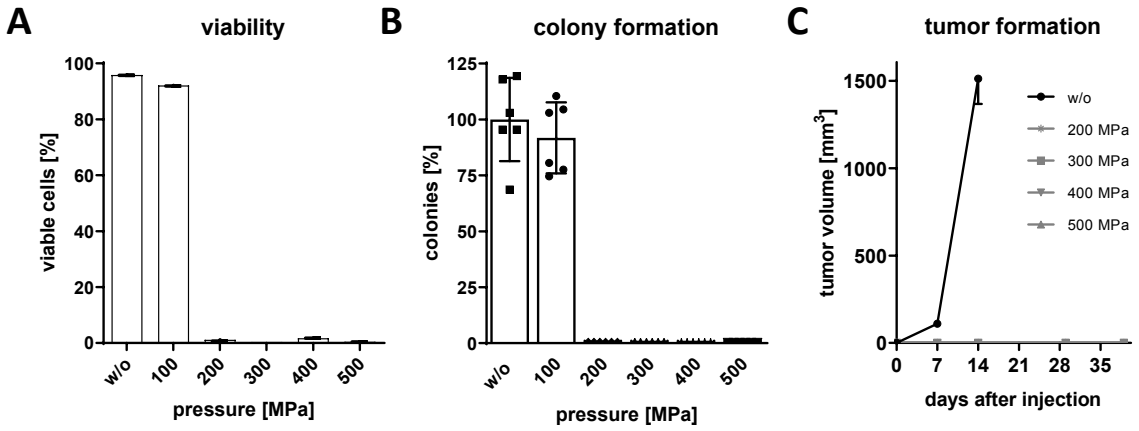

Figure 13: High hydrostatic pressure (HHP) of at least 200 MPa completely inactivates tumor cells. A-C: B16-F10 melanoma cells were treated with a pressure of 100-500 MPa for 300 s. The viability of HHP treated tumor cells was analyzed 24 h after the treatment with AnnexinV-PI staining (**A**). The ability of HHP treated cells to form colonies *in vitro* (**B**) or tumors *in vivo* (**C**) was determined by colony formation assay and subcutaneous injection of $2x10^6$ tumor cells into three syngeneic C57Bl/6 mice per group, respectively. Data from at least three independent experiments are presented as mean ± SD. These results have been previously published in (Seitz et al., 2019).

B16-F10 melanoma cells pressurized with 100 MPa for 300 s remain viable (Figure 13A) and clonogenic (Figure 13B). 24 h after the treatment with a pressure of 200 MPa or more almost no viable tumor cells are detectable with AnnexinV-FITC/PI staining anymore. 200 MPa and above HHP-treated tumor cells completely lose the ability to form colonies *in vitro* and tumors *in vivo* after subcutaneous injection into syngeneic C57Bl/6 mice (Figure 13C).

3.1.2 HPP vaccines synergize with radiotherapy to retard B16 tumor growth

To investigate the therapeutic potential of HHP-generated whole tumor cell vaccines we subcutaneously injected HHP treated B16 melanoma cells right next to established B16 tumors (Figure 14A). The experiments above (Figure 13) and previous work in our group (Weiss, Frey, et al., 2010; Weiss, Meister, et al., 2010) and by others (Urbanova et al., 2017) showed promising results and the safety of HHP vaccines generated with 200 MPa. Therefore, in all following *in vivo* vaccination approaches the tumor cells were prepared at this pressure level. As ionizing radiation has immunostimulatory properties on the tumor microenvironment (Rückert et al., 2018) we hypothesized that RT synergizes with HHP vaccines to form an even more potent anti-tumor immune response, thus, we compared single treatments with a combined approach.

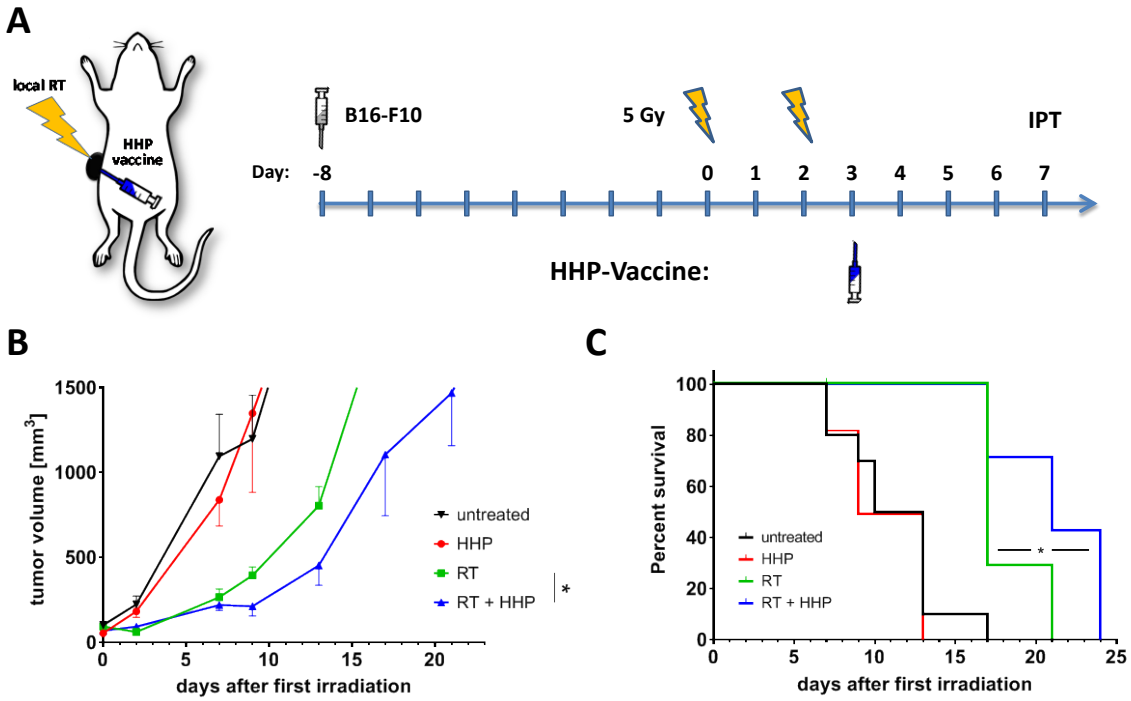

Figure 14: Whole tumor cell-based vaccines generated with high hydrostatic pressure (HHP) synergize with radiotherapy to retard tumor growth. A-C: C57Bl/6 mice were subcutaneously injected with $1x10^6$ viable B16-F10 cells. After eight days established tumors were locally irradiated with 2x5 Gy on days 0 and 2 or were left untreated. Additionally, some mice were vaccinated on day 3 with $5x10^6$ HHP (200 MPa) treated B16-F10 cells by peritumoral injection. On day 7 an immune phenotyping (IPT) by multi-color flow cytometry of immune cells infiltrating into the tumors and in the blood was performed. The tumor growth (**B**) and the survival of the mice (**C**) were monitored. Data are presented as mean ± SEM. For the tumor growth a two-way ANOVA with Geisser-Greenhouse correction and for the survival a log-rank (Mantel-Cox) test was calculated to compare the 2x5 Gy with the 2x5 Gy + HHP group; *$p < 0.05$; n = 7-11 animals per group from two independent experiments. These results have been previously published in (Seitz et al., 2019).

Irradiation of B16 tumors with 2x5 Gy achieved tumor control for about one week compared to untreated tumors (Figure 14B). Although the HHP vaccine alone had no effect, vaccination synergized with RT to retard the tumor growth significantly longer than sole RT. The benefit of the combined treatment for the tumor control was also reflected by a significantly longer survival of the mice in comparison to RT alone (Figure 14C).

3.1.3 Combined HHP and RT treatment results in increased intratumoral immune cell concentrations

To see which tumor infiltrating immune cells might be involved in the anti-tumor immune response of the combined RT and HHP treatment we sacrificed mice of each treatment group at day 7 and performed a flow cytometric immune phenotyping of a broad range of leukocyte subtypes. Furthermore, we wanted to know if T cells are potentially inactivated by the tumor cells via the PD-1/PD-L1 axis and if the PD-1 expression is acquired in the tumor or is already present in the peripheral blood.

Only RT plus HHP vaccination significantly enhanced the immune cell concentration of all leukocytes in general compared to untreated tumors (Figure 15A). This mostly originated from significantly increased concentrations of NK cells, T cells and the monocyte/macrophage compartment (Figure 15E-G) in those tumors. Additionally, all other cell types such as neutrophils, eosinophils and DCs, except B cells, showed this trend, however not significant (Figure 15B-D). B cell numbers per gram of tumor were significantly reduced in tumors treated with RT + HHP which was similar after RT alone (Figure 15H). In accordance with the higher concentration of T cells in general, all analyzed T cell subtypes were also present to a higher extent in tumors of the combined treatment (Figure 15I-M) with significant alterations for NKT cells, CD4+ T cells and Tregs (Figure 15I, K, M). Additionally, CD4+ and CD8+ T cells were analyzed for their PD-1 expression in blood and tumors. Whereas hardly any T cells positive for PD-1 were detectable in the blood in all treatment groups (Figure 15N), the majority of tumor infiltrating T cells showed PD-1 expression (Figure 15O). The percentage of PD-1+ CD4+ T cells increased to about 60 % in irradiated tumors and was significantly elevated in the combined treatment group compared to untreated controls with 35 %. No significant changes were observed for CD8+ T cells and even in control tumors about 70 % of the cells were PD-1+.

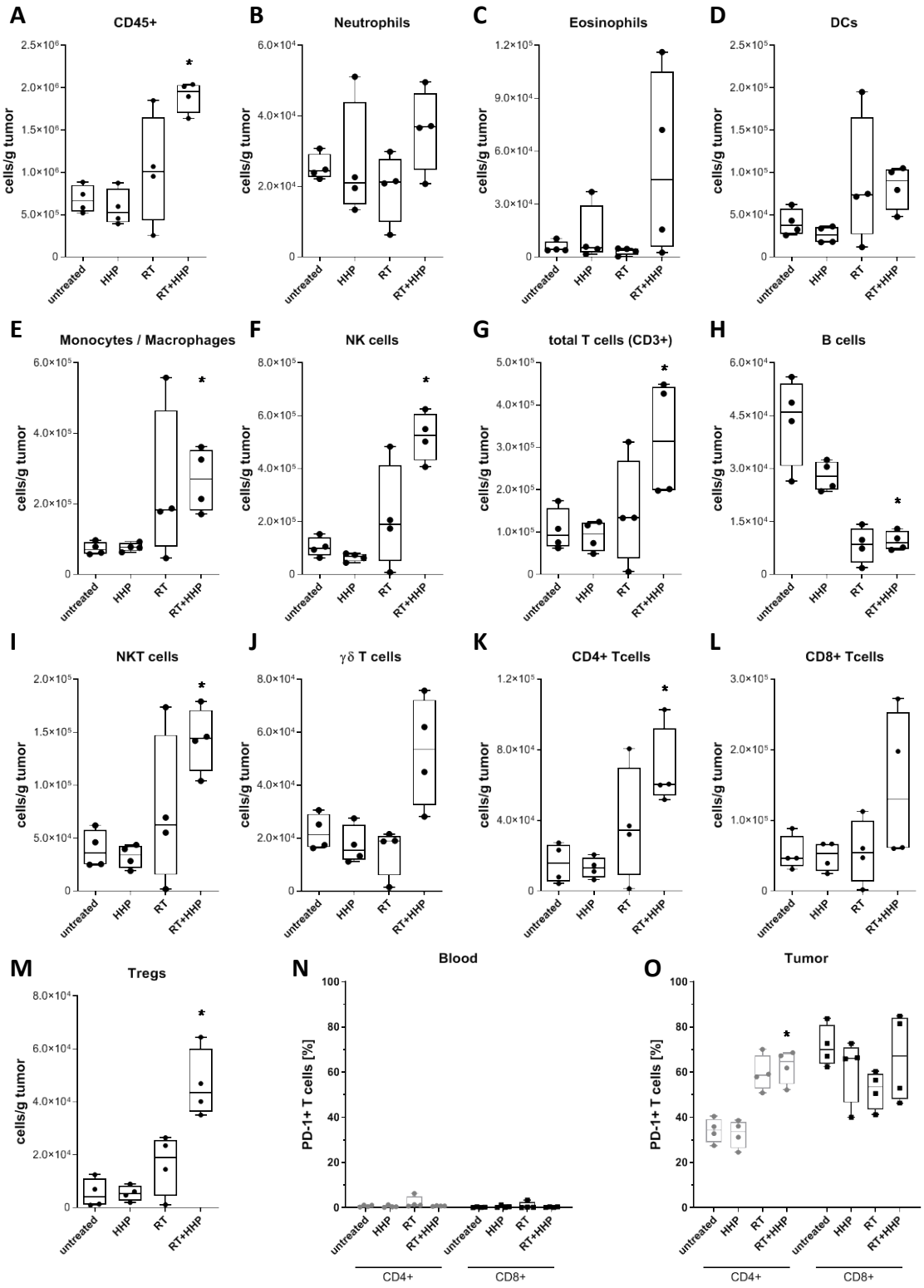

Figure 15: Combined treatment of tumors with radiotherapy and HPP vaccination increases immune cell concentrations. On day 7 after first irradiation four animals of each group were sacrificed and immune cells infiltrating into the tumors and circulating in the blood were analyzed by multi-color flow cytometry. **A-M**: The concentration of immune cells per gram of tumor is displayed. Immune cell subtypes were identified as follows: all immune cells CD45+ (**A**); neutrophils CD11b+, Ly6G+ (**B**); eosinophils CD11b+ Siglec-F+ (**C**); dendritic cells (DCs) MHC-II+, CD11c+ (**D**); monocytes/macrophages CD11b+, Ly-6C+ (**E**); natural killer (NK) cells CD49b+, CD3– (**F**); total T cells CD3+ (**G**); B cells CD19+ (**H**); NKT cells CD3+, CD49b+ (**I**); γδ T cells CD3+, γδTCR+ (**J**); regulatory T cells (Tregs) CD3+, CD4+, CD25+ FoxP3+ (**M**). CD4+ (**K**) and CD8+ (**L**) T cells in blood (**N**) and in tumors (**O**) were analyzed for PD-1 expression. Data are presented as box plots with whiskers from minimum to maximum values and Mann-Whitney U test was calculated to compare groups RT + HHP and untreated; *p < 0.05; n = 4 animals per group. Parts of these results have been previously published in (Seitz et al., 2019).

3.1.4 HHP vaccines in combination with RT significantly retard CT26 colon carcinoma growth

For the investigation if the synergistic effect of the combined RT and HHP treatment is melanoma-specific, we treated Balb/c mice bearing palpable CT26 colon carcinoma tumors 14 days after injection the same way as the C57Bl/6 mice with B16 tumors (Figure 16A).

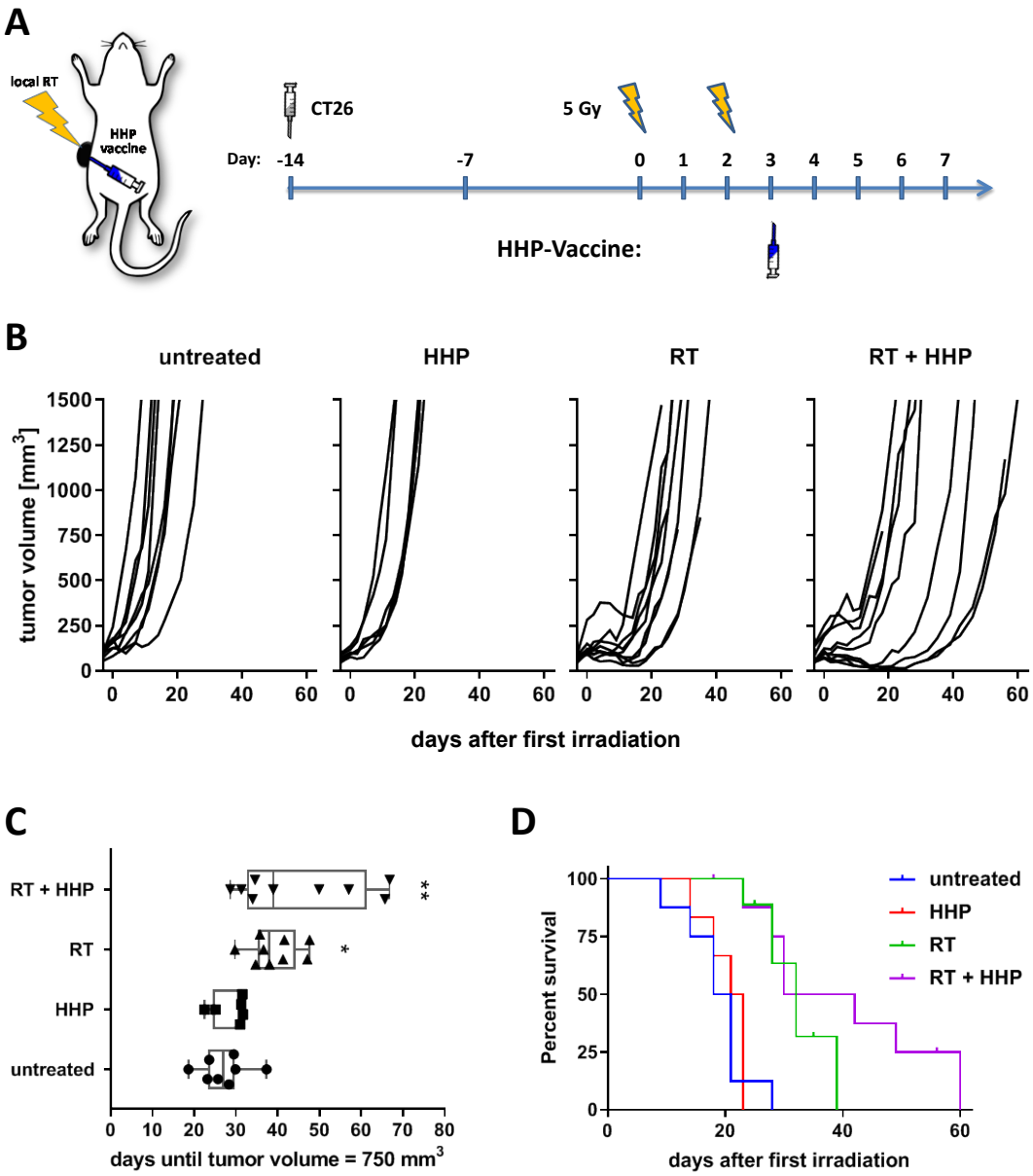

Figure 16: HHP vaccines synergize with radiotherapy in the CT26 tumor model as well. A-D: Balb/c mice were subcutaneously injected with $1.2x10^6$ viable CT26 cells. After 14 days established tumors were locally irradiated with 2x5 Gy on days 0 and 2 or were left untreated. Additionally, some mice were vaccinated on d3 with $5x10^6$ HHP (200 MPa) treated CT26 cells by peritumoral injection. The tumor growth (**B, C**) and the survival of the mice (**D**) were monitored. The time until tumors reached a volume of 750 mm^3 is presented as box plots with whiskers from minimum to maximum values and Kruskal-Wallis test with Dunn's correction for multiple testing was calculated to compare treatments with untreated controls. For the survival a log-rank (Mantel-Cox) test was calculated to compare the 2x5 Gy with the 2x5 Gy + HHP group; *p < 0.05, **p < 0.01; n= 6-9 animals per group from three independent experiments. These results have been previously published in (Seitz et al., 2019).

In the CT26 model both, RT alone and in combination with HHP, significantly delayed the tumor growth (Figure 16C). However, only half of the mice profited from the additional vaccination (Figure 16B) and the survival was not significantly improved (Figure 16D).

3.2 RIT-combinations differently affect primary and abscopal tumor growth and the tumor microenvironment

3.2.1 RT-mediated local tumor control can be improved with immunotherapies but abscopal responses are only induced together with anti-PD-1

In consequence of the promising results regarding the tumor growth retardation, we aimed to investigate if RT plus HHP vaccine combinations are also capable of inducing systemic anti-tumor immune responses in an abscopal tumor setting with B16 melanoma. Based on the high percentage of PD-1+ T cells after the therapy we also included anti-PD-1 immune checkpoint blockade in the treatment schedule (Figure 17A). Therefore, C57Bl/6 mice were injected with one tumor on each flank at a timely distance of 4 days and only the first injected primary tumor was locally irradiated. Anti-PD-1 mAbs were administered concurrently with the RT and the HPP vaccine was applied twice by subcutaneous injection in the neck.

Although injected distantly from the primary irradiated tumor the HHP vaccine was also capable to retard the tumor growth in the abscopal setting beyond the RT-mediated growth inhibition (Figure 17B). Even though RT plus anti-PD-1 had a similar effect, the triple combination did not further improve the treatment outcome. In contrast to RT alone the addition of anti-PD-1 retarded the tumor growth of the non-irradiated abscopal tumor in about half of the mice. HHP vaccination had no effect on the abscopal tumor growth and could not improve RT plus anti-PD-1-mediated abscopal responses. These results are also reflected by the time until the abscopal tumors reached a volume of 500 mm^3. Only RT plus anti-PD-1 significantly delayed the abscopal tumor growth compared to the untreated control (Figure 17C). The survival of the mice was significantly prolonged in the triple combination and RT plus anti-PD-1 group (Figure 17D).

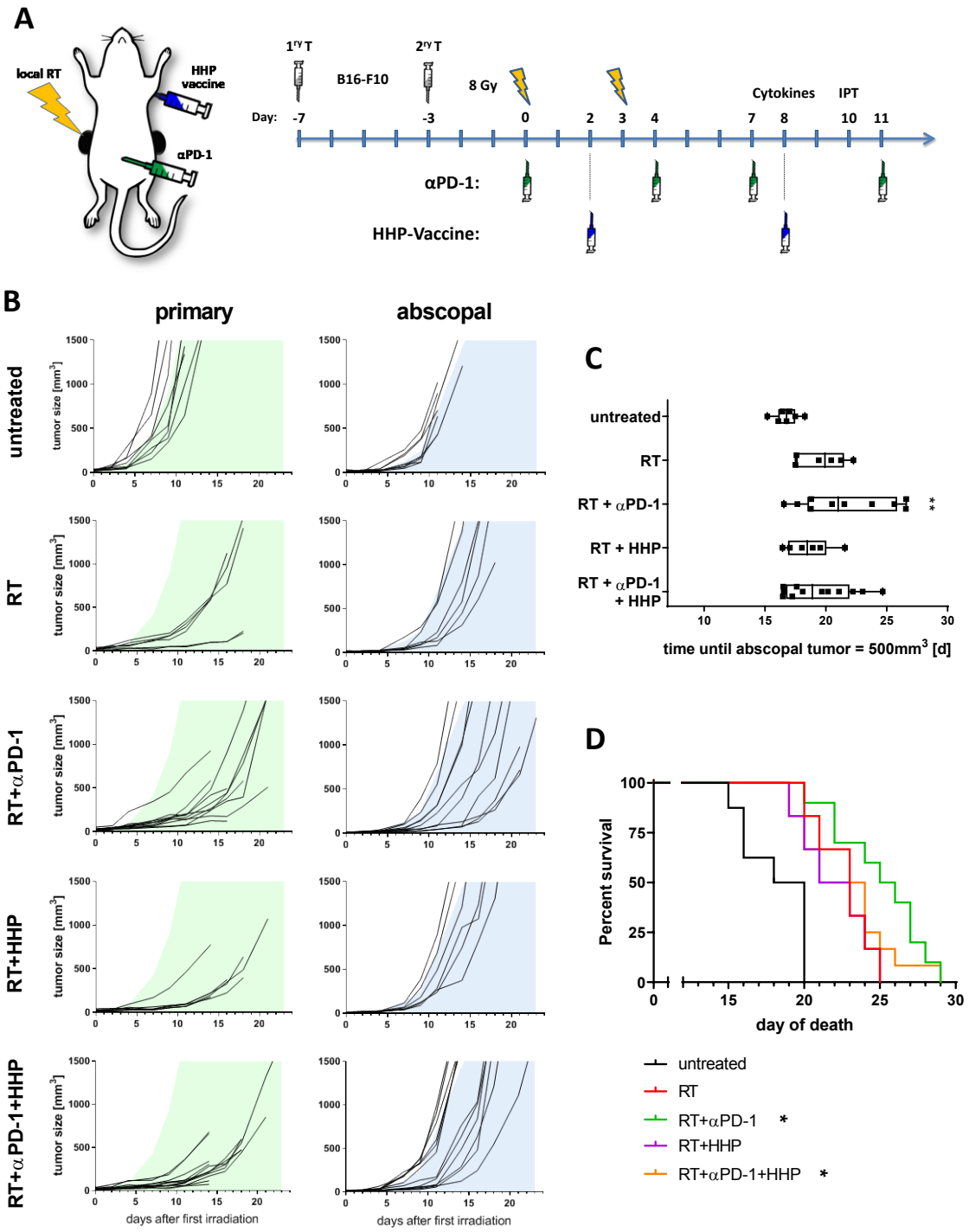

Figure 17: HHP-vaccines act systemically but only on previously irradiated tumors and fail to improve RT+PD-1 induced abscopal responses. A: C57Bl/6 mice were subcutaneously injected with $0.2x10^6$ B16-F10 tumor cells into the right flank. Four days afterwards a second tumor was injected on the left flank which later served as the non-irradiated abscopal tumor. The mice received one of the following treatments or combinations thereof. Only the first injected primary tumor was irradiated with 2x8 Gy on d0 seven days after injection and on d3. Beginning with the first irradiation on d0, the mice were intraperitoneally injected with 200 µg anti-PD-1 antibody (αPD-1) every three to four days for a total of four injections. Additionally, HHP vaccine ($5x10^6$ cells) was injected twice subcutaneously into the neck on days 2 and 8. Tumor and blood samples were collected from some animals on day 8 for cytokine analyses and on day 10 for immune phenotyping (IPT). **B**: Individual tumor growth curves are depicted. For a better comparability of the treatment groups green and blue areas indicate retarded tumor growth beyond the mean of primary and abscopal tumors of the control group, respectively. **C**: The time until the abscopal tumors reached a volume of 500 mm^3 is depicted as box and whiskers plot. A Kruskal-Wallis test with Dunn's correction for multiple testing was calculated to compare treatments with untreated controls. **D**: For the survival a log-rank (Mantel-Cox) test was calculated with Holm-Sidak correction for multiple testing to compare the treatments with the control group. *p < 0.05, **p < 0.01; n = 6-12 animals per group from two independent experiments.

3.2.2 Immune cell profiles differ between primary and abscopal tumors and between the treatment groups

As primary and abscopal tumors responded differently to the immunotherapies we hypothesized that the immune cell composition will differ between primary and abscopal tumor and between the treatment groups. Therefore, we performed multi-color flow cytometry on day 10, one week after the last fraction to identify tumor infiltrating leukocyte subtypes in primary and abscopal tumors.

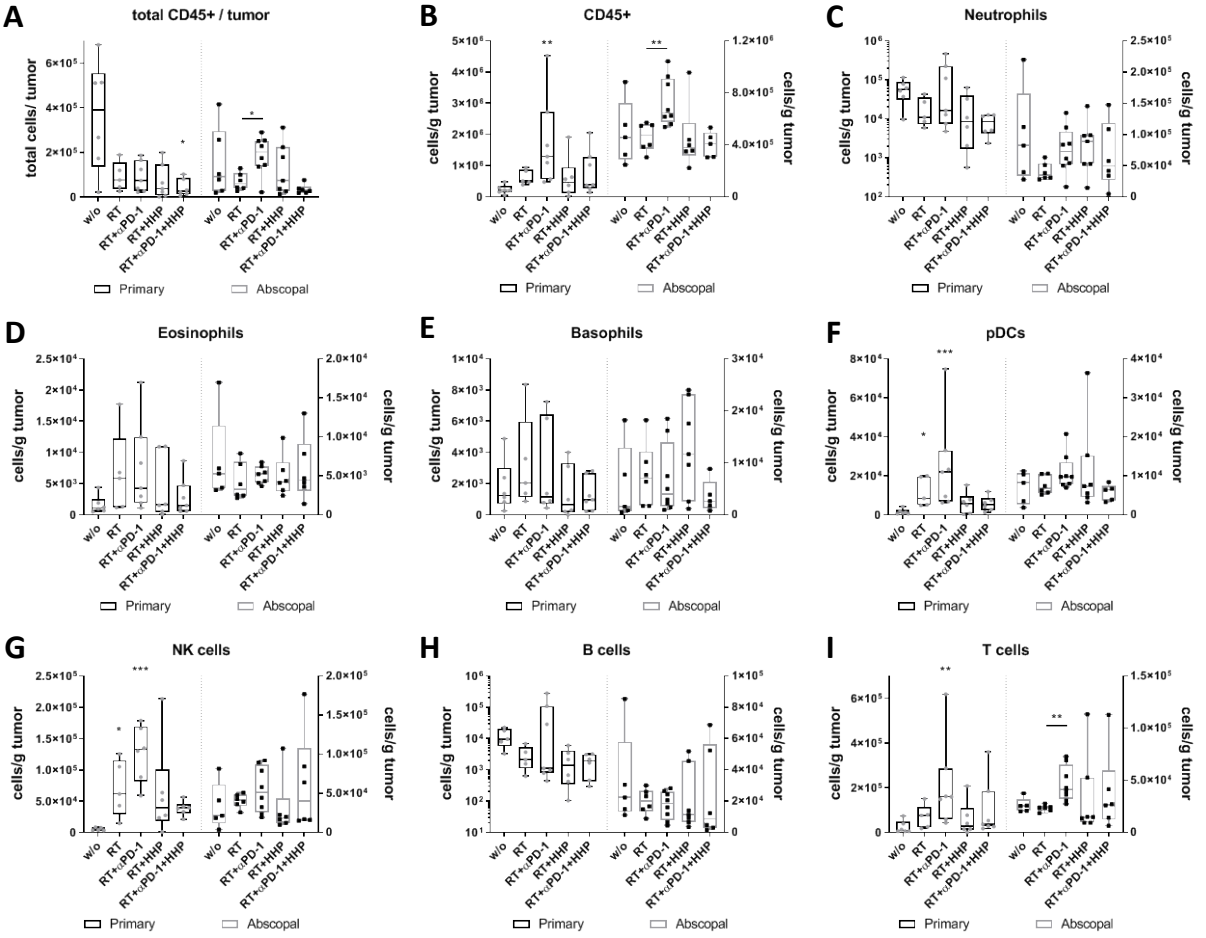

Figure 18: 2x8 Gy plus anti-PD-1 increases tumor-infiltrating leukocyte concentrations in primary and abscopal tumors. On day 10 after first irradiation mice were sacrificed and immune cells infiltrating into the tumors were analyzed by multi-color flow cytometry. The total amount of all immune cells (CD45+) per primary and abscopal tumor (**A**) and the concentration per gram of tumor (**B**) is displayed. Immune cell subtypes were identified as follows: neutrophils CD11b+, Ly6G+ (**C**); eosinophils CD11b+ Siglec-F+ (**D**); basophils FcεR1α+, CD49b+ (**E**); plasmacytoid dendritic cells (pDCs) CD11b-, Ly6G-, PDCA-1+, Ly6C+ (**F**); natural killer (NK) cells CD49b+, CD3- (**G**); B cells CD19+ (**H**); total T cells CD3+, CD49b- (**I**). Data are presented as box plots with whiskers from minimum to maximum values. A Kruskal-Wallis test with Dunn's correction for multiple testing was used to compare the primary and abscopal tumors of all treatment groups with the respective untreated control (w/o) tumors. Additionally, a Mann-Whitney U test was calculated to compare RT + anti-PD-1 and RT groups; *p < 0.05, **p < 0.01, ***p < 0.001; n = 5-8 animals per group from two independent experiments.

Although the total amount of immune cells (CD45+) in the primary tumors after any form of treatment was generally less than that in untreated controls (Figure 18A), the concentration of CD45+ cells per gram of tumor mass, was significantly increased in primary tumors of the RT plus anti-PD-1 group (Figure 18B). Additionally, in this treatment group, that also showed the most pronounced abscopal responses, the total amount of immune cells and the concentration in the abscopal tumor was significantly higher than after RT alone. The same trends in primary and abscopal tumors were found for T cells (Figure 18I). Higher concentrations of pDCs and NK cells were detected in primary tumors that had been treated with RT and concentrations even further increased after the addition of anti-PD-1 (Figure 18F, G). No significant changes were observed for all granulocyte subtypes (neutrophils, eosinophils and basophils) and B cells (Figure 18C-E, H). However, in all irradiated primary tumors the concentrations of neutrophils and B cells tend to be decreased.

Additionally, T cells were further subdivided and analyzed for their PD-1 and CD62L expression.

The concentration of NKT cells, Tregs and both, CD4+ and CD8+ T cells in primary tumors of the RT plus anti-PD-1 treatment group was significantly higher than that in untreated control tumors (Figure 19A, B, D, G). Although not significant, the same trend was observed for γδ T cells (Figure 19C). Only CD8+ T cells were found in higher concentrations in abscopal tumors of the RT plus anti-PD-1 treatment group compared to RT alone (Figure 19G). RT increased the proportion of PD-1+ and CD62L- cells among CD4+ and CD8+ T cells in primary tumors, albeit only to significant degree in some treatment combinations including RT (Figure 19E, F H, I). In abscopal tumors only the percentage of CD62L- CD4+ T cells was significantly increased in the RT and RT plus anti-PD-1 groups (Figure 19F).

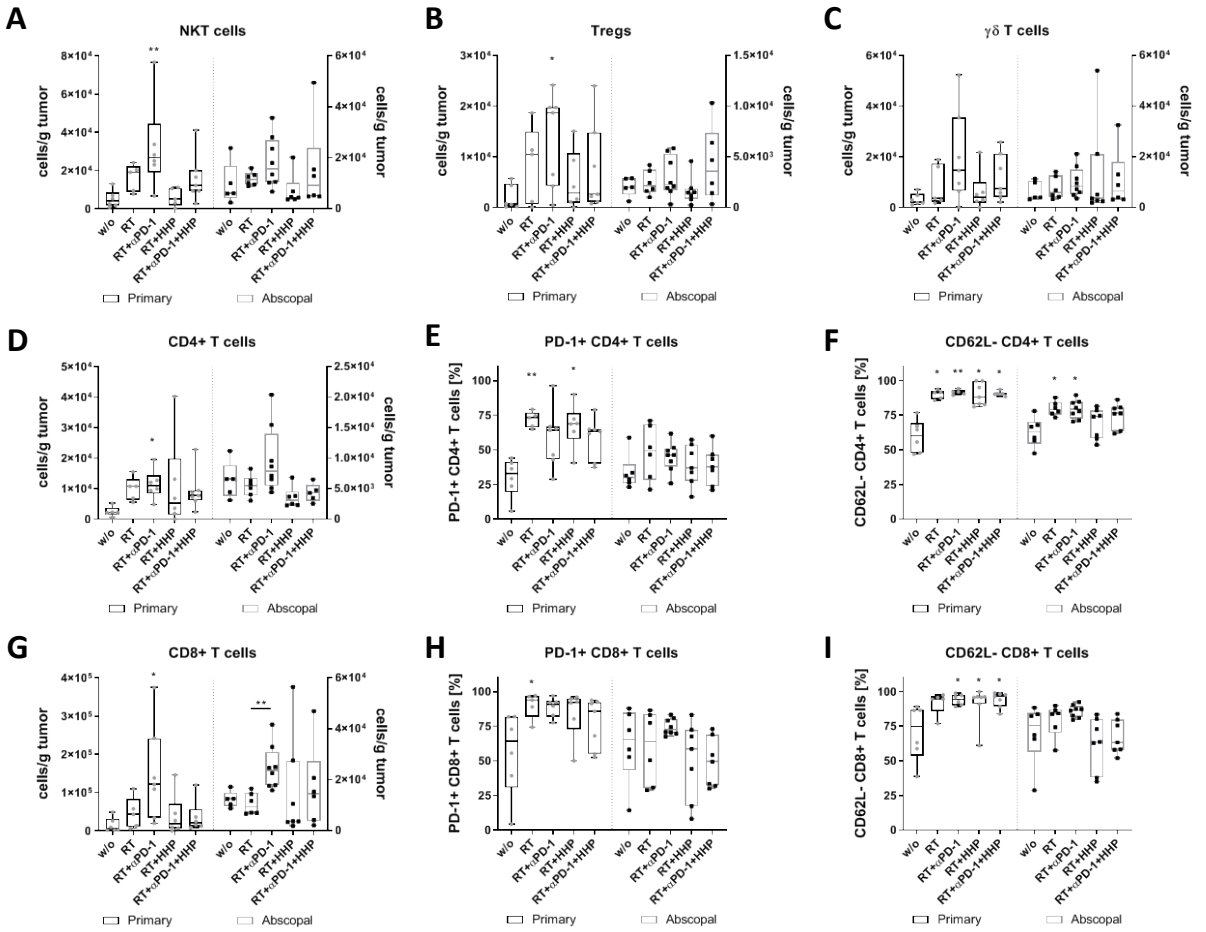

Figure 19: 2x8 Gy plus anti-PD-1 increases the concentration of tumor-infiltrating T cell subpopulations in primary and abscopal tumors. On day 10 after first irradiation mice were sacrificed and immune cells infiltrating into the tumors were analyzed by multi-color flow cytometry. **A-D, G**: The concentration of immune cells per gram of primary and abscopal tumor is displayed. Immune cell subtypes were identified as follows: NKT cells CD3+, CD49b+ (**A**); regulatory T cells (Tregs) CD3+, CD4+, CD25+ FoxP3+ (**B**); γδ T cells CD3+, γδTCR+ (**C**); CD4+ T cells (**D**), CD8+ T cells (**G**). CD4+ (**E**, **F**) and CD8+ (**H**, **I**) T cells were analyzed for their PD-1 (**E**, **H**) and CD62L (**F**, **I**) expression. Data are presented as box plots with whiskers from minimum to maximum values. A Kruskal-Wallis test with Dunn's correction for multiple testing was used to compare the primary and abscopal tumors of all treatment groups with the respective untreated control (w/o) tumors. Additionally, a Mann-Whitney U test was calculated to compare RT + anti-PD-1 and RT groups; *p < 0.05, **p < 0.01, n = 5-8 animals per group from two independent experiments.

Furthermore, DCs and the monocyte/macrophages compartment was analyzed.

In the RT plus anti-PD-1 treatment group significantly increased concentrations of DCs were detected in primary and abscopal tumors (Figure 20A), but only in primary tumors the percentage of the cDC1 subtype was significantly higher after irradiation and even higher with addition of anti-PD-1 (Figure 20B). In addition, the amount of monocytes/macrophages per gram of primary or abscopal tumor was significantly higher in the RT plus anti-PD-1 group (Figure 20C). When analyzing the composition of this compartment, no changes were observed for the percentage of monocytes among all treatment groups (Figure 20D). In primary tumors treated with RT plus anti-PD-1 the fraction of iTAMs significantly increased accompanied with a decrease in mTAMs (Figure 20E, F).

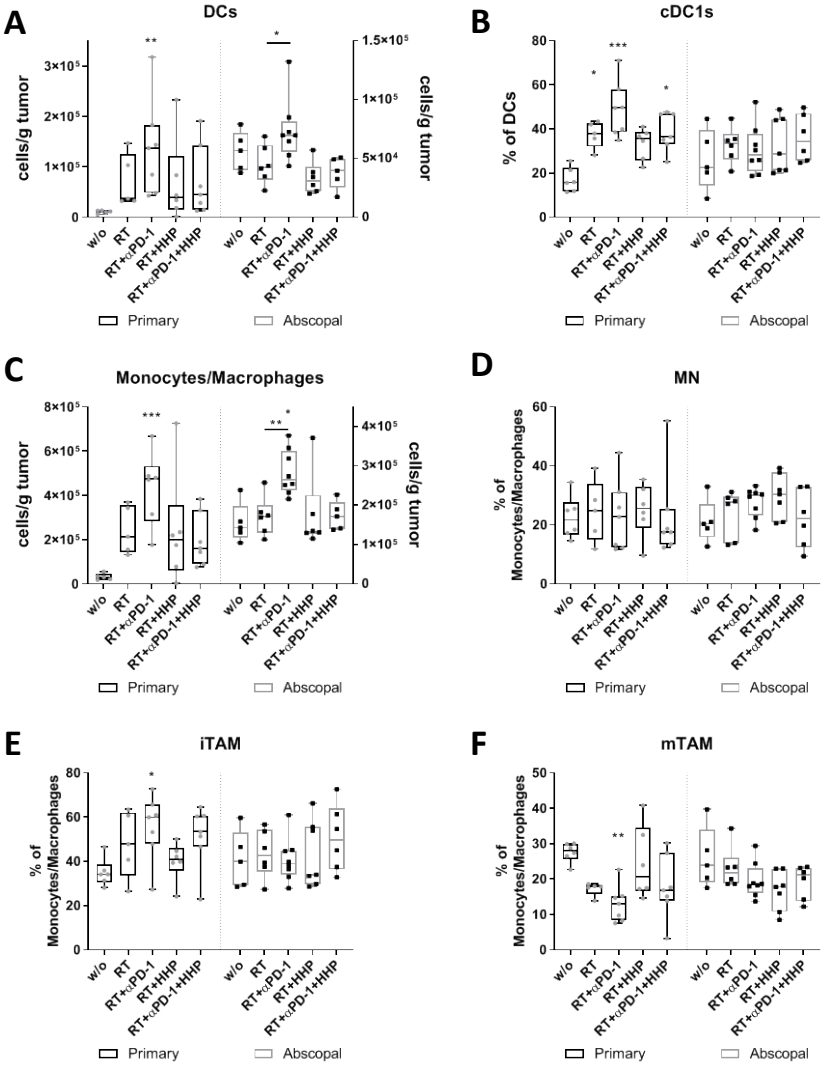

Figure 20: 2x8 Gy plus anti-PD-1 increases the concentration of tumor-infiltrating DCs and Monocytes/Macrophages in primary and abscopal tumors and alters the composition of their subtypes. On day 10 after the first irradiation mice were sacrificed and immune cells infiltrating into the tumors were analyzed by multi-color flow cytometry. **A, C**: The concentration of immune cells per gram of primary and abscopal tumor is displayed. Immune cell subtypes were identified as follows: dendritic cells (DCs) MHC-II+, CD11c+ (**A**); monocytes/macrophages CD11b+, Ly-6C+ (**C**). DCs were further subdivided in CD11b- cDC1s (**B**) and monocytes/macrophages in Ly6C+, MHC-II- monocytes (MN, **D**), Ly6C+, MHC-II+ immature tumor associated macrophages (iTAM, **E**) and Ly6C- mature TAM (mTAM, **F**). Data are presented as box plots with whiskers from minimum to maximum values. A Kruskal-Wallis test with Dunn's correction for multiple testing was used to compare the primary and abscopal tumors of all treatment groups with the respective untreated control (w/o) tumors. Additionally, a Mann-Whitney U test was calculated to compare RT + anti-PD-1 and RT groups; *p < 0.05, **p < 0.01, ***p < 0.001; n = 5-8 animals per group from two independent experiments.

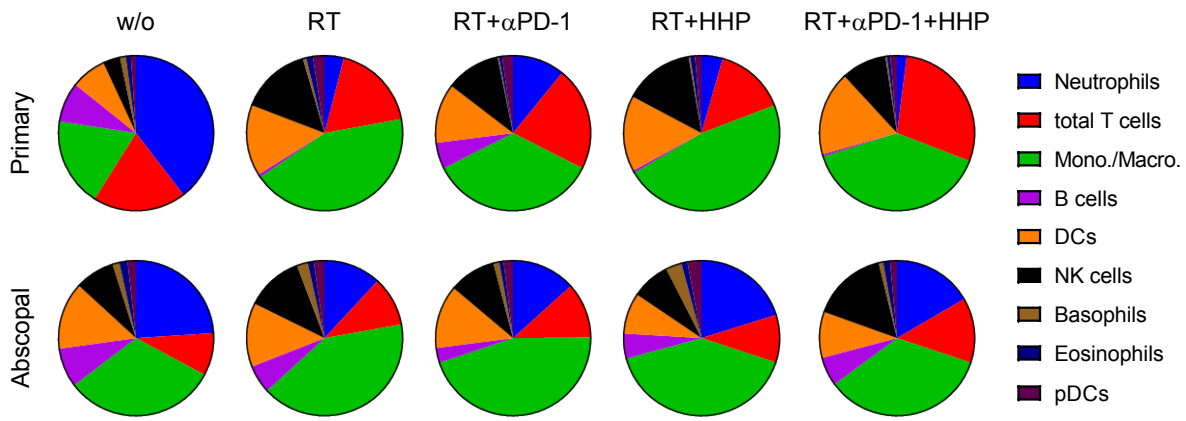

Figure 21: 2x8 Gy changes the composition of immune cells in primary and abscopal tumors. The composition of major immune cell types in primary and abscopal tumors is displayed as a pie chart with the mean of each cell type.

As depicted in Figure 21 neutrophils, T cells and monocytes/macrophages together make up more than 75 % of all identified major immune cell types in the untreated primary tumor. Among all treatment groups this composition in primary tumors is predominantly changed by RT characterized with less neutrophils, B cells and more monocytes/macrophages, DCs and NK cells. The percentage of T cells is almost not affected. Primary and abscopal tumors in the untreated control group vary to some degree. However, the composition in abscopal tumors is not drastically changed in the treatment groups.

Since not all mice responded equally to the treatment with RT plus anti-PD-1 we aimed to identify cell types that might be involved in mediating the abscopal effect by correlation analysis of the abscopal tumor weight and the tumor infiltrating immune cell concentrations.

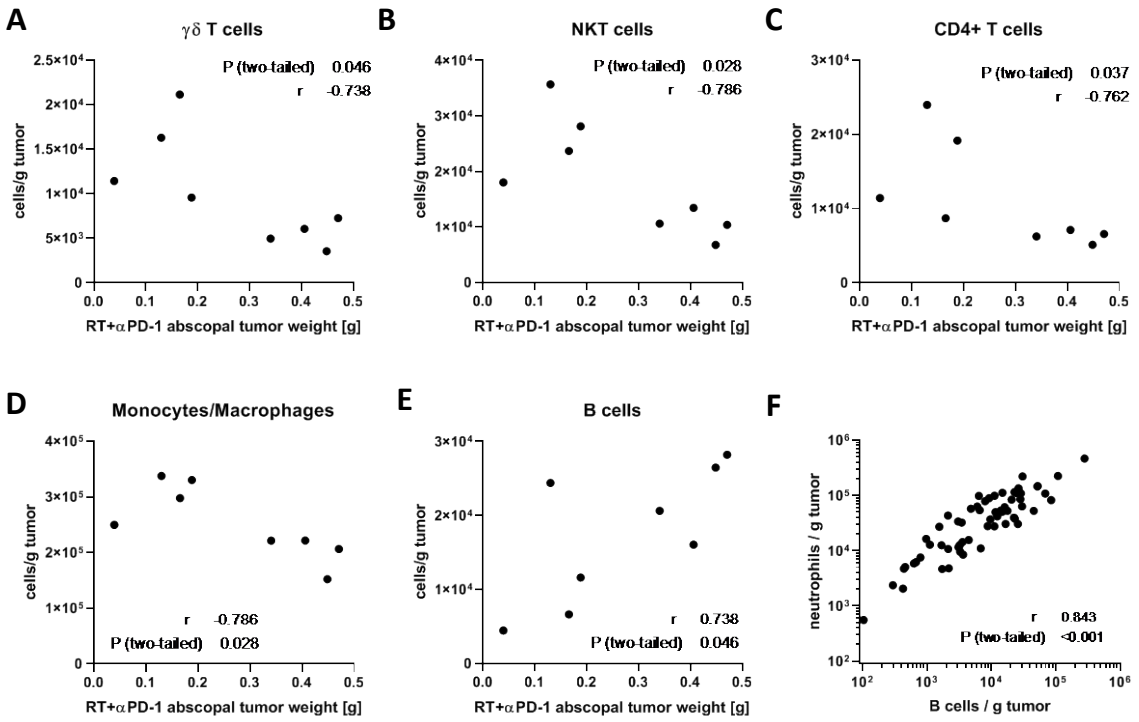

Figure 22: The abscopal tumor growth in the 2x8 Gy + anti-PD-1 group correlates with the infiltration of multiple immune cells. A-**E**: Spearman correlation was calculated for the abscopal tumor weight of the RT + anti-PD-1 group with concentration of γδ T cells (**A**), NKT cells (**B**), CD4+ T cells (**C**), monocytes/macrophages (**D**) and B cells (**E**). **F**: The Spearman correlation of neutrophil with B cell concentrations among all tumors and treatment groups is depicted.

In the RT plus anti-PD-1 treatment group a significant negative correlation of the abscopal tumor weight with the concentration of γδ T cells, NKT cells, CD4+ T cells and monocytes/macrophages was found (Figure 22A-D). In contrast, the presence of B cell positively correlates with the tumor mass (Figure 22E). As the regulation of neutrophil and B cell concentrations was very similar in all treatment groups (Figure 18B, G) we additionally wanted to know if there is a general correlation between both cell types. We found the amount of B cells per gram of tumor to be significantly correlated with the concentration of neutrophils across all tumors (primary and abscopal) and treatment groups (Figure 18F).

3.2.3 Immune cell concentrations in the peripheral blood are reduced after RT

To investigate if the changes in the tumor infiltrating immune cell concentrations can be detected in the periphery as well, immune phenotyping of the blood was performed on the same day.

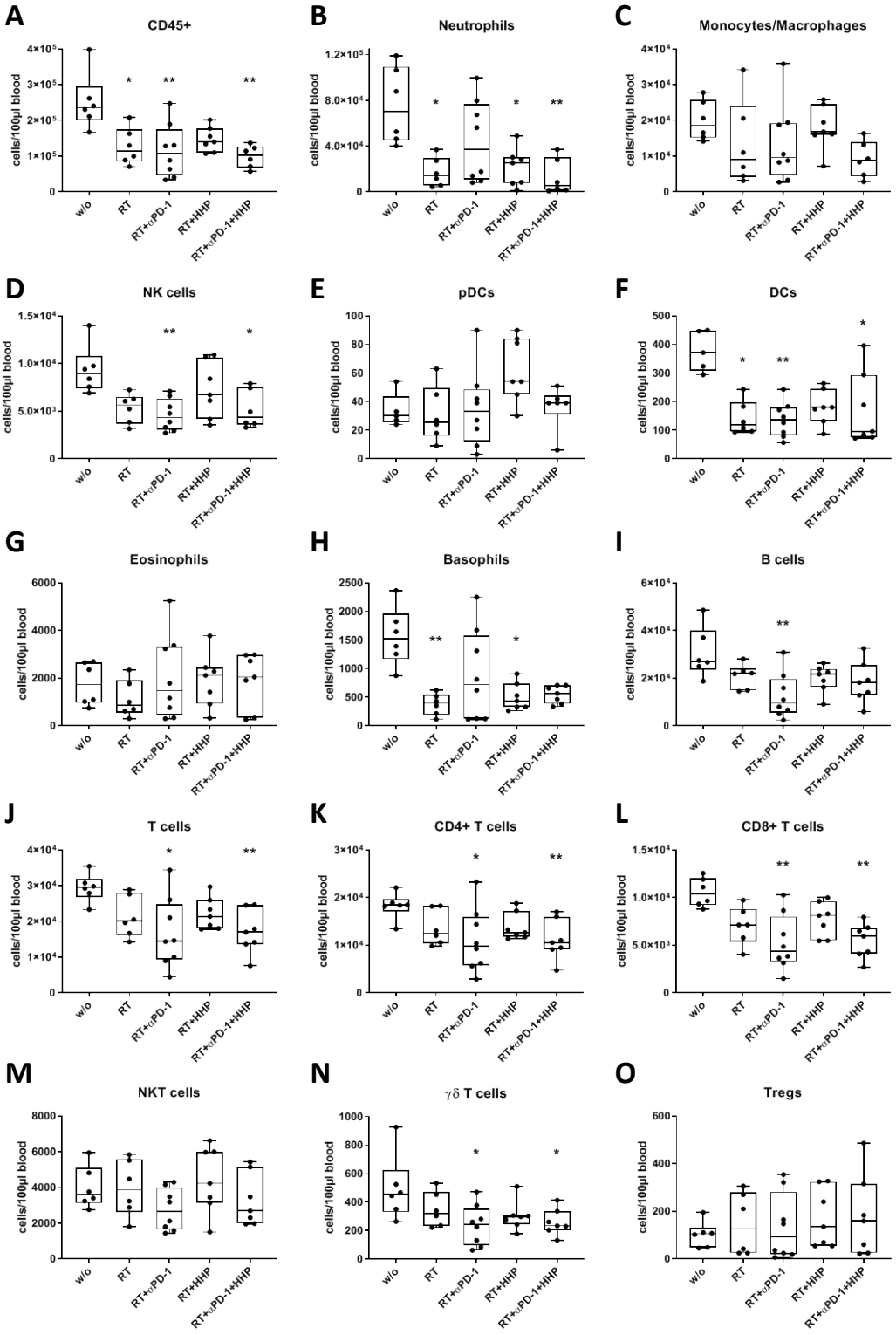

Figure 23: Immune cell numbers drop in the peripheral blood after irradiation with 2x8 Gy. On day 10 after first irradiation mice were sacrificed and immune cells in the blood were analyzed by multi-color flow cytometry. **A-O**: The concentration of immune cells per 100 µl blood is displayed. Immune cell subtypes were identified as follows: all immune cells CD45+ (**A**); neutrophils CD11b+, Ly6G+ (**B**); monocytes/macrophages CD11b+, Ly-6C+ (**C**); natural killer (NK) cells CD49b+, CD3- (**D**); plasmacytoid dendritic cells (pDCs) CD11b-, Ly6G-, PDCA-1+, Ly6C+ (**E**); dendritic cells (DCs) MHC-II+, CD11c+ (**F**); eosinophils CD11b+ Siglec-F+ (**G**); basophils FcεR1α+, CD49b+ (**H**); B cells CD19+ (**I**); total T cells CD3+, CD49b- (**J**); CD4+ (**K**) and CD8+ (**L**) Tcells; NKT cells CD3+, CD49b+ (**M**); γδ T cells CD3+, γδTCR+ (**N**); regulatory T cells (Tregs) CD3+, CD4+, CD25+ FoxP3+ (**O**). Data are presented as box plots with whiskers from minimum to maximum values. A Kruskal-Wallis test with Dunn's correction for multiple testing was used to compare all treatment groups with the untreated control (w/o); *$p < 0.05$, **$p < 0.01$; n = 6-8 animals per group from two independent experiments.

In general, the concentration of immune cells (CD45+) in the blood dropped in all treatment groups compared to untreated control mice (Figure 23A). The effect was significant in the RT treatment group, and highly significant with the addition of anti-PD-1 and in the triple combination. More precisely, similar trends were observed for neutrophils, NK cells, DCs and basophils (Figure 23B, D, F, G). In contrast, no changes were detected for the concentrations of eosinophils, NKT cells and Tregs (Figure 23G, M, O). T cells in general, as well as CD4+, CD8+ and γδ T cells were only significantly less abundant in the blood of those mice whose treatment included anti-PD-1 (Figure 23J-L, N). Monocytes/macrophages concentrations showed a declining trend in all treatment groups except RT plus HHP (Figure 23C). RT plus PD-1 was the only treatment that significantly decreased B cell concentrations in the blood (Figure 23I) and pDCs were the only cell type that showed a positive regulation which was detected in the RT plus HHP treatment group (Figure 23E).

3.2.4 Radioimmunotherapies increase the expression of immune checkpoint ligands in primary tumors

Next to the infiltration of immune cells into the tumors, the tumor microenvironment they migrate into is also of relevance for the induction and the effector phase of the anti-tumor immune response. Therefore, we analyzed the mRNA expression of immune checkpoint ligands in the tumor microenvironment. The samples for qPCR were taken from the flow through of the CD45+ MACS separation for the immune phenotyping and thus contain all cells of the tumor with the exception of immune cells.

The expression of *Cd274* (PD-L1) in primary tumors was about two-fold higher in the RT and triple combination groups and up to three-fold higher in the RT plus anti-PD-1 or plus HHP vaccine groups compared to untreated controls (Figure 24A). Similar trends were observed for the other two inhibitory immune checkpoint ligands *Pdcd1lg2* (PD-L2) and *Tnfrsf14* (HVEM) (Figure 24B, C), albeit the *Pdcd1lg2* (PD-L2) expression was only significantly elevated after RT plus HHP vaccination and the overall expression of this ligand was quite low. In contrast, the changes in the expression of the stimulatory immune checkpoint ligands *Cd70*, 4-1BBL, *Tnfsf9* (OX40L) and *Tnfsf4* (ICOS-L) were less pronounced (Figure 24D-G). Only the mRNA expression of *OX40L* was significantly higher in the primary tumors of RT plus PD-1 or plus HHP. In abscopal tumors the expression levels remained largely unchanged. RT significantly decreased the *CD70* expression in the abscopal tumors compared to the untreated control and *4-1BBL* was significantly higher expressed in the RT plus anti-PD-1 group compared to RT alone although both expression levels remained within the range of the untreated control group.

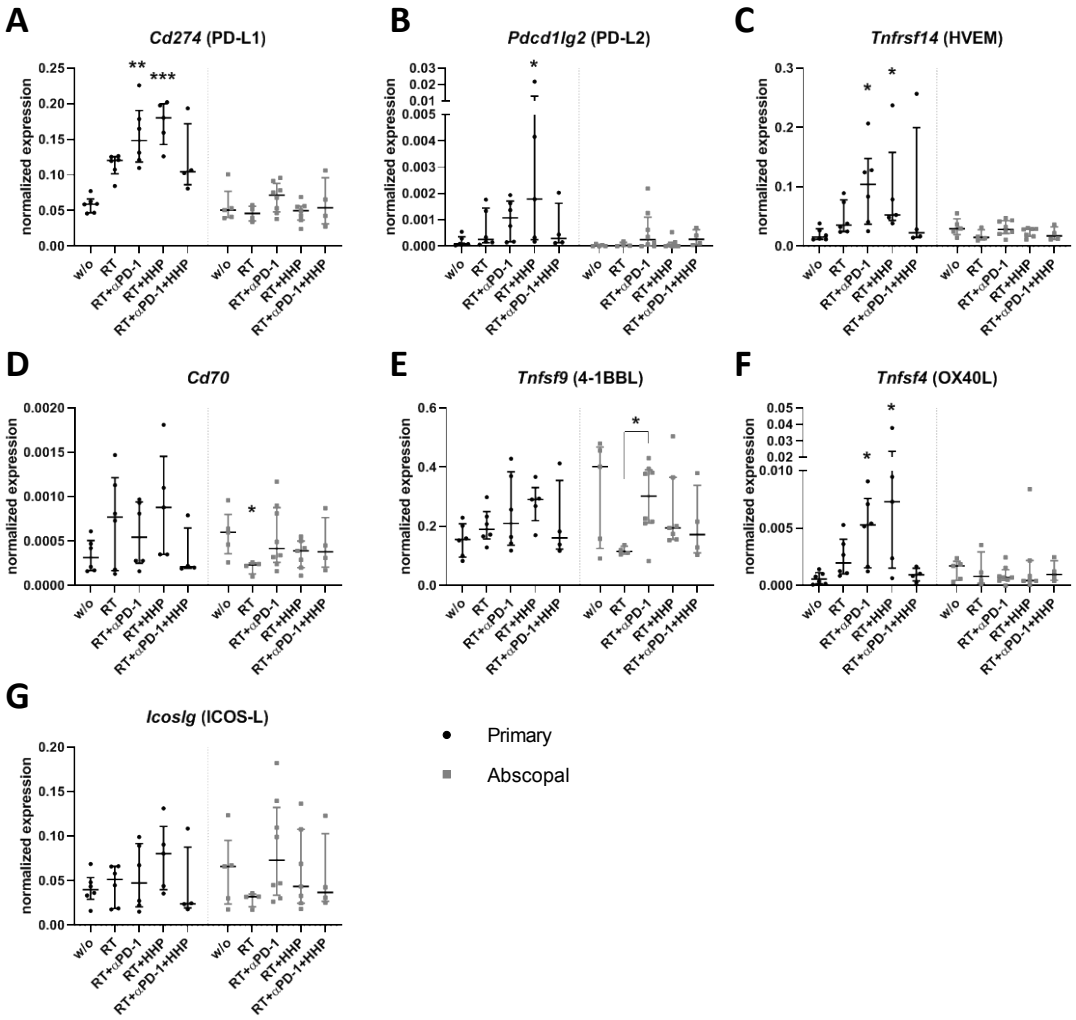

Figure 24: Radioimmunotherapies affect the expression of immune checkpoint ligands in primary tumors. On day 10 after first irradiation of the 2x8 Gy irradiation mice were sacrificed and the primary and abscopal tumors were dissociated. The flow through of the CD45-MACS containing all non-immune cells was collected for qPCR analysis. **A-G**: The expression of *Cd274* (**A**), *Pdcd1lg2* (**B**), *Tnfrsf14* (**C**), *Cd70* (**D**), *Tnfsf9* (**E**), *Tnfsf4* (**F**) and *Icoslg* (**G**) is displayed as normalized expression to the three housekeeping genes *Hprt*, *Tbp* and *Rps18*. Data are presented as median ± interquartile range. A Kruskal-Wallis test with Dunn's correction for multiple testing was used to compare all treatment groups with the untreated control (w/o). Additionally, a Mann-Whitney U test was calculated to compare RT + anti-PD-1 and RT groups; *p < 0.05, **p < 0.01, ***p < 0.001; n = 4-8 animals per group from two independent experiments.

3.2.5 Radioimmunotherapies change the cytokine profiles of primary and abscopal tumors and their serum levels

Cytokines represent another important factor in the tumor microenvironment. To investigate how the combination of each individual immunotherapy with RT modulates the cytokine profile in the tumor and how these influence the infiltration of immune cells, we generated tumor lysates for multiplex-ELISA two days before the immune phenotyping time point on day 8 of the treatment. Additionally, the concentration of those cytokines was analyzed in the serum.

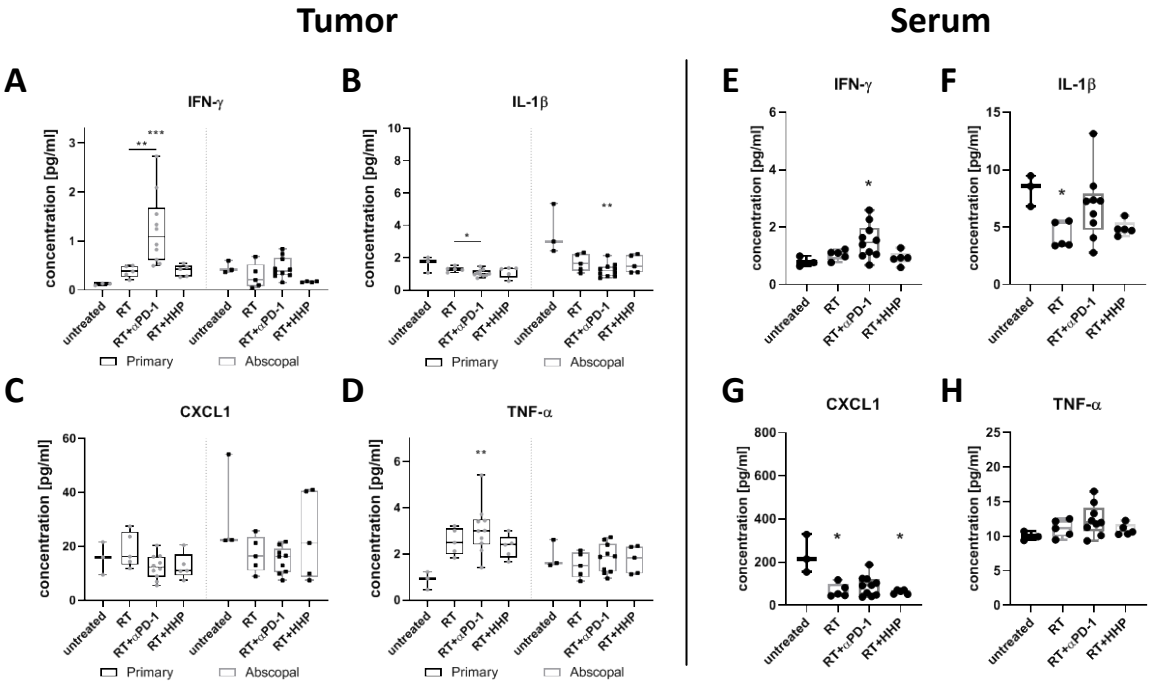

Figure 25: Radioimmunotherapies change the cytokine profils of primary and abscopal tumors and of the serum. On day 8 after first irradiation of the 2x8 Gy irradiation mice were sacrificed for the analysis of cytokines in tumors (**A**-**D**) and the serum (**E**-**H**) with multiplex-ELISA. Data for IFN-γ (**A**, **E**), IL-1β (**B**, **F**), CXCL1 (**C**, **G**) and TNF-α (**D**, **H**) are presented as box plots with whiskers from minimum to maximum values. A Kruskal-Wallis test with Dunn's correction for multiple testing was used to compare the treatment groups with the respective untreated control (w/o). Additionally, a Mann-Whitney U test was calculated to compare RT + anti-PD-1 and RT groups; *p < 0.05, **p < 0.01, ***p < 0.001; n = 3-10 animals per group.

The concentration of IFN-γ and TNF-α was found to be significantly higher in primary tumors of the RT plus anti-PD-1 treatment group than in untreated control tumors (Figure 25A, D). No changes were detected in abscopal tumors. In serum the level of IFN-γ but not TNF-α in the RT plus anti-PD-1 was significantly elevated as well (Figure 25E, H). Although CXCL1 was not regulated in primary and abscopal tumors, significantly less CXCL1 was detected in the serum of mice treated with RT and RT plus HHP vaccine (Figure 25C, G). IL-1β concentrations are decreased in primary and abscopal tumors of all treated mice but most pronounced in the RT plus anti-PD-1 group (Figure 25B). Compared to the untreated control group, IL-1β serum levels were only significantly lower in the RT group (Figure 25F).

3.3 The total number of 8 Gy fractions has impact on tumor control and multiple pathways

3.3.1 Hypofractionated irradiation with 3x8 Gy improves primary tumor control but fails to induce abscopal effects

Not all mice responded to the treatment with RT plus anti-PD-1 and HHP vaccination did not further reduce the abscopal tumor growth. By increasing the total irradiation dose we aimed to set a more potent stimulus for the abscopal anti-tumor immune response resulting in an improved treatment outcome. Therefore, we added another fraction of 8 Gy to the treatment schedule on day 1 (Figure 26A).

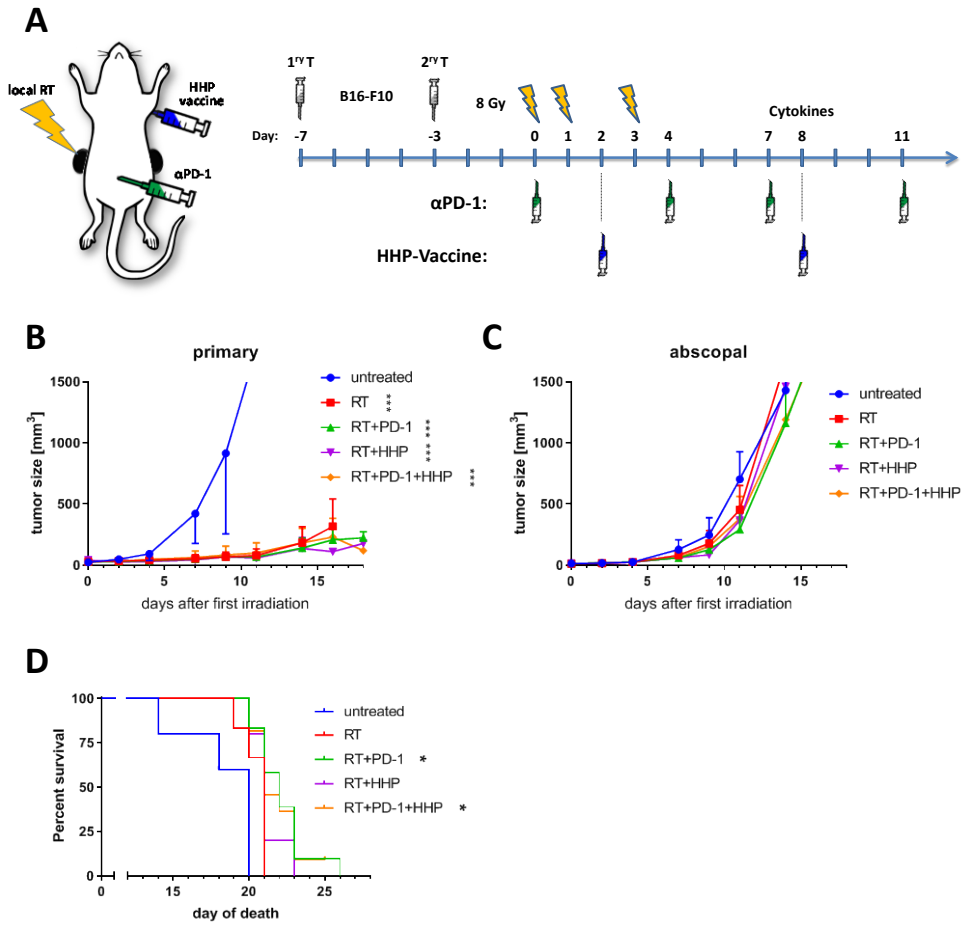

Figure 26: Hypofractionated irradiation with 3x8 Gy improves primary tumor control but fails to induce abscopal effects. **A**: C57Bl/6 mice were subcutaneously injected with $0.2x10^6$ B16-F10 tumor cells into the right flank. Four days afterwards a second tumor was injected on the left flank which later served as the non-irradiated abscopal tumor. The mice received one of the following treatments or combinations thereof. Only the first injected primary tumor was irradiated with 3x8 Gy on d0 seven days after injection and on days one and three. Beginning with the first irradiation on d0 the mice were intraperitoneally injected with 200 µg anti-PD-1 antibody (αPD-1) every three to four days for a total of four injections. Additionally, HHP vaccine ($5x10^6$ cells) was injected twice subcutaneously into the neck on days 2 and 8. The growth of the primary (**B**) and abscopal (**C**) tumors as well as the survival (**D**) was analyzed. For the tumor growth a two-way ANOVA with Geisser-Greenhouse correction was calculated to compare the treatment groups with the untreated control. For the survival a log-rank (Mantel-Cox) test was calculated with Holm-Sidak correction for multiple testing to compare the treatments with the control group. *$p < 0.05$, ***$p < 0.001$; n = 5-12 animals per group from two independent experiments.

3x8 Gy further improved the local tumor control of the primary tumor. However, immunotherapies had no additional effect on the tumor growth (Figure 26B). The abscopal tumor growth was not affected by any treatment (Figure 26C). The survival of the mice was significantly prolonged in the RT plus anti-PD-1 group and with the triple combination compared to untreated control mice.

3.3.2 3x8 Gy has only minor additional effects on cytokine levels in tumor and serum

The addition of another fraction of 8 Gy to the treatment schedule completely abrogated the abscopal effect in the RT plus anti-PD-1 group. Therefore, we wanted to know if the cytokine levels in tumors and in the serum changed compared to 2x8 Gy and analyzed the same cytokine panel as before.

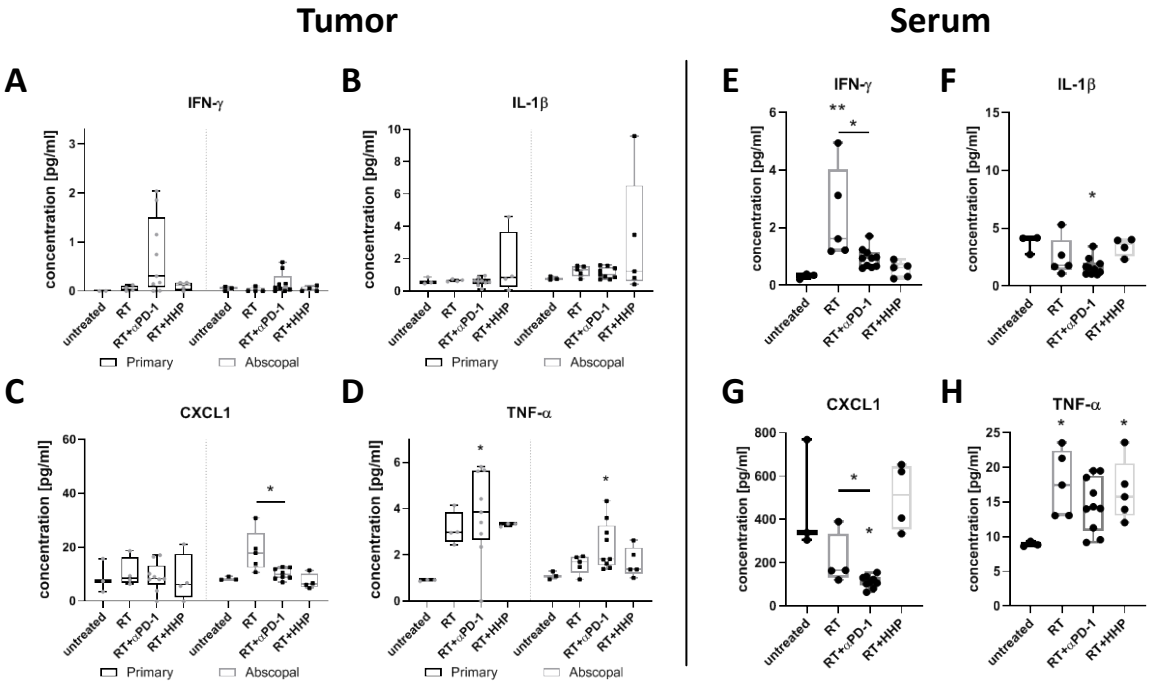

Figure 27: Radioimmunotherapies change the cytokine profils of primary and abscopal tumors and of the serum. On day 8 after first irradiation of the 3x8 Gy irradiation mice were sacrificed for the analysis of cytokines in tumors (**A**-**D**) and the serum (**E**-**H**) with multiplex-ELISA. Data for IFN-γ (**A**, **E**), IL-1β (**B**, **F**), CXCL1 (**C**, **G**) and TNF-α (**D**, **H**) are presented as box plots with whiskers from minimum to maximum values. A Kruskal-Wallis test with Dunn's correction for multiple testing was used to compare the treatment groups with the respective untreated control (w/o). Additionally, a Mann-Whitney U test was calculated to compare RT + anti-PD-1 and RT groups; *p < 0.05, **p < 0.01; n = 3-10 animals per group.

Although the concentration of IFN-γ was higher in some primary tumors after the treatment with RT plus anti-PD-1 no significant changes were observed in any treatment group (Figure 27A). In the serum however, IFN-γ was found in significantly higher concentrations after RT compared to RT plus anti-PD-1 (Figure 27E). IL-1β concentrations in tumors was not regulated,

whereas the concentration in the serum after RT plus anti-PD-1 was significantly lower (Figure 27B, F). Compared to RT alone CXCL1 was significantly less abundant in abscopal tumors and in the serum than after RT plus anti-PD-1 treatment (Figure 27C, G). TNF-α levels in primary tumors after RT and RT plus HPP were elevated and significantly higher in primary and abscopal tumors of the RT plus anti-PD-1 group compared to untreated control tumors (Figure 27D). In the serum the TNF-α concentration was lower in the control group than in any treatment group but only significant for the RT and RT plus HHP group (Figure 27H).

3.3.3 The number of 8 Gy fractions varies cytokine and immune checkpoint ligand expressions

As an additional fraction of 8 Gy did not improve abscopal immune responses but completely abrogated them, we aimed to investigate the impact of various fractions of 8 Gy on cell death, DAMPs, immune checkpoint ligands and cytokine expression *in vitro*. Therefore, B16 cells were irradiated in the same intervals as in the *in vivo* setting or with a single fractions of eight or 20 Gy and were analyzed 24 h after the last irradiation (Figure 28A).

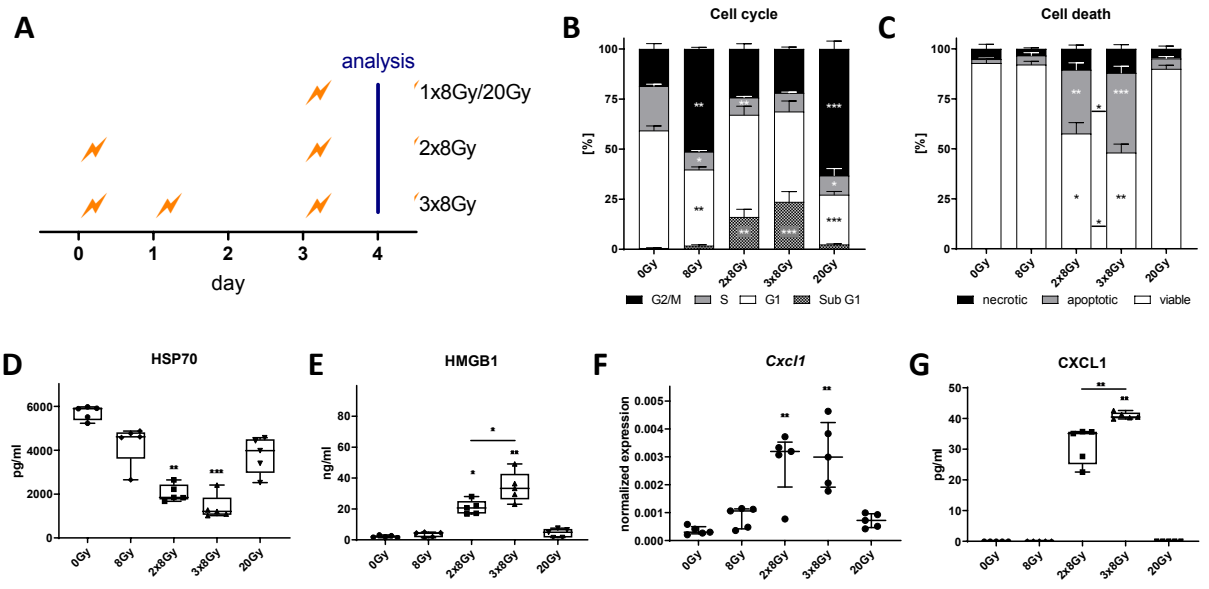

Figure 28: 3x8 Gy increases cell death, cell cycle, DAMP release and CXCL1 expression. A: B16-F10 cells were seeded 16 h before d0. The 2x8 Gy treatment group was irradiated on d0 and d3. One additional fraction of 8 Gy was applied on d1 in the 3x8 Gy group. Single fraction groups were irradiated with 8 Gy or 20 Gy on d3. 24 h after the last irradiation cell-free supernatants were harvested for ELISA and the cells for flow cytometry and qPCR. The cell cycle (**B**) and cell death (**C**) analyses are shown as stacked bar charts showing the mean ± SD. The concentration of the two DAMPs HSP70 (**D**) and HMGB1 (**E**) and CXCl1 (**G**) in the cell culture medium is depicted as box plots with whiskers from minimum to maximum values. The expression of *Cxcl1* (**F**) is displayed as normalized expression (median ± interquartile range) to the three housekeeping genes *Hprt*, *Tbp* and *Rps18*. A Kruskal-Wallis test with Dunn's correction for multiple testing was used to compare the treatment groups with the respective untreated control (0 Gy). Additionally, a Mann-Whitney U test was calculated to compare 2x8 Gy and 3x8 Gy groups; *p < 0.05, **p < 0.01, ***p < 0.001; n=5.

Irradiation of B16 cells with a single dose of either 8 Gy or 20 Gy resulted in a significantly larger proportion of cells in the G2/M phase of the cell cycle (Figure 28B) 24 h after the last irradiation. In contrast, fractionated irradiation led to a significantly higher percentage of cells with degraded DNA (sub-G1). However, there was no significant difference between 2x8 Gy and 3x8 Gy. As detected by AxV/PI staining, only fractionated irradiation induced significant amounts of cell death that was predominantly characterized by apoptosis and was significantly higher after irradiation with 3x8 Gy (Figure 28C). Although the release of the danger signal HSP70 into the cell culture medium was lower after any irradiation scheme than from untreated cells, only fractionated irradiation significantly decreased the concentration in the medium (Figure 28D). The other DAMP HMGB1 was detected only in small amounts in the cell culture medium of untreated and 8 Gy or 20 Gy irradiated cells (Figure 28E). B16 cell released significantly more HMGB1 when irradiated with 3x8 Gy than with 2x8 Gy. In the cell culture medium of non-irradiated and one time irradiated cells CXCL1 was not detectable, even though low level expression was found in qPCR analysis (Figure 28F, G). After fractionated irradiation mRNA expression significantly increased and protein release was detectable by ELISA. Furthermore, CXCL1 was significantly more abundant in the medium of 3x8 Gy than 2x8 Gy irradiated B16 cells.

The surface expression of immune checkpoint ligands after irradiation was analyzed by flow cytometry and qPCR analysis.

Even though untreated B16 already cells express PD-L1 on the cell surface, it is further up-regulated by irradiated cells in general. Especially fractionated irradiation with 3x8 Gy further increases PD-L1 expression significantly more than 2x8 Gy. The same pattern could be confirmed by qPCR analysis (Figure 29I). Although *Pdcd1lg2* (PD-L2) was significantly higher expressed on mRNA level after fractionated irradiation, no changes were found for the surface expression (Figure 29B, J). Furthermore, expression levels detected by both methods were very low. Similar to PD-L1 the highest surface expression of the other two inhibitory immune checkpoint ligands Galectin-9 (Figure 29C) and HVEM (Figure 29D) and the stimulatory counterparts CD70 (Figure 29F), ICOS-L (Figure 29G) and OX40-L (Figure 29H) was found in B16 cells irradiated with 3x8 Gy. Unlike the other checkpoint ligands, 4-1BBL was significantly higher expressed on single dose irradiated cells than on untreated cells and after fractionated irradiation (Figure 29E).

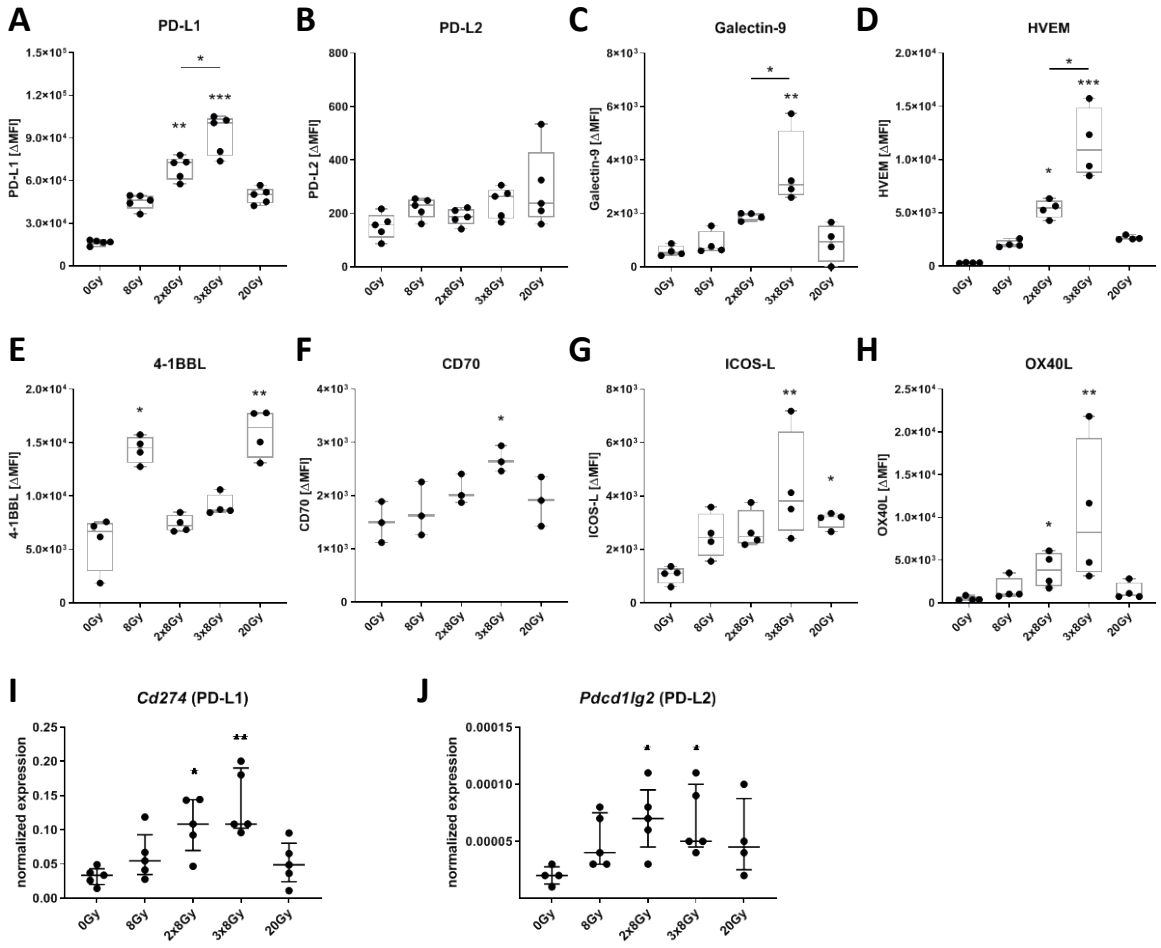

Figure 29: 3x8 Gy increases immune checkpoint ligand expression. B16-F10 cells were seeded 16 h before d0. The 2x8 Gy treatment group was irradiated on d0 and d3. One additional fraction of 8 Gy was applied on d1 in the 3x8 Gy group. Single fraction groups were irradiated with 8 Gy or 20 Gy on d3. 24 h after the last irradiation cells were harvested for flow cytometry and qPCR. **A**-**H**: The autofluorescence corrected ΔMFI (median fluorescence intensity) of PD-L1 (**A**), PD-L2 (**B**), Galectin-9 (**C**), HVEM (**D**), 4-1BBL (**E**), CD70 (**F**), ICOS-L (**G**) and OX40L (**H**) is shown as box plots with whiskers from minimum to maximum values. The expression of *Cd272* (**I**) and *Pdcd1lg2* (**J**) is displayed as normalized expression (median ± interquartile range) to the three housekeeping genes *Hprt*, *Tbp* and *Rps18*. A Kruskal-Wallis test with Dunn's correction for multiple testing was used to compare the treatment groups with the respective untreated control (0 Gy). Additionally, a Mann-Whitney U test was calculated to compare 2x8 Gy and 3x8 Gy groups; *p < 0.05, **p < 0.01, ***p < 0.001; n=3-5.

Vanpouille-Box and colleagues reported that the secretion of IFN-β, which is important for the initiation of anti-tumor immune responses, is mediated by the cGAS/STING pathway. cGAS senses DNA released into the cytosol after irradiation. The exonuclease Trex1 which is expressed after the irradiation at higher doses degrades the cytosolic DNA and thereby inhibits the expression of IFN-β (Vanpouille-Box et al., 2017). We therefore wanted to know if genes of the proteins in this pathway are expressed *in vitro* in B16 cells as well, if they are regulated by the different fractionations and if IFN-β can be found in different concentrations in the tumor lysates of the *in vivo* experiments.

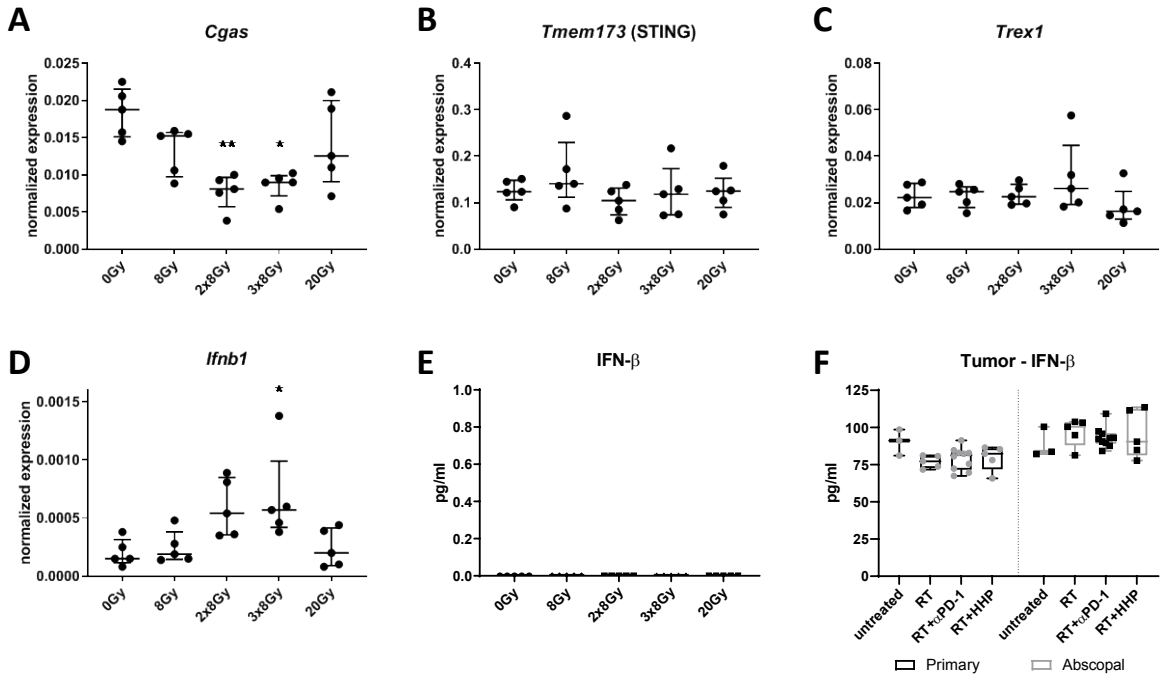

Figure 30 3x8 Gy has no impact on the cGAS/STING related IFN-β pathway. B16-F10 cells were seeded 16 h before d0. The 2x8 Gy treatment group was irradiated on d0 and d3. One additional fraction of 8 Gy was applied on d1 in the 3x8 Gy group. Single fraction groups were irradiated with 8 Gy or 20 Gy on d3. 24 h after the last irradiation cell-free supernatants were harvested for ELISA and the cells qPCR. **A**-**D**: The expression of *Cgas* (**A**), *Tmem173* (**B**), *Trex1* (**C**) and *Ifnb1* (**D**) is displayed as normalized expression (median ± interquartile range) to the three housekeeping genes *Hprt*, *Tbp* and *Rps18*. The concentration of IFN-β in the cell culture medium (**E**) and in tumor lysates (RT = 2x8 Gy) (**F**) is depicted as box plots with whiskers from minimum to maximum values. A Kruskal-Wallis test with Dunn's correction for multiple testing was used to compare the treatment groups with the respective untreated control (0 Gy). Additionally, a Mann-Whitney U test was calculated to compare 2x8 Gy and 3x8 Gy groups; *p < 0.05, **p < 0.01; n=3-5 *in vitro*, n = 3-10 animals per group *in vivo*.

The mRNA expression of *Cgas* was found to be significantly down-regulated after fractionated irradiation with 2x8 Gy and 3x8 Gy (Figure 30A). In contrast, irradiation had no effect on the expression of *Trex1* and *Tmem173* (STING) (Figure 30B, C). Although the expression of *Ifnb1* (Figure 30D) was significantly increased in the cells irradiated with 3x8 Gy compared to the untreated control cells, no IFN-β protein (Figure 30E) could be detected in the cell culture medium. In all irradiated primary tumors IFN-β appeared to be less abundant than in untreated control tumors (Figure 30F). However, those changes were not statistically significant and the different treatment groups did not change the concentrations in the abscopal tumors as well.

3.4 Intra- and extracellular IGFBP-6 has different effects on tumor cell growth

3.4.1 The IGFBP-6 concentration correlates with the response of abscopal tumors to 2x8 Gy plus anti-PD-1 therapy

To gain a broader overview over the cytokine milieu in primary and abscopal tumors after the different radioimmunotherapies (Figure 17), we performed a membrane-based cytokine array. Additionally, we wanted to investigate the difference between abscopal tumors that respond to the treatment with 2x8 Gy and anti-PD-1 and the ones that do not. Therefore, we separated the mice of this treatment for the analysis in two groups defined by the smallest ("responders") and largest abscopal tumors ("non-responders") at the time of analysis.

Almost all of the cytokines were detectable in most of the tumors (Figure 31A). However, IGFBP-6 was the most promising candidate cytokine in terms of different regulation between abscopal tumors of the responder and non-responder group was (Figure 31B). A high level of IGFBP-6 was exclusively detected in abscopal tumors of the 2x8 Gy plus anti-PD-1 responder group. The concentration of IGFBP-6 in individual tumors and additionally in untreated tumors was determined by ELISA and is depicted without differentiation between "responders" and "non-responders" in Figure 31C. Although no significant changes were detected between the treatment groups, the abscopal tumors of the 2x8 Gy plus anti-PD-1 group showed a large spread in the concentration of IGFBP-6. In these tumors the concentration of IGFBP-6 significantly correlated with the tumor weight (Figure 31D): the higher the IGFBP-6 concentration was in the tumors, the smaller was the tumor. In contrast, no correlation was detected for abscopal tumors of mice treated with 3x8 Gy and anti-PD-1 (Figure 31E).

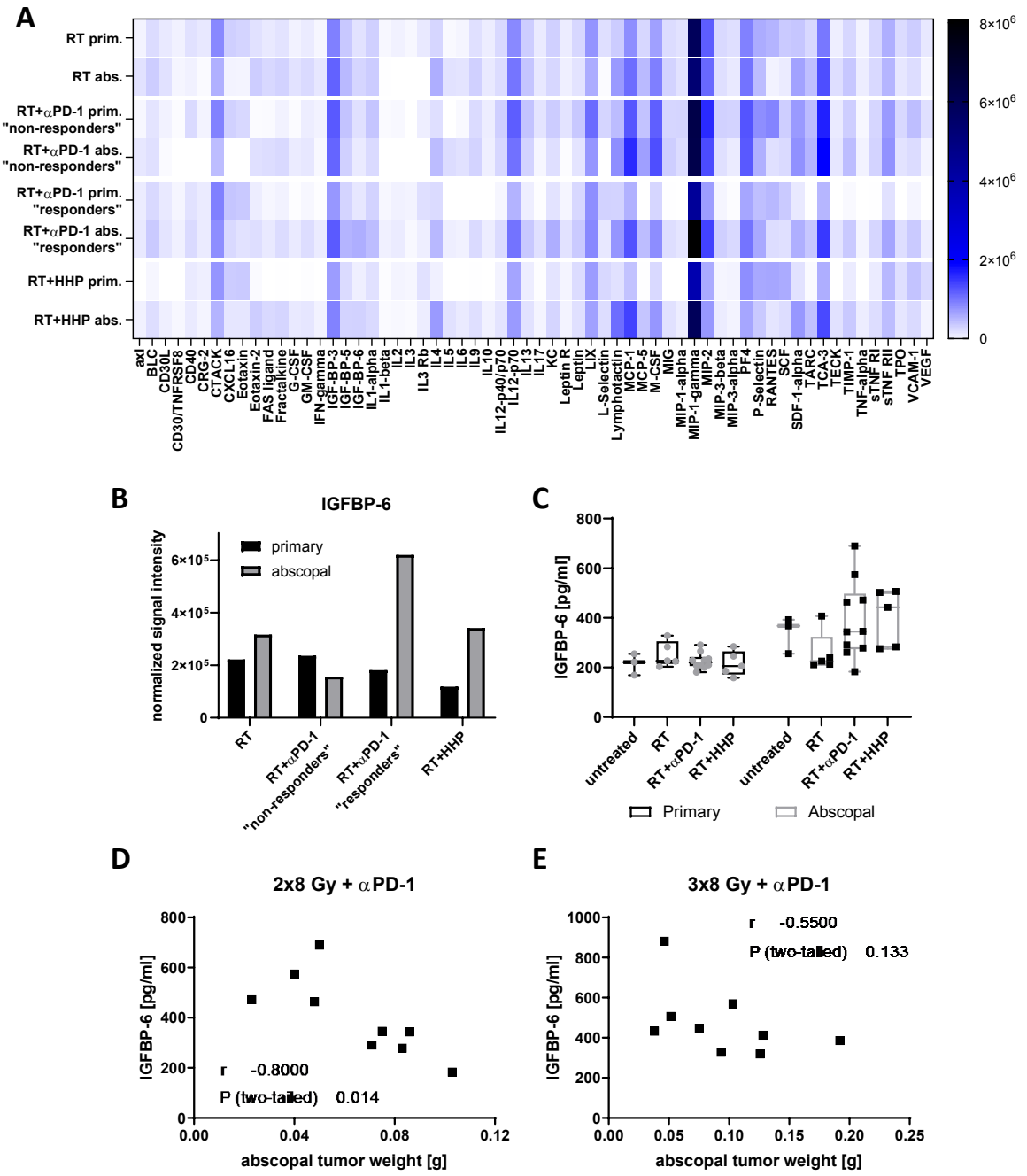

Figure 31: The IGFBP-6 concentration correlates with the response of abscopal tumors to 2x8 Gy plus anti-PD-1 therapy. On day 8 after first irradiation of the 2x8 Gy irradiation tumor lysates were prepared for a membrane-based multiplex cytokine array. Primary and abscopal tumors of the RT, RT + HHP and RT + αPD-1 group were analyzed. Therefore, the lysates of three tumors of each group were pooled. The tumors of the RT + αPD-1 treatment were divided in two groups with the three smallest and the three largest abscopal tumors and were thereby defined as the "responder" and "non-responder" group. The normalized signal intensity of all cytokines is displayed as a heat map (**A**) and the one of IGFBP-6 additionally as a bar graph (**B**). The IGFBP-6 concentrations of individual tumors were determined by ELISA and are presented as box plots with whiskers from minimum to maximum values (**C**). A Spearman correlation was calculated for the concentration of IGFBP-6 with the weight of the abscopal tumor of the RT + αPD-1 treatment group with 2x8 Gy (**D**) or 3x8 Gy (**E**) fractionations.

3.4.2 Extracellular IGFBP-6 hast no impact on the viability of B16 cells

IGFBP-6 binds the insulin-like growth factor 2 (IGF-2) and thereby regulates the availability of IGF-2 for its receptors IGF1R and IGF2R (Liso, Capitanio, Gerli, & Conese, 2018). We wanted to know if the expression of these proteins is altered by ionizing radiation and if there is a difference between irradiation with 2x8 Gy and 3x8 Gy. As before (Figure 28), the experimental set-up was designed according to the *in vivo* irradiation interval. Higher concentrations of IGFBP-6 were found in smaller tumors. Thus, we additionally investigated if IGFBP-6 is released by B16 cells and if it has direct effects on the viability of B16 cells *in vitro*.

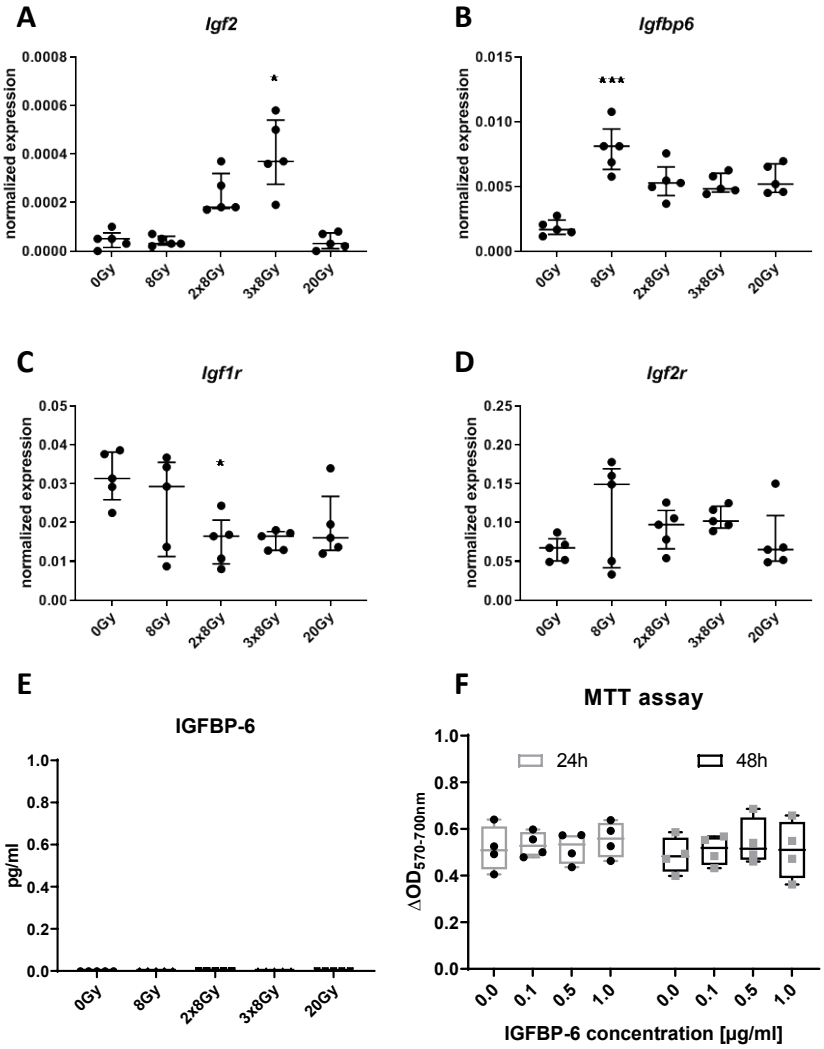

Figure 32: IGFBP-6 is not secreted by irradiated B16 cells and extracellular IGFBP-6 hast no impact on the viability of B16 cells. A-E: B16-F10 cells were seeded 16 h before d0. The 2x8 Gy treatment group was irradiated on d0 and d3. One additional fraction of 8 Gy was applied on d1 in the 3x8 Gy group. Single fraction groups were irradiated with 8 Gy or 20 Gy on d3. 24 h after the last irradiation cell-free supernatants were harvested for ELISA and the cells for qPCR. The expression of *Igf2* (**A**), *Igfbp6* (**B**), *Igf1r* (**C**), and *Igf2r* (**D**) is displayed as normalized expression (median ± interquartile range) to the three housekeeping genes *Hprt*, *Tbp* and *Rps18*. **E**: The concentration of IGFBP-6 in the cell culture medium detected by ELISA is depicted. **F**: B16 cells were seeded in increasing concentrations (0-1 µg/ml) of recombinant IGFBP-6 and the viability/proliferation was analyzed 24 h and 48 h afterwards using an MTT assay. A Kruskal-Wallis test with Dunn's correction for multiple testing was used to compare the treatment groups with the respective untreated control (0 Gy). Additionally, a Mann-Whitney U test was calculated to compare 2x8 Gy and 3x8 Gy groups; *p < 0.05, **p < 0.01, ***p < 0.001; n=4-5

Only fractionated irradiation with 2x8 Gy or 3x8 Gy increased the expression of *Igf2* but higher expression levels were found after the irradiation with 3x8 Gy (Figure 32A). Although *Igfbp6* was expressed on mRNA level and the expression was significantly higher after irradiation especially with 8 Gy as a single dose (Figure 32B), IGFBP-6 could not be detected in the cell culture medium under any treatment condition (Figure 32E). Fractionated irradiation and a high single dose of 20 Gy lowered the expression of *Igf1r* (Figure 32C). In contrast, the expression of *Igf2r* was not significantly changed (Figure 32D).

3.4.3 IGFBP-6 knockdown delays tumor growth in vivo and induces cell death in vitro

IGFBP-6 did not exhibit a direct inhibitory effect on B16 cells *in vitro*. Hence, we wanted to know if the absence of IGFBP-6 affects the abscopal tumor growth *in vivo*. As high concentrations of IGFBP-6 in abscopal tumors correlated with a good abscopal response only after treatment with 2x8 Gy plus anti-PD-1 we hypothesized that siRNA mediated knockdown of IGFBP-6 would abrogate the abscopal effect just like with a 3x8 Gy fractionation. We treated mice with 2x8 Gy and anti-PD-1 and injected Igfbp6 or negative control siRNA into abscopal tumors (Figure 33A).

Intratumoral injection of Igfbp6 siRNA into abscopal tumors had no effect on the primary tumor growth (Figure 33B). However, IGFBP-6 knockdown significantly delayed the tumor growth of the abscopal tumor compared to control siRNA (Figure 33C). The protein level of IGFBP-6 in abscopal tumors and in the serum was not affected by the siRNA knockdown 4 days after siRNA injection (Figure 33D, E).

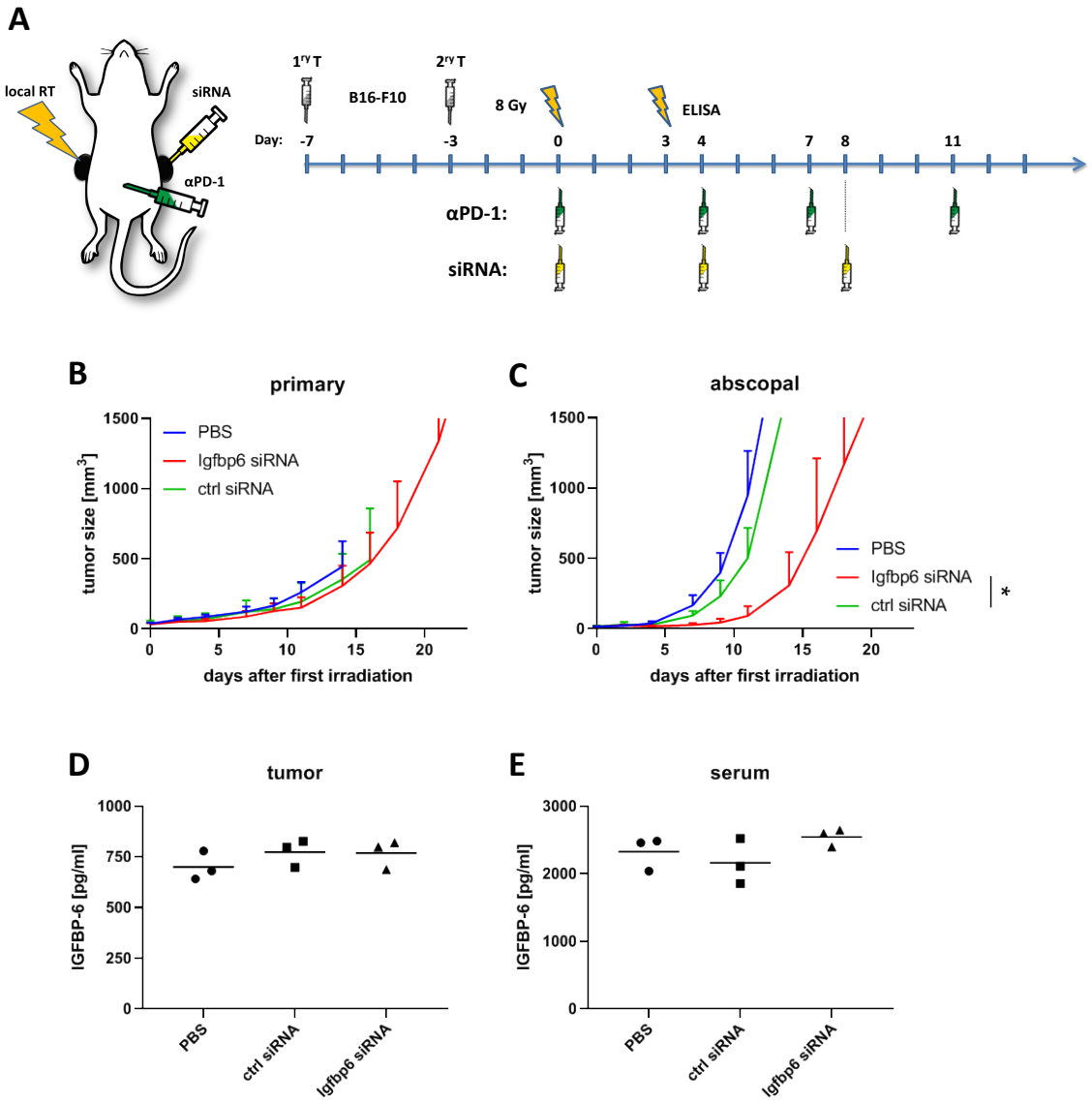

Figure 33: IGFBP-6 knockdown delays the growth of abscopal tumors *in vivo*. **A**: C57Bl/6 mice were subcutaneously injected with 0.2x10^6 B16-F10 tumor cells into the right flank. Four days afterwards a second tumor was injected on the left flank which later served as the non-irradiated abscopal tumor. Only the first injected primary tumor was irradiated with 2x8 Gy on d0 seven days after injection and on d3. Beginning with the first irradiation on d0 the mice were intraperitoneally injected with 200 µg anti-PD-1 antibody (αPD-1) every three to four days for a total of four injections. 2.5 nmol Igfbp6 siRNA, 2.5 nmol negative control siRNA (ctrl siRNA) or PBS was administered via intratumoral injection into abscopal tumors on days 0, 4 and 8. The growth of the primary (**B**) and abscopal (**C**) tumors was analyzed and is shown as mean ± SD. For the tumor growth a two-way ANOVA with Geisser-Greenhouse correction and Dunnett's multiple comparisons test was calculated to compare the treatment groups with the ctrl siRNA group. The concentration of IGFBP-6 in lysates of abscopal tumors (**D**) and in the serum (**E**) detected by ELISA is depicted. *p < 0.05; n = 5-12 animals per group from two independent experiments.

To investigate if the siRNA knockdown of IGFBP-6 has a direct effect on the proliferation or viability of B16 cells we performed IGFBP-6 knockdown *in vitro*. Because the siRNA knockdown did not reduce the IGFBP-6 protein concentration in the tumors *in vivo* we additionally wanted to check if the knockdown works *in vitro* and thereby rule out that the observed results were only due to off-target effects of the siRNA.

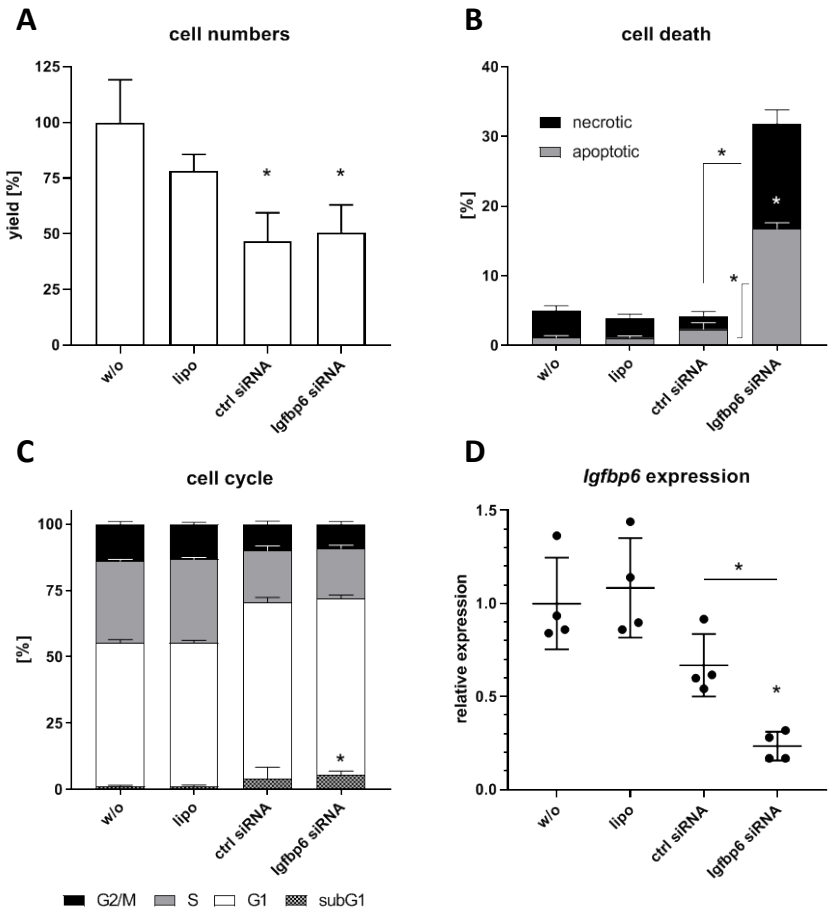

Figure 34: IGFBP-6 knockdown induces cell death *in vitro*. 5x10^4 B16 cells were seeded and incubated with a final concentration of 10 nM Igfbp6 siRNA, 10 nM negative control siRNA (ctrl siRNA), only the Lipofectamine transfection reagent (lipo), or medium (w/o). After 48 h the cells were harvested for flow cytometry and qPCR. **A**: The total cell count was normalized to the untreated medium control and is presented. The cell death (**B**) and cell cycle (**C**) analyses are shown as stacked bar charts. **D**: The mRNA expression of *Igfbp6* was normalized the housekeeping gene *Rps18* and the untreated control (ΔΔCq). All data are presented as mean ± SD. A Kruskal-Wallis test with Dunn's correction for multiple testing was used to compare the treatment groups with the respective untreated control (w/o). Additionally, a Mann-Whitney U test was calculated to compare ctrl siRNA and Igfbp6 siRNA groups; *p < 0.05; n=4

Addition of the transfection reagent alone already reduced the harvested cell numbers by about 25 %. Both, ctrl siRNA and Igfbp6 siRNA further decreased the cell numbers significantly to about 50 % compared to the untreated control (Figure 34A). However, only Igfbp6 siRNA induced apoptotic and necrotic cell death to a statistically significant extent (Figure 33B). Cells treated with siRNA showed a slightly higher proportion of cells in the G1 phase of the cell cycle (Figure 33C). In comparison to untreated cells incubation with Igfbp6 siRNA led to a significantly higher percentage of cells with degraded DNA (sub-G1). The mRNA expression of *Igfbp6* was significantly reduced by the Igfbp6 siRNA to about 20 % of the level in untreated cells (Figure 33D).

4. Discussion

4.1 HHP vaccines are safe and synergize with RT to retard tumor growth by modulating the tumor microenvironment

Using autologous whole tumor cells as a cancer vaccine has the advantage to provide all relevant patient-specific tumor antigens that do not have to be identified in advance. However, besides its advantage regarding its immunogenicity, one major aspect of such a vaccine would be its safety (Weiss et al., 2012). High hydrostatic pressure treatment with 200 MPa has been demonstrated to be an appropriate way to inactivate human cancer cell lines and to activate DCs when they take up HHP killed tumor cells (Frey et al., 2004; Fucikova et al., 2014). Applying pressure of at least 200 MPa also fully inactivated B16 melanoma cells and thereby prevented the formation of tumors after injection of the vaccine into mice (Figure 13). A fully computer-controlled and monitored system, such as the one we used (Figure 4), can guarantee the reproducibility of the tumor cell inactivation and vaccine generation process.

Unlike neoantigens, tumor-associated antigens, which are aberrantly expressed self-antigens, need to break self-tolerance to activate low affinity T cells, thus vaccines would require repeated immunization or adjuvants and co-stimulation (Hollingsworth & Jansen, 2019). Hradilova et al. have recently shown that HHP vaccines of human lung cancer cell lines profit from the adjuvant poly(I:C) to mature monocyte-derived DCs from NSCLC patients which subsequently activated tumor antigen-specific CD4+ and CD8+ T cells *in vitro* (Hradilova et al., 2017). The same group has demonstrated that DCs pulsed with HHP-killed prostate cancer cells retard orthotopic tumor growth as efficiently as chemotherapy (Mikyskova et al., 2016). Further, they currently test HHP-treated tumor cells as therapeutic cancer vaccines in clinical trials (NCT03657966, NCT02470468, NCT02111577) where they load monocyte-derived DCs (MoDCs) from patients with HHP-treated allogeneic tumor cell lines (DCVAC) *ex vivo* followed by the injection of these pulsed DCs back into the patient. We hypothesized that with the induction of ICD and its immunostimulatory properties, RT similarly acts as an adjuvant and co-stimulant. Therefore, we followed a different vaccination approach where we directly injected HHP-killed tumor cells alone in syngeneic mice thus mimicking an autologous vaccination targeted to DCs *in vivo* without the addition of any adjuvant and combined it with RT instead. In contrast to the DCVAC approach, this would obviate the need for the generation of MoDCs which have been used almost exclusively in many clinical trials for cancer vaccines because they were the only DC subtype producible *in vitro* in adequate numbers and under clinical-grade conditions (Tacken, de Vries, Torensma, & Figdor, 2007; Wimmers, Schreibelt, Skold, Figdor, & De Vries, 2014; Garg, Coulie, Van den Eynde, & Agostinis, 2017). However, in contrast to other DC subtypes (i.e. conventional type 1 DCs) MoDCs have limited capabilities to migrate to lymph nodes

and are prone to become immunosuppressive and thus, in most of the cases, adoptive cell transfer of MoDCs in clinical trials achieved only disappointing results (Cancel, Crozat, Dalod, & Mattiuz, 2019).

Whole tumor cell vaccines in general might suffer from a kind of antigen dilution effect as immunogenic tumor antigens are provided along all other normal self-antigens of the tumor cells (Hu et al., 2018). Indeed, HHP vaccine monotherapy had no effect on the growth of B16 melanomas. In the combined treatment however, HHP vaccine synergized with RT to significantly exceed RT induced tumor growth retardation and prolonged survival (Figure 14). To exclude a melanoma-specific effect, we conducted the experiment additionally with the CT26 colon carcinoma model and observed the same synergism, albeit the response to the combined treatment was more heterogeneous (Figure 16).

To date it is unknown which specific T cell numbers are needed for effective cancer vaccination and they probably vary between antigens, T cell receptor affinity and, tumor type (Hollingsworth & Jansen, 2019). Thus we analyzed the concentration and quality of tumor-infiltrating immune cells following RT and vaccination by immune phenotyping. In tumors treated with both, irradiation and vaccination, leukocytes in general were found in significantly higher concentrations (Figure 15) which is generally associated with good prognosis for most solid tumors (Vano, Petitprez, Giraldo, Fridman, & Sautes-Fridman, 2018), including melanoma (Saldanha, Flatman, Teo, & Bamford, 2017). However, a variety of immune cells of the innate and adaptive immune system were detected which can have diverse effects on tumor progression. B cells were the only cell type that was significantly reduced in irradiated tumors. Their role in melanoma is not clear yet, as B cell infiltration is partly associated with good prognosis but in other studies with tumor progression and lymph node metastases (Selitsky et al., 2019; Helmink et al., 2020). The concentration of some immune cells was not affected by the treatments whereas monocytes/macrophages, T cells, NKT cells and NK cells made up the group of significantly more abundant cells infiltrating tumors of the combined treatment. The latter have been shown to be the important mediators of anti-tumor immunity in a humanized melanoma model (Ferrari de Andrade et al., 2018) and we previously demonstrated that NK cell depletion after immunization led to a significantly accelerated melanoma growth (Finkel et al., 2016). NKT cells are not only important cells in tumor immunosurveillance but also stimulators of innate and adaptive immune cells in the tumor microenvironment (Krijgsman, Hokland, & Kuppen, 2018). All of the T cell subsets we analyzed were more abundant after RT combined with the HHP vaccine. Similarly, in experiments with immunocompetent mice They et al. demonstrated that CD8+, CD4+ and γδ T cells infiltrate B16 melanomas once the tumor microenvironment is modulated in a favorable way by immunotherapy (They et al., 2017). However, effector subtypes of those cells showed an exhausted phenotype of PD-1 and TIM-3 expression in the tumor which could be restored by anti-PD-1 treatment. In our experiment the majority of CD8+

T cells and after irradiation also the majority of CD4+ T cells expressed PD-1 on the surface while PD-1+ T cells were almost absent in the blood. That the tumor microenvironment drives the upregulation of PD-1 is also indicated by an enrichment of PD-1+ T cells found in tumors of patients with metastatic disease (Ahmadzadeh et al., 2009). Nevertheless, PD-1 expression can also be a sign of effectively primed T cell responses may be regarded as an activation marker as exhausted T cells are only a subset of PD-1+ T cells (Wei, Duffy, & Allison, 2018). Tumor-specific CD8+ T cells were shown to be enriched in the population of PD1+ T cells in the blood of patients with melanoma (Gros et al., 2016). Fernandez-Poma et al. adoptively transferred T cells selected for positive or negative PD-1 expression in mice bearing solid tumors (Fernandez-Poma et al., 2017). Only the fraction of PD-1+ T cells exhibited anti-tumor reactivity and the tumor growth was further inhibited by anti-PD-1 treatment.

Taken together, these results highlight high hydrostatic pressure treatment as a suitable method to reproducibly inactivate tumor cells for the preparation of safe whole tumor cell vaccines. HHP vaccines are well-combinable with RT and together induce anti-tumor immune responses irrespective of the tumor type by modulating the tumor microenvironment. Furthermore, the high proportion of PD-1+ T cells in tumors suggests a triple-combination with ICIs.

4.2 HHP-vaccines act systemically but only on previously irradiated tumors and fail to improve RT + anti-PD-1 induced abscopal responses

Based on the synergistic effect of RT and HHP vaccination we observed when injecting the vaccine peritumorally, we aimed to investigate if HHP vaccines can induce systemic immune responses after injection distant to the tumor. For this, we used an abscopal tumor model where we injected one tumor on each flank of the mouse and irradiated only one of the tumors (Figure 17A). Ohlfest et al. demonstrated in a murine glioma model that the anti-tumor immune response was more effective the farther away from the tumor they injected the vaccine. This was dictated by the presence of the tumor itself as the T cell priming efficiency was irrespective of the injection site in tumor-free mice (Ohlfest et al., 2013). These limitations can be explained by the immunosuppressive microenvironment of tumor draining lymph nodes mediated by Tregs and cytokines, in which tumor antigens are cross-presentation leads to tolerization (Munn & Mellor, 2006). Additionally, repeated injection has been proven to be beneficial to break self-tolerance with appropriate adjuvants. In another pre-clinical experiment we demonstrated that repeated immunization with tumor cells that had been killed by RT in combination with heat is superior to single vaccination (Finkel et al., 2016). Therefore, we injected the HHP vaccine in the abscopal model twice and distant from the tumors

subcutaneously in the neck. It was previously shown in animal models that doses per fraction of about 8 Gy are immunogenic and synergize with ICIs to induce local and abscopal anti-tumor immune responses (Schaue et al., 2012; Vanpouille-Box et al., 2017; X. Zhang & Niedermann, 2018). Therefore, we have chosen to increase the dose per fraction to 8 Gy in this treatment schedule and combined RT and HHP vaccination with further immune checkpoint inhibition using monoclonal anti-PD-1 antibodies in a concomitant treatment as suggested by the pre-clinical trial of Dovedi et al. (Dovedi et al., 2014).

Irradiation with 2x8 Gy achieved considerable local tumor control but did not induce abscopal effects (Figure 17B). Although injected distantly from the tumor, the HHP vaccine further delayed the tumor growth of the primary irradiated but not the abscopal tumor. The primary tumor response to RT plus anti-PD-1 was similar to RT plus HHP. However, the tumor growth retardation was not further improved in the triple combination. Abscopal effects in the non-irradiated tumors were observed with RT and anti-PD-1 but the response was heterogeneous with responders and non-responders. Surprisingly, the addition of the HHP vaccine partly abrogated the abscopal response. In accordance with the single tumor model, immune phenotyping of primary tumors revealed that the concentration of immune cells was increased after radioimmunotherapies, especially after RT plus anti-PD-1 (Figure 18B). This combination with the most pronounced abscopal effects was the only treatment in which the concentration of CD45+ cells was also increased significantly in abscopal tumors. These results suggest that first, HHP vaccines act systemically, but only when the tumor microenvironment is modulated by previous irradiation of the tumor. Second, as also observed for many immune cell subtypes (Figure 18-20), the concentrations of the triple combination resembles more the RT plus HHP treatment rather than RT plus anti-PD-1, indicating that the vaccination is somehow dominant and that the outcome of combining multiple (immuno)therapies is not necessarily the sum of their individual effects.

4.3 RT plus anti-PD-1 induced abscopal anti-tumor immune responses are associated with an increased infiltration of CD8+ T cells

In the literature, tumor-infiltrating immune cells are almost exclusively presented as a concentration of cells per gram of tumor or as a percentage of a parent population. Looking at the total number of immune cells in primary and abscopal tumors (Figure 18A) however suggests that an increased concentration (Figure 18B) is not always equivalent to a higher infiltration of those immune cells into the tumor after a certain treatment. While we observed elevated concentrations of leukocytes in primary irradiated tumors and an even significantly higher one when anti-PD-1 was added, total numbers dropped after RT and seemed to even further decrease with vaccination. In a

melanoma model it was found that when a peptide vaccine was injected together with incomplete Freund's adjuvant to form an antigen depot the T cells were attracted to the site of vaccination and not to the tumor resulting in impaired tumor control (Yared Hailemichael et al., 2013). At the site of HHP vaccine injection usually a nodule can be seen for several days probably consisting of residual tumor cells (not shown), indicating that the vaccine might be encapsulated instead of cleared by phagocytes and APCs. Similar to the results of Hailemichael et al., T cells, including most of the subsets and especially NKT cells, were the only cell type of which the concentration in primary tumors was negatively affected by vaccination (Figure 18I, Figure 19A, D, G). Peritumoral injection of the vaccine in the single tumor model might have bypassed this problem as in this case, T cells were among those that were significantly more abundant after combined treatment (Figure 15I). Why distant injection of HHP vaccines still improved the control of locally irradiated tumors even though T cell infiltration was impaired remains to be investigated. With regard to the dynamic of the T cell infiltration into tumors (Frey, Rückert, Weber, et al., 2017) one could speculate that this is a matter of the time point of analysis. Although not significant, T cell concentrations in abscopal tumors tended to be lower than those in the untreated group which corroborates the hypothesis that T cells are sequestered by HHP vaccine depots.

Additionally to the lower immune cell numbers in irradiated tumors, most of the immune cells decreased in the peripheral blood after RT as well (Figure 23). Leukopenia and impaired functionality of lymphocytes, monocytes and neutrophils has also been reported during and after RT of patients with cervical, rectal, oral and breast cancer (van Meir et al., 2017; Dovsak et al., 2018; Y. J. Lee et al., 2018). Further, from the conditioning of patients suffering from hematologic malignancies for bone marrow transplantation with total body irradiation it is known that RT is very immunosuppressive and toxic for immune cells (Paix et al., 2018). Therefore, immune cells have long been considered to be upon the most radiosensitive cells in the body and indeed, we have previously shown *ex vivo* that human immune cells are susceptible even for single doses of ionizing radiation but the radiosensitivity differs between immune cell types. Monocytes appeared to be the most resistant cell type while lymphocytes and NK cells died even after irradiation with doses typically used for the irradiation of tumors. However, even at higher doses T cells were not fully eradicated suggesting that the surviving fraction could still exert their tumor killing activity even after irradiation (Falcke et al., 2018). Arina et al. investigated this issue in a very elegant *in vivo* setting using a mouse model where they differently labeled T cells in the tumor and in the periphery to discriminate pre-existing T cells from those that newly infiltrated after RT. In accordance with our results they found that fractionated irradiation or a high single dose decimated pre-existing T cells in the tumor but the majority remained viable and new T cells infiltrated after RT. However, they have shown that these newly tumor-infiltrating T cells contribute to the anti-tumor immune response but pre-existing

irradiated T cells can do so as well. Blocking the egress of T cells from lymph nodes with FTY720 just before RT and thereby also the subsequent infiltration into tumors had no negative impact on the tumor growth. Although the proliferative capacity of the surviving T cells was diminished, they retained their motility and produced even more IFN-γ than non-irradiated T cells (A. Arina et al., 2019). Activated and memory T cells have been shown to be more radioresistant than naïve T cells (P. L. Dunn & North, 1991; Grayson, Harrington, Lanier, Wherry, & Ahmed, 2002) and Arina et al. additionally found TGF-β in the tumor microenvironment to contribute to the resistance of tumor infiltrating T cells (A. Arina et al., 2019). We conclude that although ionizing radiation is harmful for immune cells, the net outcome for the tumor control after IR is positive as it increases the functionality of surviving or newly infiltrating leukocytes and provides the basis for efficient immunotherapies.

In contrast to primary tumors, the significantly higher concentration of CD45+ cells in the abscopal tumors of the RT plus anti-PD-1 group was accompanied with a higher total number. The higher concentrations in the primary tumors therefore likely originated from an enhanced tumor growth inhibition or tumor cell killing by RT and immune cells which decreases the tumor cells to a greater extent than the immune cells. However, this does not exclude that there is no infiltration after RT at all. Abscopal tumors of RT plus anti-PD-1 in contrast seem to show a true immune cell infiltration as both, total numbers and concentration increased. These newly infiltrating immune cells largely consisted of monocytes/macrophages (Figure 20C), DCs (Figure 20A) and T cells (Figure 18I) of which CD8+ T cells were the main subset (Figure 19G). According to their main function as phagocytes, APCs and effector cells, respectively, one could assume that infiltrating CD8+ T cells first killed tumor cells and this cell death subsequently attracted both other cell types. In line with our findings, the success of immune checkpoint blockade with anti-PD-1 in basal or squamous cell carcinoma patients was mediated by novel T cell clones which had not been present in the same tumors before (Yost et al., 2019), underlining the different mechanisms in abscopal and primary irradiated tumors.

Equivalent to the single tumor model the percentage of PD-1+ T cells in the tumors was high (Figure 19E, H). The minority of CD4+ T cells in untreated primary and all abscopal tumors expressed PD-1 but this percentage was significantly increased after RT. For CD8+ T cells the proportion was already high in untreated tumors but was further elevated upon irradiation. CD62L is another marker of T cell activation and effector functions. In a melanoma model Yang et al. demonstrated that CD62L which is found on naïve T cells is shedded upon T cell activation and is associated with lytic activity (S. Yang, Liu, Wang, Rosenberg, & Morgan, 2011). In our model, the percentage of CD4+ and CD8+ T cells negative for CD62L significantly increased in irradiated tumors (Figure 19F, I) indicating increased T cell functionality.

In primary and abscopal tumors of mice treated with RT and anti-PD-1 we detected significantly higher concentrations of DCs than in untreated or solely irradiated tumors (Figure 20A). All irradiated primary tumors, and especially those where anti-PD-1 was added, were further enriched for CD11b- DCs (Figure 20B). This subset of DCs can be referred to as conventional type 1 DCs (cDC1s) which are specialized to cross-present antigen to CD8+ T cells and stimulate NK, NKT and CTLs by producing high amounts of IL-12 (Cancel et al., 2019). In the tumor microenvironment cDC1s are associated with the recruitment of effector CD8+ T cells and thus better prognosis for several tumor entities (Broz et al., 2014). Further, in pre-clinical trials cDC1s have been shown to be essential for the treatment with ICIs as the treatment efficacy is abrogated in cDC1 deficient $Batf3^{-/-}$ mice (Spranger & Gajewski, 2015; Sanchez-Paulete et al., 2016). As cDC1s express receptors specific for the recognition of dead and dying cells (Audsley, McDonnell, & Waithman, 2020) they might not only be important to initiate CTL responses in irradiated tumors where ICD is induced but might also be required for the cross-presentation of HHP vaccines and could be targets for further improvements of those vaccines.

TAMs are generally thought to contribute to tumor progression and immunosuppression by various mechanisms such as supporting metastasis, angiogenesis or T cell inhibition (Jiang, Li, & Zhu, 2015). Some subsets however, are associated with good prognosis. Etzerodt et al. classified three different monocyte and macrophage subsets in the TME based on their Ly6-C and MHC-II expression. These are monocytes (MN), immature TAMs (iTAM) and mature TAMs (mTAM) which contained a very suppressive CD163+ TAMs subset. In a melanoma model tumor infiltrating MNs were polarized towards immunosuppressive mTAMs. Depletion of these CD163+ cells resulted in increased infiltration of iTAMs which had an inflammatory phenotype and subsequently activated T cells were attracted to promote tumor regression (Etzerodt et al., 2019). Similar to CD163+ mTAM depletion RT and anti-PD-1 significantly shifted the balance towards more iTAMs and less mTAM in primary tumors (Figure 20D-F).

Both, monocytes/macrophages and DCs were found together with CD8+ T cells in higher concentrations in tumors with abscopal responses. This might indicate that first CTLs, which were primed in consequence of irradiation of the primary tumor and checkpoint inhibition, infiltrated into abscopal tumors and killed tumor cells as seen by reduced tumor growth. Subsequently tumor cell death might have attracted these phagocytes and APCs.

The most abundant cell type found in untreated primary tumors were neutrophils followed by monocytes/macrophages and T cells (Figure 21). Abscopal tumors which were injected four days after the primary tumor were infiltrated by less neutrophils and T cells but more monocytes/macrophages DCs and NK cells. Comparable immune cell compositions for untreated B16 tumors at about the same time point after tumor injection have been found by others as well

(Courau et al., 2016). Irradiation of primary tumors changed the immune cell composition drastically. Monocytes/macrophages were now, by far, the dominant cell type and NK cell percentages markedly expanded whereas B cells and neutrophils largely disappeared. Further immunotherapies had little impact on this composition. Only minor changes in abscopal tumors across all treatment groups were observed compared to the untreated controls. This indicates that RT is the main stimulus that changes the immunological tumor microenvironment on the cellular level.

As the response of abscopal tumors to RT plus anti-PD-1 was quite heterogeneous we analyzed which cell types might contribute to abscopal responses by correlating the immune cell concentrations with the weight of the abscopal tumor (Figure 22). Additionally to the generally increased infiltration of monocytes/macrophages and T cells in those tumors, higher concentrations of monocytes/macrophages and the γδ, NKT and CD4+ T cell subsets correlated with good abscopal responses (lower tumor weight) in those tumors. In contrast, B cell numbers positively correlated with abscopal tumor growth. Thus, immune cells seem to have differential roles in abscopal responses even though functional tests are missing.

In line with the *in vitro* results for the immune checkpoint ligands (Figure 29), RT up-regulated the expression of PD-L1, HVEM and OX40L in primary but not abscopal tumors (Figure 24). Adding either of both immunotherapies further enhanced this effect. Similarly, Dovedi et al. showed that PD-L1 was significantly more abundant on tumor cells of CT26 tumors up to seven days after fractionated RT in combination with anti-PD-L1. *In vitro* they found that the surface expression was dependent on IFN-γ and could be further increased with TNF-α (Dovedi et al., 2014). Both are cytokines which we found in higher concentrations in tumor lysates of primary tumors treated with RT or RT plus anti-PD-1 (Figure 25).

In conclusion, tumor growth retardation of locally irradiated primary tumors was accompanied by changes of the immunological microenvironment. The total number of immune cells per tumor was reduced mainly by the elimination of B cells and neutrophils. Although the addition of either HPP vaccines or anti-PD-1 did not change immune cell numbers, primary tumor growth was further reduced. Immunotherapies thus seem to have improved the functionality of immune cells present in the tumors. In contrast, the most prominent difference which we observed between abscopal tumors of treatment combinations that failed to elicit abscopal effects and RT plus anti-PD-1 was the elevated CD8+ T cell infiltration. Other changes in immune cell infiltration, cytokine milieu and immune checkpoint ligand expression were rather small. This suggests that among all effector cells, including NK cells and the other T cell subsets which we investigated, only CD8+ T cells mediated abscopal responses and that these are probably newly infiltrating cells rather than pre-existing ones.

4.4 The sum of small changes in the immunological and oncogenic phenotype and cytokine secretion of B16 cells after irradiation with an additional fraction of 8 Gy (3x8 Gy) abrogates abscopal effects

Albeit the local tumor control of primary irradiated tumors was improved by adding another fraction of 8 Gy, the abscopal anti-tumor immune responses we observed when we treated mice with 2x8 Gy and anti-PD-1 (Figure 17) were completely abrogated using 3x8 Gy (Figure 26). To investigate the underlying mechanism on the tumor cell level we used the same irradiation schedules *in vitro* compared to a single irradiation with 8 Gy or a single high dose (20 Gy) and analyzed the cell death, DAMPs and cytokine secretion, immune checkpoint expression and the cGAS/STING pathway. Cell death in 3x8 Gy irradiated B16 cells was higher than with 2x8 Gy which was characterized by a significantly increased rate of apoptosis (Figure 28B-C). The phagocytosis of apoptotic cells was shown to polarize macrophages towards an immunosuppressive phenotype (W. J. Zhang & Zheng, 2005) and thus contributes to tumor progression (Werfel et al., 2019). As one of the best known DAMPs and characteristics of ICD, HMGB1 is a potent stimulus for immune responses (Kang, Zhang, Zeh, Lotze, & Tang, 2013). The release of HMGB1 by irradiated tumor cells that we have detected especially with 3x8 Gy (Figure 28E), was however shown to promote proliferation of living tumor cells (He et al., 2018). CXCL1, a chemokine originally identified in melanoma, is associated with oncogenesis, tumor progression and metastasis across several tumor entities (C. Yang et al., 2019) by recruiting tumor-associated neutrophils (Yuan et al., 2016). Moreover, CXCL1 expression was reported to be higher in immunotherapy-resistant tumor cell clones (Li et al., 2018). *Cxcl1* expression was low in B16 cells but increased upon fractionated irradiation (Figure 28F) and only there CXCL1 could be detected in the cell culture supernatant in significant higher amounts with 3x8 Gy (Figure 28G). In the serum of patients with colorectal cancer CXCL1 is a predictive marker for lung and liver metastases (Divella et al., 2017). Although tumor levels were not affected by the different treatments (Figure 25C, Figure 27C) we found significantly lower serum concentrations of CXCL1 in most of the mice that had been treated with 2x8 Gy or 3x8 Gy with or without additional immunotherapies (Figure 25G, Figure 27G). Albeit ionizing radiation, administered either fractionated or as a single dose, increased the surface expression of most of the immune checkpoint ligands on B16 cells, it were predominantly the immunosuppressive ones (PD-L1, Galectin-9 and HVEM) that were up-regulated. Further, the very same were significantly higher after 3x8 Gy compared to 2x8 Gy whereas no differences between both fractionations were found for the stimulatory ligands 4-1BBL, CD70, ICOS-L and OX40L (Figure 29), in sum indicating a more suppressive tumor cell phenotype at 3x8 Gy. Additionally, we detected higher IFN-γ levels in tumors irradiated with 2x8 Gy plus anti-PD-1 checkpoint inhibition (Figure 25A) than in the counterparts irradiated with 3x8 Gy (Figure 27A). IFN-γ

has been found to be a predictive marker for the efficiency of radiotherapy in a murine model (Gerber et al., 2013) and breast cancer patients (Weichselbaum et al., 2008) as well as anti-PD-1 therapy in multiple tumor entities including melanoma (Ayers et al., 2017; Karachaliou et al., 2018). Vanpouille-Box et al. reported that upon irradiation (e.g. 3x8 Gy) DNA is released into the cytosol of the cell which is sensed by the cGAS/STING pathway and ultimately leads to the secretion of the inflammatory cytokine IFN-β. If the dose is too high (e.g. 20 Gy) however the exonuclease Trex1 is expressed and degrades cytosolic DNA and thereby shuts down the type I IFN response (Vanpouille-Box et al., 2017). Therefore, we have investigated this pathway and compared the fractionated schedule to a single dose of 20 Gy. While *Ifnb1* expression on mRNA level was significantly increased in B16 cells irradiated with 3x8Gy, no IFN-β could be detected in the cell culture supernatant at any condition and the cytokine level inside the tumor *in vivo* was not affected by any treatment (Figure 30), suggesting that this pathway does not play a role in B16 melanoma.

Although most of the differences between irradiation with 2x8 Gy and 3x8 Gy *in vitro* and *in vivo* were significant, the absolute changes were however little and so far no further experiments were conducted to clarify the importance of each mechanism. Nevertheless, these effects eventually might sum up and together contribute to the failure of 3x8 Gy to elicit abscopal effects. In the work by Zhang et al. a comparable irradiation scheme with 3x9.18 Gy plus anti-PD-1 checkpoint inhibition was able to induce abscopal anti-tumor immune responses in the B16-CD133 model. When they used the B16 wildtype model without exogenous antigen however, similar to ours results, no abscopal effects were observed (X. Zhang & Niedermann, 2018).

4.5 Knockdown of IGFBP-6 expression but not extracellular IGFBP-6 induces tumor cell death in B16 melanomas *in vitro* and *in vivo*

The deregulation of insulin-like growth factors (IGFs), which are essential for normal growth and development, is associated with diseases, such as neurodegeneration, diabetes or cancer. Migration, proliferation and survival of several cell types is influenced by binding of IGF-I and IGF-II to their receptors, including IGF-IR and IGF-IIR and many cancers overexpress IGF-II. The availability of IGFs is regulated by a family of six IGF binding proteins (IGFBP-1-6). IGFBP-6 has a much higher affinity for IGF-II than for IGF-I and therefore primarily regulates mitosis, proliferation and survival in an IGF-II dependent manner. In many adult and pediatric cancers IGFBP-6 was demonstrated to inhibit tumor growth and survival. However, IGF-independent actions on proliferation and apoptosis have been shown for IGFBP-6 as well. The role of IGFBP-6 in tumors and its cellular source is however largely unknown (Reviewed by (Liso et al., 2018)).

We detected similar concentrations of IGFBP-6 in tumor lysates of irradiated primary as well as abscopal tumors. Only in abscopal tumors of the 2x8 Gy plus anti-PD-1 group we found a correlation of a high IGFBP-6 concentration with a smaller tumor mass, representing those mice with good abscopal responses (Figure 31). Therefore, we wanted to know if IGFBP-6-related proteins are expressed in B16 cells and if IGFBP-6 has direct effects on the tumor cells. B16 cells expressed both IGF-II receptors IGF-IR and IGF-IIR, but IGF-II only to a small extent after fractionated irradiation (Figure 32A, C, D). IGFBP-6 was expressed on mRNA level in untreated B16 melanoma cells and even higher after irradiation but no extracellular protein could be detected under any condition in the cell culture supernatant by ELISA, indicating that the tumor cells are not the source of intratumoral IGFBP-6 (Figure 32B, E). Single-cell RNA-Seq data of B16 tumors, which are available in the Single Cell Expression Atlas, reveal that IGFBP-6 (ENSMUSG00000023046) is highly expressed by a subset of cancer-associated fibroblasts (Davidson et al., 2018a, 2018b). The addition of recombinant IGFBP-6 to the cell culture had no impact on B16 growth and survival, as detected by a MTT assay (Figure 32F). In contrast, although similar IGFBP-6 mRNA expression was detected in TS/A mammary carcinoma cells, protein was released especially after fractionated irradiation (data not shown). However, also these cells did not respond to the addition of IGFBP-6 (data not shown). These results suggest that no direct effect of extracellular IGFBP-6 on B16 cell growth or survival is responsible for the smaller tumor mass with higher IGFBP-6 concentrations.

IGBP-3, 5 and 6 have nuclear localization sequences and overexpression of IGFBP-6 led to apoptosis in rhabdomyosarcoma cells independent of IGF-II (Iosef, Gkourasas, Jia, Li, & Han, 2008). Very recently, Zhao et al. found a correlation of decreased IGFBP-6 expression with poor survival in patients with colorectal cancer and an increased migration, proliferation and invasion *in vitro* (C. Zhao et al., 2020). Additionally, Kuo et al. reported that overexpression of IGFBP-6 increased apoptosis in nasopharyngeal carcinoma cells and suppressed their proliferation, invasion and metastatic activity (Kuo, Tang, Lu, Wu, & Lin, 2010). These results indicate a putative role as a tumor suppressor gene. Further, *in vitro* IGFBP-6 was shown to have chemoattractant features towards monocytes, T cells and neutrophils (Liso et al., 2017; Conese et al., 2018). To address these mechanisms we performed *in vivo* knockdown of IGFBP-6 by injecting siRNA into abscopal tumors of mice treated with 2x8 Gy plus anti-PD-1 which should abrogate the abscopal effect. Surprisingly, IGFBP-6 knockdown resulted in delayed tumor growth and did not diminish protein levels in the tumor (Figure 33A-D). As IGFBP-6 in humans is found in cerebrospinal fluid and serum (Levitt Katz, Rosenfeld, & Cohen, 1995) we also checked serum levels and detected high concentrations unaffected by the knockdown (Figure 33E), indicating that intratumoral IGFBP-6 levels might be replenished by serum IGFBP-6 after the knockdown. *In vitro* transfection of B16 and TS/A cells with the siRNA confirmed the successful IGFBP-6 knockdown and although control siRNA inhibited the

proliferation as well, only Igfbp6 siRNA led to significant amounts of apoptosis and necrosis (Figure 34, data not shown). Cell death induction and reduced proliferation upon IGFBP-6 knockdown was also reported for human fibroblasts (Micutkova et al., 2011). Thus, knockdown experiments argue against IGFBP-6 as a tumor suppressor gene in melanoma and mammary carcinoma tumor models.

In conclusion, there might be two different mechanisms for IGFBP-6 underlying our results. *In vitro* and IGFBP-6 knockdown experiments suggest intracellular actions of IGFBP-6 involved in cell survival. However, these results are contradictory to our initial finding that high concentrations in tumor lysates were associated with smaller tumors. Extracellular IGFBP-6 had no direct inhibitory effect on B16 cells *in vitro* but other IGF-II independent mechanisms, such as attraction of immune cells cannot be excluded.

4.6 Conclusions and outlook

Altogether, our results highlight high hydrostatic pressure as a safe method to generate whole tumor cell vaccines. Potent anti-tumor immune responses are elicited across different tumor entities by combining radiotherapy with HHP vaccines which can be either injected peritumorally or at distant sites. However, in the abscopal tumor model, HHP vaccines had systemic effects only on previously irradiated tumors. Furthermore, vaccination partly abrogated abscopal effects induced by RT and anti-PD-1 checkpoint inhibition, indicating that both immunotherapies act through different mechanisms which negatively influence each other. These limitations might be overcome in the future by improving HHP vaccines with adjuvants such as poly(I:C) (Cicchelero, de Rooster, & Sanders, 2014) or anti-CTLA-4 to aid in the priming of CTLs (Y. Hailemichael et al., 2018).

Urbanova et al. have previously shown that antigens start to degrade after the treatment with HHP (Urbanova et al., 2017). So far, we generate the vaccine one day prior to the injection. Immediate injection or preservation of the pressurized cells until injection might further improve the immunogenicity of the vaccine. The amount of cells injected might be another point for optimization. To prevent the formation of a depot which redirects T cell to the injection site instead of the tumor, injecting less HHP treated cells might ensure that the vaccine is taken up completely. Conventional type 1 DCs which we found to be more abundant in irradiated tumors, are becoming increasingly recognized for their importance to prime and activate CD8+ T cells by the uptake and cross-presentation of tumor antigens (Audsley et al., 2020). Direct targeting of those cells or relocating the injection point to a peritumoral injection of the vaccine after irradiation, a point where cDC1s are already present, might additionally improve HHP vaccine efficiency.

Initially we hypothesized that primary and abscopal tumors of different treatment groups differ in their tumor microenvironment. Indeed, we found that RT has great impact on the immune

cell composition, immune checkpoint expression, and the cytokine milieu in primary tumors and even in the peripheral blood. Abscopal tumors however were not changed by RT alone. Although the addition of HHP vaccines ameliorated primary tumor growth retardation, no further changes were observed. In contrast, anti-PD-1 mostly amplified RT-mediated effects in primary tumors. The latter combination of RT plus anti-PD-1 was the only treatment which had an effect on the abscopal tumor microenvironment which was characterized by the infiltration of CD8+ T cells, monocytes/macrophages and DCs. These results suggest that the immunotherapies profit from the RT-induced TME modulations but instead of pure infiltration of immune cells in general or specific subsets it is rather a functional alteration of pre-existing or newly infiltrating immune cells that mediate the improved anti-tumor immune response. In the future we will thus focus on the activation status and functionality of immune cells to further investigate the underlying mechanisms of local tumor control and abscopal effects induced by RIT combinations. As we have previously shown, immune cell infiltration upon irradiation is a very dynamic process (Frey, Rückert, Weber, et al., 2017). Looking at earlier time points after RIT might give further insight into the time course of local and abscopal anti-tumor immune responses.

Finally, although we could not find a causative mechanism for the correlation of high intratumoral IGFBP-6 levels with abscopal responses, targeting of intracellular IGFBP-6 expression might emerge as new strategy for the treatment of melanoma.

VI. References

Abuodeh, Y., Venkat, P., & Kim, S. (2016). Systematic review of case reports on the abscopal effect. *Curr Probl Cancer, 40*(1), 25-37. doi:10.1016/j.currproblcancer.2015.10.001

Adkins, I., Hradilova, N., Palata, O., Sadilkova, L., Palova-Jelinkova, L., & Spisek, R. (2018). High hydrostatic pressure in cancer immunotherapy and biomedicine. *Biotechnol Adv, 36*(3), 577-582. doi:10.1016/j.biotechadv.2018.01.015

Ahmadzadeh, M., Johnson, L. A., Heemskerk, B., Wunderlich, J. R., Dudley, M. E., White, D. E., & Rosenberg, S. A. (2009). Tumor antigen-specific CD8 T cells infiltrating the tumor express high levels of PD-1 and are functionally impaired. *Blood, 114*(8), 1537-1544. doi:10.1182/blood-2008-12-195792

Albini, A., Bruno, A., Noonan, D. M., & Mortara, L. (2018). Contribution to Tumor Angiogenesis From Innate Immune Cells Within the Tumor Microenvironment: Implications for Immunotherapy. *Front Immunol, 9*, 527. doi:10.3389/fimmu.2018.00527

Arina, A., Beckett, M., Fernandez, C., Zheng, W., Pitroda, S., Chmura, S. J., ..., Weichselbaum, R. R. (2019). Tumor-reprogrammed resident T cells resist radiation to control tumors. *Nat Commun, 10*(1), 3959. doi:10.1038/s41467-019-11906-2

Arina, A., Gutiontov, S. I., & Weichselbaum, R. R. (2020). Radiotherapy and immunotherapy for cancer: From "systemic" to "multi-site". *Clinical Cancer Research*. doi:10.1158/1078-0432.Ccr-19-2034

Asur, R., Butterworth, K. T., Penagaricano, J. A., Prise, K. M., & Griffin, R. J. (2015). High dose bystander effects in spatially fractionated radiation therapy. *Cancer Lett, 356*(1), 52-57. doi:10.1016/j.canlet.2013.10.032

Audsley, K. M., McDonnell, A. M., & Waithman, J. (2020). Cross-Presenting XCR1(+) Dendritic Cells as Targets for Cancer Immunotherapy. *Cells, 9*(3). doi:10.3390/cells9030565

Ayers, M., Lunceford, J., Nebozhyn, M., Murphy, E., Loboda, A., Kaufman, D. R., ..., McClanahan, T. K. (2017). IFN-gamma-related mRNA profile predicts clinical response to PD-1 blockade. *J Clin Invest, 127*(8), 2930-2940. doi:10.1172/JCI91190

BfS. (2019). Was ist ionisierende Strahlung? Access date 13.02.2020 from https://www.bfs.de/DE/themen/ion/einfuehrung/einfuehrung_node.html

Boonyaratanakornkit, B. B., Park, C. B., & Clark, D. S. (2002). Pressure effects on intra- and intermolecular interactions within proteins. *Biochim Biophys Acta, 1595*(1-2), 235-249. doi:10.1016/s0167-4838(01)00347-8

Borst, J., Ahrends, T., Babala, N., Melief, C. J. M., & Kastenmuller, W. (2018). CD4(+) T cell help in cancer immunology and immunotherapy. *Nat Rev Immunol, 18*(10), 635-647. doi:10.1038/s41577-018-0044-0

Brown, J. A., Dorfman, D. M., Ma, F. R., Sullivan, E. L., Munoz, O., Wood, C. R., ..., Freeman, G. J. (2003). Blockade of programmed death-1 ligands on dendritic cells enhances T cell activation and cytokine production. *J Immunol, 170*(3), 1257-1266. doi:10.4049/jimmunol.170.3.1257

Broz, M. L., Binnewies, M., Boldajipour, B., Nelson, A. E., Pollack, J. L., Erle, D. J., ..., Krummel, M. F. (2014). Dissecting the tumor myeloid compartment reveals rare activating antigen-presenting cells critical for T cell immunity. *Cancer Cell, 26*(5), 638-652. doi:10.1016/j.ccell.2014.09.007

Cancel, J. C., Crozat, K., Dalod, M., & Mattiuz, R. (2019). Are Conventional Type 1 Dendritic Cells Critical for Protective Antitumor Immunity and How? *Front Immunol, 10*, 9. doi:10.3389/fimmu.2019.00009

Cerwenka, A., Baron, J. L., & Lanier, L. L. (2001). Ectopic expression of retinoic acid early inducible-1 gene (RAE-1) permits natural killer cell-mediated rejection of a MHC class I-bearing tumor in vivo. *Proc Natl Acad Sci U S A, 98*(20), 11521-11526. doi:10.1073/pnas.201238598

Chakravarty, P. K., Alfieri, A., Thomas, E. K., Beri, V., Tanaka, K. E., Vikram, B., & Guha, C. (1999). Flt3-Ligand Administration after Radiation Therapy Prolongs Survival in a Murine Model of Metastatic Lung Cancer. *Cancer Research, 59*(24), 6028.

Chen, D., Xie, J., Fiskesund, R., Dong, W., Liang, X., Lv, J., ..., Huang, B. (2018). Chloroquine modulates antitumor immune response by resetting tumor-associated macrophages toward M1 phenotype. *Nat Commun, 9*(1), 873. doi:10.1038/s41467-018-03225-9

Chen, D. S., & Mellman, I. (2013). Oncology meets immunology: the cancer-immunity cycle. *Immunity, 39*(1), 1-10. doi:10.1016/j.immuni.2013.07.012

Cicchelero, L., de Rooster, H., & Sanders, N. N. (2014). Various ways to improve whole cancer cell vaccines. *Expert Rev Vaccines, 13*(6), 721-735. doi:10.1586/14760584.2014.911093

Conese, M., D'Oria, S., Castellani, S., Trotta, R., Montemurro, P., & Liso, A. (2018). Insulin-like growth factor-6 (IGFBP-6) stimulates neutrophil oxidative burst, degranulation and chemotaxis. *Inflamm Res, 67*(2), 107-109. doi:10.1007/s00011-017-1107-6

Courau, T., Nehar-Belaid, D., Florez, L., Levacher, B., Vazquez, T., Brimaud, F., ..., Klatzmann, D. (2016). TGF-beta and VEGF cooperatively control the immunotolerant tumor environment and the efficacy of cancer immunotherapies. *JCI Insight, 1*(9), e85974. doi:10.1172/jci.insight.85974

Dagoglu, N., Karaman, S., Caglar, H. B., & Oral, E. N. (2019). Abscopal Effect of Radiotherapy in the Immunotherapy Era: Systematic Review of Reported Cases. *Cureus, 11*(2), e4103. doi:10.7759/cureus.4103

Davidson, S., Efremova, M., Riedel, A., Mahata, B., Pramanik, J., Huuhtanen, J., ..., Teichmann, S. A. (2018a). Single-cell RNA sequencing reveals a dynamic stromal niche within the evolving tumour microenvironment. *bioRxiv*, 467225-467225. doi:10.1101/467225

Davidson, S., Efremova, M., Riedel, A., Mahata, B., Pramanik, J., Huuhtanen, J., ..., Teichmann, S. A. (2018b). Single-cell RNA sequencing reveals a dynamic stromal niche within the evolving tumour microenvironment. Access date 25.02.2020 from https://www.ebi.ac.uk/gxa/sc/experiments/E-EHCA-2/results/tsne?geneId=ENSMUSG00000023046&colourBy=metadata&metadata=inferred_cell_type

Deloch, L., Derer, A., Hartmann, J., Frey, B., Fietkau, R., & Gaipl, U. S. (2016). Modern Radiotherapy Concepts and the Impact of Radiation on Immune Activation. *Front Oncol, 6*, 141. doi:10.3389/fonc.2016.00141

Demaria, S., & Formenti, S. C. (2020). The abscopal effect 67 years later: from a side story to center stage. *Br J Radiol*, 20200042. doi:10.1259/bjr.20200042

Demaria, S., Kawashima, N., Yang, A. M., Devitt, M. L., Babb, J. S., Allison, J. P., & Formenti, S. C. (2005). Immune-Mediated Inhibition of Metastases after Treatment with Local Radiation and CTLA-4 Blockade in a Mouse Model of Breast Cancer. *Clinical Cancer Research, 11*(2), 728.

Demaria, S., Ng, B., Devitt, M. L., Babb, J. S., Kawashima, N., Liebes, L., & Formenti, S. C. (2004). Ionizing radiation inhibition of distant untreated tumors (abscopal effect) is immune mediated. *Int J Radiat Oncol Biol Phys, 58*(3), 862-870. doi:10.1016/j.ijrobp.2003.09.012

Derer, A., Spiljar, M., Bäumler, M., Hecht, M., Fietkau, R., Frey, B., & Gaipl, U. S. (2016). Chemoradiation Increases PD-L1 Expression in Certain Melanoma and Glioblastoma Cells. *Front Immunol, 7*, 610. doi:10.3389/fimmu.2016.00610

Dewan, M. Z., Galloway, A. E., Kawashima, N., Dewyngaert, J. K., Babb, J. S., Formenti, S. C., & Demaria, S. (2009). Fractionated but not single-dose radiotherapy induces an immune-mediated abscopal effect when combined with anti-CTLA-4 antibody. *Clin Cancer Res, 15*(17), 5379-5388. doi:10.1158/1078-0432.CCR-09-0265

Diehl, P., Reuning, U., Gollwitzer, H., Magdolen, U., Gerdesmeyer, L., Schauwecker, J., ..., Schmitt, M. (2004). Effect of extracorporal high hydrostatic pressure on tumor cell adherence and viability. *Oncol Rep, 12*(2), 369-373.

Diehl, P., Schauwecker, J., Mittelmeier, W., & Schmitt, M. (2008). High hydrostatic pressure, a novel approach in orthopedic surgical oncology to disinfect bone, tendons and cartilage. *Anticancer Res, 28*(6B), 3877-3883.

Divella, R., Daniele, A., R, D. E. L., Simone, M., Naglieri, E., Savino, E., ..., Ranieri, G. (2017). Circulating Levels of VEGF and CXCL1 Are Predictive of Metastatic Organotropismin in Patients with Colorectal Cancer. *Anticancer Res, 37*(9), 4867-4871. doi:10.21873/anticanres.11895

Dovedi, S. J., Adlard, A. L., Lipowska-Bhalla, G., McKenna, C., Jones, S., Cheadle, E. J., ..., Illidge, T. M. (2014). Acquired resistance to fractionated radiotherapy can be overcome by concurrent PD-L1 blockade. *Cancer Res, 74*(19), 5458-5468. doi:10.1158/0008-5472.CAN-14-1258

Dovsak, T., Ihan, A., Didanovic, V., Kansky, A., Verdenik, M., & Hren, N. I. (2018). Effect of surgery and radiotherapy on complete blood count, lymphocyte subsets and inflammatory response in patients with advanced oral cancer. *BMC Cancer, 18*(1), 235. doi:10.1186/s12885-018-4136-9

Dunn, G. P., Old, L. J., & Schreiber, R. D. (2004). The three Es of cancer immunoediting. *Annu Rev Immunol, 22*, 329-360. doi:10.1146/annurev.immunol.22.012703.104803

Dunn, P. L., & North, R. J. (1991). Selective radiation resistance of immunologically induced T cells as the basis for irradiation-induced T-cell-mediated regression of immunogenic tumor. *J Leukoc Biol, 49*(4), 388-396. doi:10.1002/jlb.49.4.388

Dyck, L., & Mills, K. H. G. (2017). Immune checkpoints and their inhibition in cancer and infectious diseases. *Eur J Immunol, 47*(5), 765-779. doi:10.1002/eji.201646875

Etzerodt, A., Tsalkitzi, K., Maniecki, M., Damsky, W., Delfini, M., Baudoin, E., ..., Lawrence, T. (2019). Specific targeting of CD163 + TAMs mobilizes inflammatory monocytes and promotes T cell–mediated tumor regression. *The Journal of Experimental Medicine, 216*(10), 2394-2411. doi:10.1084/jem.20182124

Falcke, S. E., Ruhle, P. F., Deloch, L., Fietkau, R., Frey, B., & Gaipl, U. S. (2018). Clinically Relevant Radiation Exposure Differentially Impacts Forms of Cell Death in Human Cells of the Innate and Adaptive Immune System. *Int J Mol Sci, 19*(11). doi:10.3390/ijms19113574

Fernandez-Poma, S. M., Salas-Benito, D., Lozano, T., Casares, N., Riezu-Boj, J. I., Mancheno, U., ..., Hervas-Stubbs, S. (2017). Expansion of Tumor-Infiltrating CD8(+) T cells Expressing PD-1 Improves the Efficacy of Adoptive T-cell Therapy. *Cancer Res, 77*(13), 3672-3684. doi:10.1158/0008-5472.CAN-17-0236

Ferrari de Andrade, L., Tay, R. E., Pan, D., Luoma, A. M., Ito, Y., Badrinath, S., ..., Wucherpfennig, K. W. (2018). Antibody-mediated inhibition of MICA and MICB shedding promotes NK cell-driven tumor immunity. *Science, 359*(6383), 1537-1542. doi:10.1126/science.aao0505

Fife, B. T., & Bluestone, J. A. (2008). Control of peripheral T-cell tolerance and autoimmunity via the CTLA-4 and PD-1 pathways. *Immunol Rev, 224*, 166-182. doi:10.1111/j.1600-065X.2008.00662.x

Finkel, P., Frey, B., Mayer, F., Bosl, K., Werthmoller, N., Mackensen, A., ..., Ullrich, E. (2016). The dual role of NK cells in antitumor reactions triggered by ionizing radiation in combination with hyperthermia. *Oncoimmunology, 5*(6), e1101206. doi:10.1080/2162402X.2015.1101206

Freeman, G. J., Long, A. J., Iwai, Y., Bourque, K., Chernova, T., Nishimura, H., ..., Honjo, T. (2000). Engagement of the PD-1 immunoinhibitory receptor by a novel B7 family member leads to negative regulation of lymphocyte activation. *J Exp Med, 192*(7), 1027-1034. doi:10.1084/jem.192.7.1027

Frey, B., Franz, S., Sheriff, A., Korn, A., Bluemelhuber, G., Gaipl, U. S., ..., Herrmann, M. (2004). Hydrostatic pressure induced death of mammalian cells engages pathways related to apoptosis or necrosis. *Cell Mol Biol (Noisy-le-grand), 50*(4), 459-467.

Frey, B., Janko, C., Ebel, N., Meister, S., Schlucker, E., Meyer-Pittroff, R., ..., Gaipl, U. S. (2008). Cells under pressure - treatment of eukaryotic cells with high hydrostatic pressure, from physiologic aspects to pressure induced cell death. *Curr Med Chem, 15*(23), 2329-2336. doi:10.2174/092986708785909166

Frey, B., Rubner, Y., Kulzer, L., Werthmoller, N., Weiss, E. M., Fietkau, R., & Gaipl, U. S. (2014). Antitumor immune responses induced by ionizing irradiation and further immune stimulation. *Cancer Immunol Immunother, 63*(1), 29-36. doi:10.1007/s00262-013-1474-y

Frey, B., Rückert, M., Deloch, L., Rühle, P. F., Derer, A., Fietkau, R., & Gaipl, U. S. (2017). Immunomodulation by ionizing radiation-impact for design of radio-immunotherapies and for treatment of inflammatory diseases. *Immunol Rev, 280*(1), 231-248. doi:10.1111/imr.12572

Frey, B., Rückert, M., & Gaipl, U. S. (2019). Immune Modulatory Effects of Radiotherapy. In *Radiation Oncology* (pp. 1-12).

Frey, B., Rückert, M., Weber, J., Mayr, X., Derer, A., Lotter, M., ..., Gaipl, U. S. (2017). Hypofractionated Irradiation Has Immune Stimulatory Potential and Induces a Timely Restricted Infiltration of Immune Cells in Colon Cancer Tumors. *Front Immunol, 8*, 231. doi:10.3389/fimmu.2017.00231

Fucikova, J., Moserova, I., Truxova, I., Hermanova, I., Vancurova, I., Partlova, S., ..., Spisek, R. (2014). High hydrostatic pressure induces immunogenic cell death in human tumor cells. *Int J Cancer, 135*(5), 1165-1177. doi:10.1002/ijc.28766

Fukumura, D., Xavier, R., Sugiura, T., Chen, Y., Park, E. C., Lu, N., ..., Seed, B. (1998). Tumor induction of VEGF promoter activity in stromal cells. *Cell, 94*(6), 715-725. doi:10.1016/s0092-8674(00)81731-6

Gaipl, U. S., Multhoff, G., Scheithauer, H., Lauber, K., Hehlgans, S., Frey, B., & Rodel, F. (2014). Kill and spread the word: stimulation of antitumor immune responses in the context of radiotherapy. *Immunotherapy, 6*(5), 597-610. doi:10.2217/imt.14.38

Galluzzi, L., Buque, A., Kepp, O., Zitvogel, L., & Kroemer, G. (2015). Immunological Effects of Conventional Chemotherapy and Targeted Anticancer Agents. *Cancer Cell, 28*(6), 690-714. doi:10.1016/j.ccell.2015.10.012

Galluzzi, L., Buque, A., Kepp, O., Zitvogel, L., & Kroemer, G. (2017). Immunogenic cell death in cancer and infectious disease. *Nat Rev Immunol, 17*(2), 97-111. doi:10.1038/nri.2016.107

Galluzzi, L., Vitale, I., Warren, S., Adjemian, S., Agostinis, P., Martinez, A. B., ..., Marincola, F. M. (2020). Consensus guidelines for the definition, detection and interpretation of immunogenic cell death. *Journal for ImmunoTherapy of Cancer, 8*(1), e000337. doi:10.1136/jitc-2019-000337

Garg, A. D., Coulie, P. G., Van den Eynde, B. J., & Agostinis, P. (2017). Integrating Next-Generation Dendritic Cell Vaccines into the Current Cancer Immunotherapy Landscape. *Trends Immunol, 38*(8), 577-593. doi:10.1016/j.it.2017.05.006

Gerber, S. A., Sedlacek, A. L., Cron, K. R., Murphy, S. P., Frelinger, J. G., & Lord, E. M. (2013). IFN-gamma mediates the antitumor effects of radiation therapy in a murine colon tumor. *Am J Pathol, 182*(6), 2345-2354. doi:10.1016/j.ajpath.2013.02.041

Grayson, J. M., Harrington, L. E., Lanier, J. G., Wherry, E. J., & Ahmed, R. (2002). Differential sensitivity of naive and memory CD8+ T cells to apoptosis in vivo. *J Immunol, 169*(7), 3760-3770. doi:10.4049/jimmunol.169.7.3760

Griffioen, A. W., Damen, C. A., Blijham, G. H., & Groenewegen, G. (1996). Tumor angiogenesis is accompanied by a decreased inflammatory response of tumor-associated endothelium. *Blood, 88*(2), 667-673.

Gros, A., Parkhurst, M. R., Tran, E., Pasetto, A., Robbins, P. F., Ilyas, S., ..., Rosenberg, S. A. (2016). Prospective identification of neoantigen-specific lymphocytes in the peripheral blood of melanoma patients. *Nat Med, 22*(4), 433-438. doi:10.1038/nm.4051

Guo, F., Wang, Y., Liu, J., Mok, S. C., Xue, F., & Zhang, W. (2016). CXCL12/CXCR4: a symbiotic bridge linking cancer cells and their stromal neighbors in oncogenic communication networks. *Oncogene, 35*(7), 816-826. doi:10.1038/onc.2015.139

Hailemichael, Y., Dai, Z., Jaffarzad, N., Ye, Y., Medina, M. A., Huang, X.-F., ..., Overwijk, W. W. (2013). Persistent antigen at vaccination sites induces tumor-specific CD8+ T cell sequestration, dysfunction and deletion. *Nature Medicine, 19*(4), 465-472. doi:10.1038/nm.3105

Hailemichael, Y., Woods, A., Fu, T., He, Q., Nielsen, M. C., Hasan, F., ..., Overwijk, W. W. (2018). Cancer vaccine formulation dictates synergy with CTLA-4 and PD-L1 checkpoint blockade therapy. *J Clin Invest, 128*(4), 1338-1354. doi:10.1172/JCI93303

Hanahan, D., & Weinberg, R. A. (2000). The hallmarks of cancer. *Cell, 100*(1), 57-70. doi:10.1016/s0092-8674(00)81683-9

Hanahan, D., & Weinberg, R. A. (2011). Hallmarks of cancer: the next generation. *Cell, 144*(5), 646-674. doi:10.1016/j.cell.2011.02.013

Haskin, C. L., Athanasiou, K. A., Klebe, R., & Cameron, I. L. (1993). A heat-shock-like response with cytoskeletal disruption occurs following hydrostatic pressure in MG-63 osteosarcoma cells. *Biochem Cell Biol, 71*(7-8), 361-371. doi:10.1139/o93-054

He, S., Cheng, J., Sun, L., Wang, Y., Wang, C., Liu, X., ..., Huang, Q. (2018). HMGB1 released by irradiated tumor cells promotes living tumor cell proliferation via paracrine effect. *Cell Death Dis, 9*(6), 648. doi:10.1038/s41419-018-0626-6

Helmink, B. A., Reddy, S. M., Gao, J., Zhang, S., Basar, R., Thakur, R., ..., Wargo, J. A. (2020). B cells and tertiary lymphoid structures promote immunotherapy response. *Nature, 577*(7791), 549-555. doi:10.1038/s41586-019-1922-8

Herskind, C., Ma, L., Liu, Q., Zhang, B., Schneider, F., Veldwijk, M. R., & Wenz, F. (2017). Biology of high single doses of IORT: RBE, 5 R's, and other biological aspects. *Radiat Oncol, 12*(1), 24. doi:10.1186/s13014-016-0750-3

Hettich, M., Lahoti, J., Prasad, S., & Niedermann, G. (2016). Checkpoint Antibodies but not T Cell-Recruiting Diabodies Effectively Synergize with TIL-Inducing gamma-Irradiation. *Cancer Res, 76*(16), 4673-4683. doi:10.1158/0008-5472.CAN-15-3451

Hollingsworth, R. E., & Jansen, K. (2019). Turning the corner on therapeutic cancer vaccines. *NPJ Vaccines, 4*, 7. doi:10.1038/s41541-019-0103-y

Hradilova, N., Sadilkova, L., Palata, O., Mysikova, D., Mrazkova, H., Lischke, R., ..., Adkins, I. (2017). Generation of dendritic cell-based vaccine using high hydrostatic pressure for non-small cell lung cancer immunotherapy. *PLoS One, 12*(2), e0171539. doi:10.1371/journal.pone.0171539

Hu, Z., Ott, P. A., & Wu, C. J. (2018). Towards personalized, tumour-specific, therapeutic vaccines for cancer. *Nat Rev Immunol, 18*(3), 168-182. doi:10.1038/nri.2017.131

Iosef, C., Gkourasas, T., Jia, C. Y., Li, S. S., & Han, V. K. (2008). A functional nuclear localization signal in insulin-like growth factor binding protein-6 mediates its nuclear import. *Endocrinology, 149*(3), 1214-1226. doi:10.1210/en.2007-0959

Janssen, E. M., Lemmens, E. E., Wolfe, T., Christen, U., von Herrath, M. G., & Schoenberger, S. P. (2003). CD4+ T cells are required for secondary expansion and memory in CD8+ T lymphocytes. *Nature, 421*(6925), 852-856. doi:10.1038/nature01441

Jiang, Y., Li, Y., & Zhu, B. (2015). T-cell exhaustion in the tumor microenvironment. *Cell Death Dis, 6*, e1792. doi:10.1038/cddis.2015.162

Kang, R., Zhang, Q., Zeh, H. J., 3rd, Lotze, M. T., & Tang, D. (2013). HMGB1 in cancer: good, bad, or both? *Clin Cancer Res, 19*(15), 4046-4057. doi:10.1158/1078-0432.CCR-13-0495

Karachaliou, N., Gonzalez-Cao, M., Crespo, G., Drozdowskyj, A., Aldeguer, E., Gimenez-Capitan, A., ..., Rosell, R. (2018). Interferon gamma, an important marker of response to immune checkpoint blockade in non-small cell lung cancer and melanoma patients. *Ther Adv Med Oncol, 10*, 1758834017749748. doi:10.1177/1758834017749748

Klempner, S. J., Fabrizio, D., Bane, S., Reinhart, M., Peoples, T., Ali, S. M., ..., Reddy, P. (2020). Tumor Mutational Burden as a Predictive Biomarker for Response to Immune Checkpoint Inhibitors: A Review of Current Evidence. *Oncologist, 25*(1), e147-e159. doi:10.1634/theoncologist.2019-0244

Klug, F., Prakash, H., Huber, P. E., Seibel, T., Bender, N., Halama, N., ..., Beckhove, P. (2013). Low-dose irradiation programs macrophage differentiation to an iNOS(+)/M1 phenotype that orchestrates effective T cell immunotherapy. *Cancer Cell, 24*(5), 589-602. doi:10.1016/j.ccr.2013.09.014

Knudson, K. M., Hicks, K. C., Luo, X., Chen, J. Q., Schlom, J., & Gameiro, S. R. (2018). M7824, a novel bifunctional anti-PD-L1/TGFbeta Trap fusion protein, promotes anti-tumor efficacy as monotherapy and in combination with vaccine. *Oncoimmunology, 7*(5), e1426519. doi:10.1080/2162402X.2018.1426519

Krijgsman, D., Hokland, M., & Kuppen, P. J. K. (2018). The Role of Natural Killer T Cells in Cancer-A Phenotypical and Functional Approach. *Front Immunol, 9*, 367. doi:10.3389/fimmu.2018.00367

Kuo, Y. S., Tang, Y. B., Lu, T. Y., Wu, H. C., & Lin, C. T. (2010). IGFBP-6 plays a role as an oncosuppressor gene in NPC pathogenesis through regulating EGR-1 expression. *J Pathol, 222*(3), 299-309. doi:10.1002/path.2735

Lauro, F. M., & Bartlett, D. H. (2008). Prokaryotic lifestyles in deep sea habitats. *Extremophiles, 12*(1), 15-25. doi:10.1007/s00792-006-0059-5

Leach, D. R., Krummel, M. F., & Allison, J. P. (1996). Enhancement of antitumor immunity by CTLA-4 blockade. *Science, 271*(5256), 1734-1736. doi:10.1126/science.271.5256.1734

LeBleu, V. S., & Kalluri, R. (2018). A peek into cancer-associated fibroblasts: origins, functions and translational impact. *Dis Model Mech, 11*(4). doi:10.1242/dmm.029447

Lee, S., & Margolin, K. (2011). Cytokines in cancer immunotherapy. *Cancers (Basel), 3*(4), 3856-3893. doi:10.3390/cancers3043856

Lee, Y. J., Lee, S. B., Beak, S. K., Han, Y. D., Cho, M. S., Hur, H., ..., Min, B. S. (2018). Temporal changes in immune cell composition and cytokines in response to chemoradiation in rectal cancer. *Sci Rep, 8*(1), 7565. doi:10.1038/s41598-018-25970-z

Levitt Katz, L. E., Rosenfeld, R. G., & Cohen, S. P. (1995). Clinical Significance of Insulin-Like Growth Factor Binding Proteins (IGFBPs). *The Endocrinologist, 5*(1), 36-43. doi:10.1097/00019616-199501000-00006

Li, J., Byrne, K. T., Yan, F., Yamazoe, T., Chen, Z., Baslan, T., ..., Stanger, B. Z. (2018). Tumor Cell-Intrinsic Factors Underlie Heterogeneity of Immune Cell Infiltration and Response to Immunotherapy. *Immunity, 49*(1), 178-193 e177. doi:10.1016/j.immuni.2018.06.006

Lim, Y. J., Koh, J., Kim, S., Jeon, S. R., Chie, E. K., Kim, K., ..., Wu, H. G. (2017). Chemoradiation-Induced Alteration of Programmed Death-Ligand 1 and CD8(+) Tumor-Infiltrating Lymphocytes Identified Patients With Poor Prognosis in Rectal Cancer: A Matched Comparison Analysis. *Int J Radiat Oncol Biol Phys, 99*(5), 1216-1224. doi:10.1016/j.ijrobp.2017.07.004

Liso, A., Capitanio, N., Gerli, R., & Conese, M. (2018). From fever to immunity: A new role for IGFBP-6? *J Cell Mol Med, 22*(10), 4588-4596. doi:10.1111/jcmm.13738

Liso, A., Castellani, S., Massenzio, F., Trotta, R., Pucciarini, A., Bigerna, B., ..., Falini, B. (2017). Human monocyte-derived dendritic cells exposed to hyperthermia show a distinct gene expression profile and selective upregulation of IGFBP6. *Oncotarget, 8*(37), 60826-60840. doi:10.18632/oncotarget.18338

Liu, Z., Kuang, W., Zhou, Q., & Zhang, Y. (2018). TGF-beta1 secreted by M2 phenotype macrophages enhances the stemness and migration of glioma cells via the SMAD2/3 signalling pathway. *Int J Mol Med, 42*(6), 3395-3403. doi:10.3892/ijmm.2018.3923

Macgregor, R. B., Jr. (1998). Effect of hydrostatic pressure on nucleic acids. *Biopolymers, 48*(4), 253-263. doi:10.1002/(sici)1097-0282(1998)48:4<253::aid-bip5>3.3.co;2-6

Martincorena, I., Raine, K. M., Gerstung, M., Dawson, K. J., Haase, K., Van Loo, P., ..., Campbell, P. J. (2017). Universal Patterns of Selection in Cancer and Somatic Tissues. *Cell, 171*(5), 1029-1041 e1021. doi:10.1016/j.cell.2017.09.042

Mayor, P. C., Eng, K. H., Singel, K. L., Abrams, S. I., Odunsi, K., Moysich, K. B., ..., Segal, B. H. (2018). Cancer in primary immunodeficiency diseases: Cancer incidence in the United States Immune Deficiency Network Registry. *J Allergy Clin Immunol, 141*(3), 1028-1035. doi:10.1016/j.jaci.2017.05.024

Mentre, P., Hamraoui, L., Hui Bon Hoa, G., & Debey, P. (1999). Pressure-sensitivity of endoplasmic reticulum membrane and nucleolus as revealed by electron microscopy. *Cell Mol Biol (Noisy-le-grand), 45*(3), 353-362.

Micutkova, L., Diener, T., Li, C., Rogowska-Wrzesinska, A., Mueck, C., Huetter, E., ..., Jansen-Duerr, P. (2011). Insulin-like growth factor binding protein-6 delays replicative senescence of human fibroblasts. *Mech Ageing Dev, 132*(10), 468-479. doi:10.1016/j.mad.2011.07.005

Mikyskova, R., Stepanek, I., Indrova, M., Bieblova, J., Simova, J., Truxova, I., ..., Reinis, M. (2016). Dendritic cells pulsed with tumor cells killed by high hydrostatic pressure induce strong immune responses and display therapeutic effects both in murine TC-1 and TRAMP-C2 tumors when combined with docetaxel chemotherapy. *Int J Oncol, 48*(3), 953-964. doi:10.3892/ijo.2015.3314

Mole, R. H. (1953). Whole body irradiation; radiobiology or medicine? *Br J Radiol, 26*(305), 234-241. doi:10.1259/0007-1285-26-305-234

Morisada, M., Clavijo, P. E., Moore, E., Sun, L., Chamberlin, M., Van Waes, C., ..., Allen, C. T. (2018). PD-1 blockade reverses adaptive immune resistance induced by high-dose hypofractionated but not low-dose daily fractionated radiation. *Oncoimmunology, 7*(3), e1395996. doi:10.1080/2162402X.2017.1395996

Mortaz, E., Tabarsi, P., Mansouri, D., Khosravi, A., Garssen, J., Velayati, A., & Adcock, I. M. (2016). Cancers Related to Immunodeficiencies: Update and Perspectives. *Front Immunol, 7*, 365. doi:10.3389/fimmu.2016.00365

Morvan, M. G., & Lanier, L. L. (2016). NK cells and cancer: you can teach innate cells new tricks. *Nat Rev Cancer, 16*(1), 7-19. doi:10.1038/nrc.2015.5

Munn, D. H., & Mellor, A. L. (2006). The tumor-draining lymph node as an immune-privileged site. *Immunol Rev, 213*, 146-158. doi:10.1111/j.1600-065X.2006.00444.x

Murphy, K., Weaver, C. T., Mowat, A., & Janeway, C. A., Jr. (2017). *Janeway's immunobiology*. New York, N.Y.; London: Garland Science.

NobelPrize.org. (2020). The Nobel Prize in Physiology or Medicine 2018 [Press release]. Retrieved from https://www.nobelprize.org/prizes/medicine/2018/press-release/

Ohlfest, J. R., Andersen, B. M., Litterman, A. J., Xia, J., Pennell, C. A., Swier, L. E., ..., Olin, M. R. (2013). Vaccine injection site matters: qualitative and quantitative defects in CD8 T cells primed as a function of proximity to the tumor in a murine glioma model. *J Immunol, 190*(2), 613-620. doi:10.4049/jimmunol.1201557

Paix, A., Antoni, D., Waissi, W., Ledoux, M. P., Bilger, K., Fornecker, L., & Noel, G. (2018). Total body irradiation in allogeneic bone marrow transplantation conditioning regimens: A review. *Crit Rev Oncol Hematol, 123*, 138-148. doi:10.1016/j.critrevonc.2018.01.011

Peggs, K. S., Quezada, S. A., & Allison, J. P. (2009). Cancer immunotherapy: co-stimulatory agonists and co-inhibitory antagonists. *Clin Exp Immunol, 157*(1), 9-19. doi:10.1111/j.1365-2249.2009.03912.x

Porrello, A., Leslie, P. L., Harrison, E. B., Gorentla, B. K., Kattula, S., Ghosh, S. K., ..., Pecot, C. V. (2018). Factor XIIIA-expressing inflammatory monocytes promote lung squamous cancer through fibrin cross-linking. *Nat Commun, 9*(1), 1988. doi:10.1038/s41467-018-04355-w

Prasanna, A., Ahmed, M. M., Mohiuddin, M., & Coleman, C. N. (2014). Exploiting sensitization windows of opportunity in hyper and hypo-fractionated radiation therapy. *J Thorac Dis, 6*(4), 287-302. doi:10.3978/j.issn.2072-1439.2014.01.14

Qin, S., Xu, L., Yi, M., Yu, S., Wu, K., & Luo, S. (2019). Novel immune checkpoint targets: moving beyond PD-1 and CTLA-4. *Mol Cancer, 18*(1), 155. doi:10.1186/s12943-019-1091-2

Qureshi, O. S., Zheng, Y., Nakamura, K., Attridge, K., Manzotti, C., Schmidt, E. M., ..., Sansom, D. M. (2011). Trans-endocytosis of CD80 and CD86: a molecular basis for the cell-extrinsic function of CTLA-4. *Science, 332*(6029), 600-603. doi:10.1126/science.1202947

Reits, E. A., Hodge, J. W., Herberts, C. A., Groothuis, T. A., Chakraborty, M., Wansley, E. K., ..., Neefjes, J. J. (2006). Radiation modulates the peptide repertoire, enhances MHC class I expression, and induces successful antitumor immunotherapy. *J Exp Med, 203*(5), 1259-1271. doi:10.1084/jem.20052494

Riley, R. S., June, C. H., Langer, R., & Mitchell, M. J. (2019). Delivery technologies for cancer immunotherapy. *Nat Rev Drug Discov, 18*(3), 175-196. doi:10.1038/s41573-018-0006-z

Rosenberg, S. A., Yang, J. C., & Restifo, N. P. (2004). Cancer immunotherapy: moving beyond current vaccines. *Nat Med, 10*(9), 909-915. doi:10.1038/nm1100

Rückert, M., Deloch, L., Fietkau, R., Frey, B., & Gaipl, U. S. (2017). Interaktionen von Strahlen- und Immuntherapie. *23*(10), 823-830. doi:10.1007/s00761-017-0267-x

Rückert, M., Deloch, L., Fietkau, R., Frey, B., Hecht, M., & Gaipl, U. S. (2018). Immune modulatory effects of radiotherapy as basis for well-reasoned radioimmunotherapies. *Strahlenther Onkol, 194*(6), 509-519. doi:10.1007/s00066-018-1287-1

Sainz-Perez, A., Lim, A., Lemercier, B., & Leclerc, C. (2012). The T-cell receptor repertoire of tumor-infiltrating regulatory T lymphocytes is skewed toward public sequences. *Cancer Res, 72*(14), 3557-3569. doi:10.1158/0008-5472.CAN-12-0277

Saldanha, G., Flatman, K., Teo, K. W., & Bamford, M. (2017). A Novel Numerical Scoring System for Melanoma Tumor-infiltrating Lymphocytes Has Better Prognostic Value Than Standard Scoring. *Am J Surg Pathol, 41*(7), 906-914. doi:10.1097/PAS.0000000000000848

Sanchez-Paulete, A. R., Cueto, F. J., Martinez-Lopez, M., Labiano, S., Morales-Kastresana, A., Rodriguez-Ruiz, M. E., ..., Melero, I. (2016). Cancer Immunotherapy with Immunomodulatory Anti-CD137 and Anti-PD-1 Monoclonal Antibodies Requires BATF3-Dependent Dendritic Cells. *Cancer Discov, 6*(1), 71-79. doi:10.1158/2159-8290.CD-15-0510

Sarvaria, A., Madrigal, J. A., & Saudemont, A. (2017). B cell regulation in cancer and anti-tumor immunity. *Cell Mol Immunol, 14*(8), 662-674. doi:10.1038/cmi.2017.35

Schadendorf, D., Hodi, F. S., Robert, C., Weber, J. S., Margolin, K., Hamid, O., ..., Wolchok, J. D. (2015). Pooled Analysis of Long-Term Survival Data From Phase II and Phase III Trials of Ipilimumab in Unresectable or Metastatic Melanoma. *J Clin Oncol, 33*(17), 1889-1894. doi:10.1200/JCO.2014.56.2736

Schaue, D., Ratikan, J. A., Iwamoto, K. S., & McBride, W. H. (2012). Maximizing tumor immunity with fractionated radiation. *Int J Radiat Oncol Biol Phys, 83*(4), 1306-1310. doi:10.1016/j.ijrobp.2011.09.049

Schreiber, R. D., Old, L. J., & Smyth, M. J. (2011). Cancer immunoediting: integrating immunity's roles in cancer suppression and promotion. *Science, 331*(6024), 1565-1570. doi:10.1126/science.1203486

Seetharam, S., Staba, M. J., Schumm, L. P., Schreiber, K., Schreiber, H., Kufe, D. W., & Weichselbaum, R. R. (1999). Enhanced eradication of local and distant tumors by genetically produced interleukin-12 and radiation. *Int J Oncol, 15*(4), 769-773. doi:10.3892/ijo.15.4.769

Seidel, J. A., Otsuka, A., & Kabashima, K. (2018). Anti-PD-1 and Anti-CTLA-4 Therapies in Cancer: Mechanisms of Action, Efficacy, and Limitations. *Front Oncol, 8*, 86. doi:10.3389/fonc.2018.00086

Seitz, C., Rückert, M., Deloch, L., Weiss, E. M., Utz, S., Izydor, M., ..., Frey, B. (2019). Tumor Cell-Based Vaccine Generated With High Hydrostatic Pressure Synergizes With Radiotherapy by Generating a Favorable Anti-tumor Immune Microenvironment. *Front Oncol, 9*, 805. doi:10.3389/fonc.2019.00805

Selitsky, S. R., Mose, L. E., Smith, C. C., Chai, S., Hoadley, K. A., Dittmer, D. P., ..., Vincent, B. G. (2019). Prognostic value of B cells in cutaneous melanoma. *Genome Med, 11*(1), 36. doi:10.1186/s13073-019-0647-5

Shankaran, V., Ikeda, H., Bruce, A. T., White, J. M., Swanson, P. E., Old, L. J., & Schreiber, R. D. (2001). IFNgamma and lymphocytes prevent primary tumour development and shape tumour immunogenicity. *Nature, 410*(6832), 1107-1111. doi:10.1038/35074122

Shitara, K., & Nishikawa, H. (2018). Regulatory T cells: a potential target in cancer immunotherapy. *Ann N Y Acad Sci, 1417*(1), 104-115. doi:10.1111/nyas.13625

Spranger, S., & Gajewski, T. F. (2015). A new paradigm for tumor immune escape: beta-catenin-driven immune exclusion. *J Immunother Cancer, 3*, 43. doi:10.1186/s40425-015-0089-6

Tacken, P. J., de Vries, I. J., Torensma, R., & Figdor, C. G. (2007). Dendritic-cell immunotherapy: from ex vivo loading to in vivo targeting. *Nat Rev Immunol, 7*(10), 790-802. doi:10.1038/nri2173

They, L., Michaud, H. A., Becquart, O., Lafont, V., Guillot, B., Boissiere-Michot, F., ..., Gros, L. (2017). PD-1 blockade at the time of tumor escape potentiates the immune-mediated antitumor effects of a melanoma-targeting monoclonal antibody. *Oncoimmunology, 6*(10), e1353857. doi:10.1080/2162402X.2017.1353857

Thomas, A., Routh, E. D., Pullikuth, A., Jin, G., Su, J., Chou, J. W., ..., Miller, L. D. (2018). Tumor mutational burden is a determinant of immune-mediated survival in breast cancer. *Oncoimmunology, 7*(10), e1490854. doi:10.1080/2162402X.2018.1490854

Urbanova, L., Hradilova, N., Moserova, I., Vosahlikova, S., Sadilkova, L., Hensler, M., ..., Adkins, I. (2017). High hydrostatic pressure affects antigenic pool in tumor cells: Implication for dendritic cell-based cancer immunotherapy. *Immunol Lett, 187*, 27-34. doi:10.1016/j.imlet.2017.05.005

Valipour, B., Velaei, K., Abedelahi, A., Karimipour, M., Darabi, M., & Charoudeh, H. N. (2019). NK cells: An attractive candidate for cancer therapy. *J Cell Physiol, 234*(11), 19352-19365. doi:10.1002/jcp.28657

van Meir, H., Nout, R. A., Welters, M. J., Loof, N. M., de Kam, M. L., van Ham, J. J., ..., van der Burg, S. H. (2017). Impact of (chemo)radiotherapy on immune cell composition and function in cervical cancer patients. *Oncoimmunology, 6*(2), e1267095. doi:10.1080/2162402X.2016.1267095

Vano, Y. A., Petitprez, F., Giraldo, N. A., Fridman, W. H., & Sautes-Fridman, C. (2018). Immune-based identification of cancer patients at high risk of progression. *Curr Opin Immunol, 51*, 97-102. doi:10.1016/j.coi.2018.03.005

Vanpouille-Box, C., Alard, A., Aryankalayil, M. J., Sarfraz, Y., Diamond, J. M., Schneider, R. J., ..., Demaria, S. (2017). DNA exonuclease Trex1 regulates radiotherapy-induced tumour immunogenicity. *Nat Commun, 8*, 15618. doi:10.1038/ncomms15618

Veglia, F., Perego, M., & Gabrilovich, D. (2018). Myeloid-derived suppressor cells coming of age. *Nat Immunol, 19*(2), 108-119. doi:10.1038/s41590-017-0022-x

Velcheti, V., & Schalper, K. (2016). Basic Overview of Current Immunotherapy Approaches in Cancer. *Am Soc Clin Oncol Educ Book, 35*, 298-308. doi:10.14694/EDBK_156572

10.1200/EDBK_156572

Wang, S., He, Z., Wang, X., Li, H., & Liu, X. S. (2019). Antigen presentation and tumor immunogenicity in cancer immunotherapy response prediction. *Elife, 8*. doi:10.7554/eLife.49020

Wei, S. C., Duffy, C. R., & Allison, J. P. (2018). Fundamental Mechanisms of Immune Checkpoint Blockade Therapy. *Cancer Discov, 8*(9), 1069-1086. doi:10.1158/2159-8290.CD-18-0367

Weichselbaum, R. R., Ishwaran, H., Yoon, T., Nuyten, D. S., Baker, S. W., Khodarev, N., ..., Minn, A. J. (2008). An interferon-related gene signature for DNA damage resistance is a predictive marker for chemotherapy and radiation for breast cancer. *Proc Natl Acad Sci U S A, 105*(47), 18490-18495. doi:10.1073/pnas.0809242105

Weiss, E.-M., Frey, B., Rödel, F., Herrmann, M., Schlücker, E., Voll, R. E., ..., Gaipl, U. S. (2010). Ex vivo- and in vivo-induced dead tumor cells as modulators of antitumor responses. *Annals of the New York Academy of Sciences, 1209*, 109-117. doi:10.1111/j.1749-6632.2010.05743.x

Weiss, E.-M., Meister, S., Janko, C., Ebel, N., Schlücker, E., Meyer-Pittroff, R., ..., Frey, B. (2010). High hydrostatic pressure treatment generates inactivated mammalian tumor cells with immunogeneic features. *Journal of immunotoxicology, 7*(3), 194-204. doi:10.3109/15476911003657414

Weiss, E.-M., Wunderlich, R., Ebel, N., Rubner, Y., Schlücker, E., Meyer-Pittroff, R., ..., Frey, B. (2012). Selected anti-tumor vaccines merit a place in multimodal tumor therapies. *Frontiers in oncology, 2*, 132-132. doi:10.3389/fonc.2012.00132

Wennerberg, E., Lhuillier, C., Vanpouille-Box, C., Pilones, K. A., Garcia-Martinez, E., Rudqvist, N. P., ..., Demaria, S. (2017). Barriers to Radiation-Induced In Situ Tumor Vaccination. *Front Immunol, 8*, 229. doi:10.3389/fimmu.2017.00229

Werfel, T. A., Elion, D. L., Rahman, B., Hicks, D. J., Sanchez, V., Gonzales-Ericsson, P. I., ..., Cook, R. S. (2019). Treatment-Induced Tumor Cell Apoptosis and Secondary Necrosis Drive Tumor

Progression in the Residual Tumor Microenvironment through MerTK and IDO1. *Cancer Res, 79*(1), 171-182. doi:10.1158/0008-5472.CAN-18-1106

Werthmöller, N., Frey, B., Rückert, M., Lotter, M., Fietkau, R., & Gaipl, U. S. (2016). Combination of ionising radiation with hyperthermia increases the immunogenic potential of B16-F10 melanoma cells in vitro and in vivo. *Int J Hyperthermia, 32*(1), 23-30. doi:10.3109/02656736.2015.1106011

Williams, M. A., & Bevan, M. J. (2007). Effector and memory CTL differentiation. *Annu Rev Immunol, 25*, 171-192. doi:10.1146/annurev.immunol.25.022106.141548

Wilson, R. G., Jr., Trogadis, J. E., Zimmerman, S., & Zimmerman, A. M. (2001). Hydrostatic pressure induced changes in the cytoarchitecture of pheochromocytoma (PC-12) cells. *Cell Biol Int, 25*(7), 649-666. doi:10.1006/cbir.2000.0692

Wimmers, F., Schreibelt, G., Skold, A. E., Figdor, C. G., & De Vries, I. J. (2014). Paradigm Shift in Dendritic Cell-Based Immunotherapy: From in vitro Generated Monocyte-Derived DCs to Naturally Circulating DC Subsets. *Front Immunol, 5*, 165. doi:10.3389/fimmu.2014.00165

Wouters, M. C. A., & Nelson, B. H. (2018). Prognostic Significance of Tumor-Infiltrating B Cells and Plasma Cells in Human Cancer. *Clin Cancer Res, 24*(24), 6125-6135. doi:10.1158/1078-0432.CCR-18-1481

Xing, D., Siva, S., & Hanna, G. G. (2019). The Abscopal Effect of Stereotactic Radiotherapy and Immunotherapy: Fool's Gold or El Dorado? *Clin Oncol (R Coll Radiol), 31*(7), 432-443. doi:10.1016/j.clon.2019.04.006

Yang, C., Yu, H., Chen, R., Tao, K., Jian, L., Peng, M., ..., Liu, S. (2019). CXCL1 stimulates migration and invasion in ERnegative breast cancer cells via activation of the ERK/MMP2/9 signaling axis. *Int J Oncol, 55*(3), 684-696. doi:10.3892/ijo.2019.4840

Yang, S., Liu, F., Wang, Q. J., Rosenberg, S. A., & Morgan, R. A. (2011). The shedding of CD62L (L-selectin) regulates the acquisition of lytic activity in human tumor reactive T lymphocytes. *PLoS One, 6*(7), e22560. doi:10.1371/journal.pone.0022560

Yost, K. E., Satpathy, A. T., Wells, D. K., Qi, Y., Wang, C., Kageyama, R., ..., Chang, H. Y. (2019). Clonal replacement of tumor-specific T cells following PD-1 blockade. *Nature Medicine, 25*(8), 1251-1259. doi:10.1038/s41591-019-0522-3

Young, K. H., Baird, J. R., Savage, T., Cottam, B., Friedman, D., Bambina, S., ..., Crittenden, M. R. (2016). Optimizing Timing of Immunotherapy Improves Control of Tumors by Hypofractionated Radiation Therapy. *PLoS One, 11*(6), e0157164. doi:10.1371/journal.pone.0157164

Yu, Y. R., & Ho, P. C. (2019). Sculpting tumor microenvironment with immune system: from immunometabolism to immunoediting. *Clin Exp Immunol, 197*(2), 153-160. doi:10.1111/cei.13293

Yuan, M., Zhu, H., Xu, J., Zheng, Y., Cao, X., & Liu, Q. (2016). Tumor-Derived CXCL1 Promotes Lung Cancer Growth via Recruitment of Tumor-Associated Neutrophils. *J Immunol Res, 2016*, 6530410. doi:10.1155/2016/6530410

Zhang, W. J., & Zheng, S. S. (2005). In vitro study of immunosuppressive effect of apoptotic cells. *J Zhejiang Univ Sci B, 6*(9), 919-925. doi:10.1631/jzus.2005.B0919

Zhang, X., & Niedermann, G. (2018). Abscopal Effects With Hypofractionated Schedules Extending Into the Effector Phase of the Tumor-Specific T-Cell Response. *Int J Radiat Oncol Biol Phys, 101*(1), 63-73. doi:10.1016/j.ijrobp.2018.01.094

Zhao, C., Zhu, X., Wang, G., Wang, W., Ju, S., & Wang, X. (2020). Decreased expression of IGFBP6 correlates with poor survival in colorectal cancer patients. *Pathology - Research and Practice*. doi:10.1016/j.prp.2020.152909

Zhao, P., Wang, Y., Kang, X., Wu, A., Yin, W., Tang, Y., ..., Huang, Y. (2018). Dual-targeting biomimetic delivery for anti-glioma activity via remodeling the tumor microenvironment and directing macrophage-mediated immunotherapy. *Chem Sci, 9*(10), 2674-2689. doi:10.1039/c7sc04853j

VII. List of Publications

Peer-reviewed publications

2019 Seitz, C.*, **Rückert, M.***, Deloch, L., Weiss, E.-M., Utz, S., Izydor, M., et al.. Tumor Cell-Based Vaccine Generated With High Hydrostatic Pressure Synergizes With Radiotherapy by Generating a Favorable Anti-tumor Immune Microenvironment. *Frontiers in Oncology* 9, 805. doi: 10.3389/fonc.2019.00805.

2019 Deloch, L., Fuchs, J., **Rückert, M.**, Fietkau, R., Frey, B., and Gaipl, U.S.. Low-Dose Irradiation Differentially Impacts Macrophage Phenotype in Dependence of Fibroblast-Like Synoviocytes and Radiation Dose. *Journal of Immunology Research*, 1-11. doi: 10.1155/2019/3161750.

2019 Frey B., **Rückert M.**, Gaipl U.S. Immune Modulatory Effects of Radiotherapy. In: Wenz F. (eds) *Radiation Oncology*. Springer, Cham

2018 Deloch, L., **Rückert, M.**, Fietkau, R., Frey, B., and Gaipl, U.. Low-Dose Radiotherapy Has No Harmful Effects on Key Cells of Healthy Non-Inflamed Joints. *International Journal of Molecular Sciences* 19(10). doi: 10.3390/ijms19103197.

2018 **Rückert, M**.*, Deloch, L. *, Fietkau, R., Frey, B., Hecht, M., and Gaipl, U.S.. Immune modulatory effects of radiotherapy as basis for well-reasoned radioimmunotherapies. *Strahlentherapie und Onkologie* 194(6), 509-519. doi: 10.1007/s00066-018-1287-1.

2017 Frey, B., **Rückert, M.**, Deloch, L., Rühle, P.F., Derer, A., Fietkau, R., et al.. Immunomodulation by ionizing radiation-impact for design of radio-immunotherapies and for treatment of inflammatory diseases. *Immunological Reviews* 280(1)**,** 231-248. doi: 10.1111/imr.12572.

2017 **Rückert M.***, Deloch L.*, Fietkau R., Frey B., Gaipl U.S.. Interaktionen von Strahlen- und Immuntherapie. *Der Onkologe*, 23(10), 823-830. doi:10.1007/s00761-017-0267-x

2017 Frey, B., **Rückert, M.**, Weber, J., Mayr, X., Derer, A., Lotter, M., et al.. Hypofractionated Irradiation Has Immune Stimulatory Potential and Induces a Timely Restricted Infiltration of Immune Cells in Colon Cancer Tumors. *Frontiers in Immunology* 8, 231. doi: 10.3389/fimmu.2017.00231.

2017 Jara-Avaca M, Kempf H, **Rückert M**, Robles-Diaz D, Franke A, de la Roche J, Fischer M, Malan D, Sasse P, Solodenko W, et al. EBIO Does Not Induce Cardiomyogenesis in Human Pluripotent Stem Cells but Modulates Cardiac Subtype Enrichment by Lineage-Selective Survival. *Stem Cell Reports* 8(2), 305-317. doi: 10.1016/j.stemcr.2016.12.012.

2016 Werthmöller, N., Frey, B., **Rückert, M.**, Lotter, M., Fietkau, R., and Gaipl, U.S. (2016). Combination of ionising radiation with hyperthermia increases the immunogenic potential of B16-F10 melanoma cells in vitro and in vivo.

International Journal of Hyperthermia 32(1), 23-30. doi: 10.3109/02656736.2015.1106011.

2014 Kempf, H., Olmer, R., Kropp, C., **Rückert, M.**, Jara-Avaca, M., Robles-Diaz, D., et al.. Controlling Expansion and Cardiomyogenic Differentiation of Human Pluripotent Stem Cells in Scalable Suspension Culture. *Stem Cell Reports* 3(6), 1132-1146. doi: 10.1016/j.stemcr.2014.09.017.

* *authors contributed equally*

Short publications

2019 **Rückert M.**, S.C., Deloch L., Weiss E.-M., Utz S., Izydor M., Ebel N., Schlücker E., Fietkau R., Gaipl U.S., Frey B.. Mit hydrostatischem Hochdruck generierte Ganzzell-Tumorvakzine erzeugen in Kombination mit Strahlentherapie ein immunogenes Tumor-Mikromilieu. *Strahlentherapie und Onkologie* 195(S1), 1-218. doi: 10.1007/s00066-019-01465-2.

2019 Deloch, L., **Rückert, M.**, Seeling, M., Nimmerjahn, F., Fietkau, R., Frey, B., et al.. P154 Local low dose radiation induces systemic immune alterations in two experimental models of inflammatory arthritis. *Annals of the Rheumatic Diseases* 78(Suppl 1), A67. doi: 10.1136/annrheumdis-2018-EWRR2019.136.

2018 Deloch, L., **Rückert, M.**, Hueber, A.J., Herrmann, M., Fietkau, R., Frey, B., et al.. P115 Low dose radiation has a positive impact on bone metabolism in an experimental model of inflammatory arthritis. *Annals of the Rheumatic Diseases* 77(Suppl 1), A62. doi: 10.1136/annrheumdis-2018-EWRR2018.130.

2018 **Rückert M.**, F.B., Fietkau R., Gaipl U.S.. Anti-tumor immune responses in primary and abscopal tumors differently depend on radiotherapy fractionation and immunotherapy modalities. *Strahlentherapie und Onkologie* 194(S1), 1-222. doi: 10.1007/s00066-018-1301-7.

2017 Frey B., Seitz C., Weiss E.-M., **Rückert M.**, Schlücker E., Schaft N., Fietkau R., Gaipl U. S.. Autologous whole tumor cell-based vaccines generated with high hydrostatic pressure bear immunogenic potential and act synergistically with radiotherapy to retard tumor growth. *European Journal of Immunology* 47, 1-333. doi: 10.1002/eji.201770300.

2017 Deloch, L., Liberg, J., **Rückert, M.**, Hueber, A.J., Fietkau, R., Frey, B., et al.. 06.06 Low dose radiation alters the inflammatory phenotype of fibroblast-like synoviocytes and macrophages and stimulates osteoblasts. *Annals of the Rheumatic Diseases* 76(Suppl 1), A61. doi: 10.1136/annrheumdis-2016-211053.6.

2017 **Rückert M.**, Frey B., Fietkau R., Gaipl U. S.. Immunological basis of local and abscopal antitumor responses induced with radio-immunotherapy. *European Journal of Immunology* 47, 1-333. doi: 10.1002/eji.201770300.

2017 **Rückert M.**, F.B., Fietkau R., Gaipl U.S.. Immunological basis of abscopal antitumor responses induced with radio-immunotherapy. *Strahlentherapie und Onkologie* 193(S1)**,** 1-194. doi: 10.1007/s00066-017-1137-6.

2016 Frey B., S.C., **Rückert M.**,Weiss E.-M., Wunderlich R., Schlücker E., Schaft N., Fietkau R.,Gaipl U.S.. Combination of ionizing radiation with an autologous whole tumour cell-based vaccine induces immunogenic melanoma and colorectal cancer cells and significantly retards tumour growth in syngenic mouse models. *Strahlentherapie und Onkologie* 192(S1), 1-161. doi: 10.1007/s00066-016-0974-z.